IMPLEMENTATION OF THE ENSEMBLE KALMAN FILTER IN THE CHARACTERIZATION OF HYDRAULIC FRACTURES IN SHALE GAS RESERVOIRS BY INTEGRATING DOWNHOLE TEMPERATURE SENSING TECHNOLOGY

A Thesis

by

JOSE ANDRES MORENO

Submitted to the Office of Graduate and Professional Studies of
Texas A&M University
in partial fulfillment of the requirements for the degree of

MASTER OF SCIENCE

Chair of Committee,	Eduardo Gildin
Co-Chair of Committee,	Ding Zhu
Committee Member,	Shankar Bhattacharyya
Head of Department,	Daniel Hill

August 2014

Major Subject: Petroleum Engineering

ABSTRACT

Multi-stage hydraulic fracturing in horizontal wells has demonstrated successful results for developing unconventional low-permeability oil and gas reservoirs. Despite being vastly implemented by different operators across North America, hydraulic fracture treatments are still not fully comprehended and have proved to have a more complex behavior than initially thought. To fill this knowledge gap and monitor the performance of hydraulic fracture treatments, fracture diagnostic tools are deployed in order to obtain information that can give a better insight of the reservoir and hydraulic fracture conditions. A technique that has demonstrated great potential in the monitoring of hydraulic fracture treatments is distributed temperature sensing technology. In situations where pressure and/or flow rate data is not reliable or in conflict with the known physics of the reservoir, continuous temperature data can be used as an alternative source of information since it effectively responds to pressure or flow rate changes when looked at a finer scale. Qualitative information such as fracture initiation points, vertical coverage and number of created fractures can be identified via distributed temperature sensors however; more quantitative results are needed in order to accurately characterize hydraulic fractures in shale gas reservoirs.

In this study, a stochastic inverse problem is set up with the objective of inferring hydraulic fracture characteristics, such as fracture half-length and permeability, by assimilating data from downhole temperature sensors. The ensemble Kalman filter is implemented to assimilate DTS data and estimate fracture parameters. This inverse

method is suitable for applications to non-linear assimilation problems and is, by nature, an appropriate approach for monitoring. In this way, the ensemble Kalman filter enables a quantitative fracture characterization and automatic history matching. Furthermore, the EnKF offers several advantages for this application, including the ensemble formulation for uncertainty assessment, convenient gradient-free implementation, and the flexibility to incorporate additional monitoring data types. The validity of the method is examined using synthetic models, and finally, field data from a horizontal gas well in the Marcellus shale.

DEDICATION

To my mother, for being the most influential person in my life and my best friend.

ACKNOWLEDGEMENTS

I would like to thank my committee chair, Dr. Gildin, and my committee members, Dr. Zhu and Dr. Bhattacharyya, for their guidance and support throughout the course of this research.

Thanks also go to my friends and colleagues and the department faculty and staff for making my time at Texas A&M University a great experience. I also want to extend my gratitude to the Department of Energy and the Research Partnership to Secure Energy for America, which provided funding for this research under contract DE-AC26-07NT42677.

Finally, thanks to my family and friends for their encouragement and support.

TABLE OF CONTENTS

Page

LIST OF FIGURES

Page

LIST OF TABLES

Page

1. INTRODUCTION

1.1 Background

In the last decade, unconventional hydrocarbon resources have become a predominant component of North America's energy supply. The development and economic viability of these unconventional reservoirs, specifically shale formations, relies on the effective stimulation of extremely low-permeability rock through a technique known as hydraulic fracturing. This technique consists of pumping specially engineered fluids at high pressure and rate into the reservoir interval to create complex fracture networks that connect a large reservoir surface area to the wellbore (Cipolla et al, 2010). As a result, hydraulic fracturing has become an indispensable technology in today's North American onshore development by enabling the development of once thought unattainable resources.

Despite being vastly implemented by different operators across North America, hydraulic fracture treatments (HFT) are still not fully comprehended and have proved to have a more complex behavior than initially thought. To fill this knowledge gap, fracture diagnostic tools are used in order to directly or indirectly measure parameters that can provide relevant information to asses a fracture treatment. Conventional diagnostic tools can be classified in to three different groups: Direct-Far Field, Direct-Near Wellbore and Indirect Mapping tools. A technique with great potential in the area of HFT diagnostics is distributed temperature sensing technology (DTS). In situations where pressure and/or flow rate data is not reliable or in conflict with the known physics of the reservoir,

continuous temperature data can be used as an alternative source of information since it effectively responds to pressure or flow rate changes when looked at a finer scale (Duru and Horne, 2009).

Prior to the advent of hydraulic fracturing, DTS had been mostly used for the assessment of flow contribution or injection distribution from comingled reservoirs (Sierra et al, 2008). Today, DTS is started to be used in a myriad of HFT diagnosis applications such as estimating number of generated fractures, pad fluid placement, perforation effectiveness, interval isolation and flowback (Sierra et al, 2008). These applications are suitable for qualitative assessments however; more quantitative results are needed if a more accurate reservoir/HFT characterization is sought.

In the quest for more quantitative results, a statistical framework is preferred rather than a deterministic one. The issue of strong non-linearity between the measurements (e.g. temperature along the wellbore) and unknown parameters (e.g. fracture half-length) makes the development of analytical reservoir models a very challenging task. On the other hand, Bayesian inversion modeling techniques present a suitable framework for problems involving large amount of data and severe nonlinearities. Today's computational power and the introduction of better data assimilation techniques have facilitated the handling of such problems in petroleum science. In recent years, the ensemble Kalman Filter (EnKF) has shown great potential as an alternative to traditional history matching due to its ability to continuously update reservoir models (Skjervheim et al, 2005). Commonly used in atmospheric and oceanographic sciences, the EnKF is a sequential Bayesian inversion that results in an

ensemble of solutions approximating the posterior probability density function for the model input parameters, state variables, and other output data conditioned to measured dynamic data (Skjervheim et al, 2005).

In this study, the EnKF filter method is used to update hydraulic fracture model parameters using a combination of production and continuous DTS data. A sensitivity analysis is performed to determine which parameters affect the reservoir temperature the most and assist in the calibration of the forward model. In addition, field data from a horizontal gas well from the Marcellus shale is integrated to further improve on the reservoir model. The goal is to use EnKF and determine as many hydraulic fracture parameters as possible using all the provided data.

1.2 Literature Review

1.2.1 Unconventional Resources

Hydrocarbon reservoirs can be classified based on the petrophysical traits that characterize them. This is based upon the predominant produced fluid (oil, gas or both) or whether they are conventional or unconventional reservoirs. (Belvalkar and Oyewole, 2010). Formations that require higher technical expertise and are less economical are defined as unconventional. When it comes to unconventional gas supplies, these can be classified as deep gas, tight gas, shale gas, coalbed methane geopressurized zones and Artic and sub-sea hydrates (Belvalkar and Oyewole, 2010). In the United States, shale gas constitutes a large portion of the country's natural gas reserves and has become a predominant component of its current energy supply.

In the past, gas-containing shale was often overlooked and considered uneconomical due to the ultra-low permeability found in these formations. Shale is defined as a fine-grained, fissile, detrital sedimentary rock which is formed as a result of deposition of clay and silt-sized particles over each other and consolidated over time (Belvalkar and Oyewole, 2010). Often acting as a seal to conventional reservoirs, shales can contain significant amount of gas trapped in the pore space as well as adsorbed on the organic matter (Belvalkar and Oyewole, 2010). In most cases, shale's low-permeability does not allow the gas to flow and hydraulic fracture treatments are executed to connect the reservoir to the wellbore via a network of artificially created fractures.

The Marcellus shale is an example of gas-containing shale. Located in the Appalachian basin, the Marcellus shale crosses the states of Pennsylvania, New York, Ohio and West Virginia. Located at approximately 5000 ft total vertical depth (TVD) with at least 50 ft formation thickness, the Marcellus shale is believed to hold up to 500 Tcf gas in place with estimates of recoverable gas at 50 Tcf (Belvalkar and Oyewole, 2010). As is the case in most gas shales, hydrocarbons are stored as free gas in natural fractures and intergranular porosity. Furthermore, the Marcellus is a dual porosity reservoir with gas flowing faster from natural fractures in comparison to the gas produced from desorption, which only occurs in the presence of hydraulic fractures. Evidently, the intersection with the reservoir's natural fractures and the effectiveness of the created fracture network is often the difference between success and failure of a well.

1.2.2 Fracture Diagnostic Technology

The assessment of a hydraulic fracture treatment (HFT) is often very complicated given that fractures grow thousands of feet below the surface and partly because hydraulic fracture behavior is still not fully understood. As a result, fracture geometry from fracture models is often inaccurate or at least, difficult to verify. For this reason, different tools have been designed with the purpose of collecting data that could lead to the proper assessment of fracture parameters.

The main purpose of fracture diagnostics is to help the producer optimize field development and well economics (Cipolla and Wright, 2000). Today, there are three main categories of commercially available diagnostic tools: Direct-Far Field, Direct-Near Wellbore and Indirect. Tiltmeter fracture mapping and microseismic fracture mapping are examples of the first group. These are often conducted from offset wellbores or from the surface during the deployment of the fracture treatment and provide a "big picture" far-field fracture growth (Cipolla and Wright, 2000). Despite mapping the total extent of hydraulic fracture growth, these tools do not offer an accurate representation of the effective propped fracture length or conductivity. Furthermore, the resolution of these is only reliable as longs as it is proximate to the testing site.

The second group of diagnostic tools is often deployed for specific applications and can be run inside the treatment wellbore before and/or after the fracture treatment. Radioactive tracer technology, production logging and DTS are examples of direct-near wellbore diagnostic techniques. Note that the first two examples are commonly deployed

post-completion while DTS is permanently installed during the drilling/completion process. Today, the main application of Near-Wellbore Fracture Diagnostic tools is the identification of fluid/proppant entry or production from each zone in multi-zone completions (Sierra et al, 2008).

Lastly, indirect-fracture diagnostic methods provide estimates of fracture parameters based on indirect measurements such as pressure responses after the propped fracture treatment (Cipolla and Wright, 2000). These methods rely on analytical and numerical solutions in order to process the collected data and generate an estimate of the desired fracture parameters. Consequently, the results obtained from these are not always unique and require calibration with direct observations. Nevertheless, a good estimate for effective dimensions and conductivity, as well as a diagnostic to identify problems in the fracture treatment, is often obtained from these techniques.

1.2.3 Downhole Temperature Technology

1.2.3.1 Downhole Temperature Sensors (DTS)

Downhole temperature sensing technology is a direct measurement diagnostic tool capable of detecting small temperature variations along a wellbore. Previously used to determine fluid placement in acidizing treatments and monitor flow in comingled reservoirs, DTS is an emerging technology in the field of fracture diagnostics (Cipolla and Wright, 2000).

The conventional way to monitor fractured wells is through production and temperature logs. These are capable of generating a production and temperature profiles

during a shut-in period before or after fracturing. Different from conventional temperature logs, DTS is permanently installed on the wellbore and enables the observation of a dynamic temperature profile along the well without stopping production and for extended periods of time. For reservoir characterization and monitoring purposes, prolonged and continuous real-time temperature measurements are more beneficial than the snapshots a traditional temperature logging tool can provide.

DTS is able to capture temperature measurements along the well via fiber optic. First, a pulsed laser sources sends a pulse of light down the optical fiber and the properties of the returning light are then recorded (Sierra et al, 2008). The returning light, also known as "backscatter", includes the absorption and retransmission of light energy. The different spectral components that comprise the backscattered light are Rayleigh, Brillouin, and Raman bands. The latter ones are able to collect temperature information transmitted in the optical fiber since its two components, Stokes and Anti-Stokes, are influenced by temperature. The relative intensities between these two components are a function of temperature at which the backscattering occurred (Sierra et al, 2008) . By tracking the arrival time of the reflected and backscattered light, the location where the light originated is then determined. This location is referred as a sample point. A DTS profile is developed by combining a set of temperature measurements or sample points, equally spaced along the fiber length. **Fig. 1.1** illustrates these concepts.

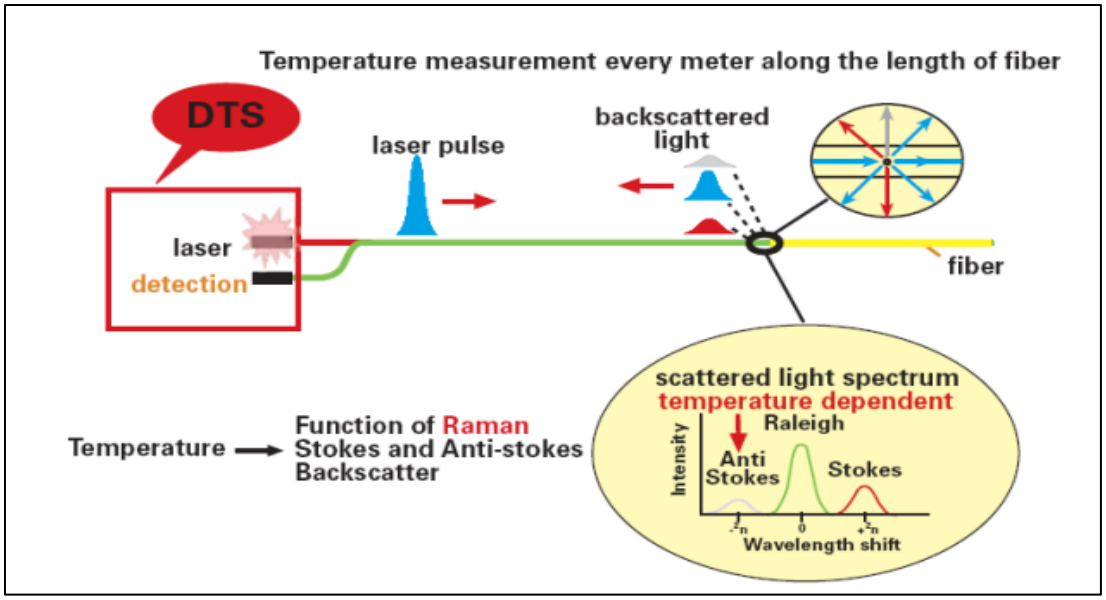

Fig. 1.1—Raman-based distributed temperature sensing concept (Sierra et al, 2008)

1.2.3.2 Installation and Deployment

The installation of DTS varies depending on its application. Flow profiling, fluid placement and fracture diagnostic applications share the same DTS analysis techniques however, the way in which the data is collected may vary for each case. A downhole cable that houses an optical fiber is required in order to carry out any monitoring application using DTS. The difference lies in the deployment and positioning of the housing cable in the wellbore. Some installations place the cable directly in the flow path while other deployment methods secure the cable to the outside of casing or production tubing (Sierra et al, 2008). When interested in monitoring HFT's, the best method for deployment is probably strapping the housing cable to the outside of the production casing. The limitation is that production casing needs to run back to the surface. An alternative to this issue is liner lap installations but these have not been successfully

tested in the field yet (Sierra et al, 2008). An additional concern is perforating with the cable running across the pay zone. Various completion designs are already being implemented in order to avoid perforating the fiber optic-cable. These techniques include oriented perforating, sliding sleeves, tubing conveyed perorating (TCP) guns ran outside the casing, and hydraulically controlled casing valves (Sierra et al, 2008). **Fig.** 1.2 shows a schematic of a DTS cable for both installation configurations.

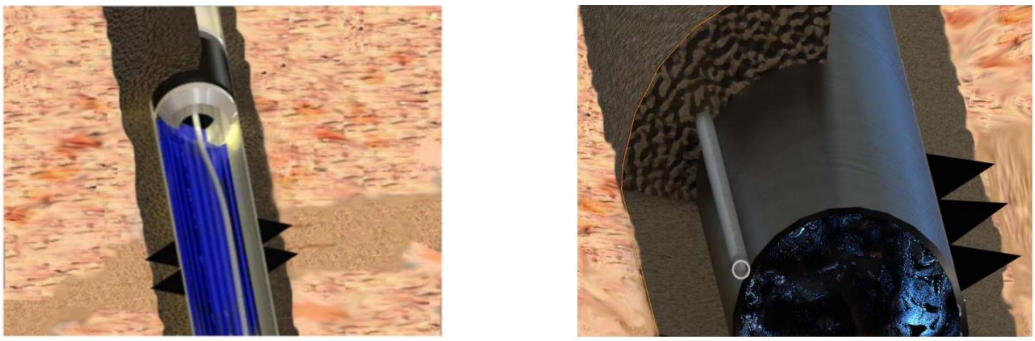

In flow path **Behind casing**

Fig. 1.2—Installation of fiber optic cable housing DTS: in flow path (left) and behind casing (right).

The deployment and installation of DTS is definitely an important factor to consider when selecting well monitoring tools. Complications during the installation/completion phase tend to deter operators in selecting DTS however, many operators have successfully figured out how to best install this tool and use it for a variety of applications in fields across the globe(Sierra et al, 2008). The next big challenge is to learn how to use DTS data more effectively, surpass the qualitative benchmark and reach more quantitative results. Special data assimilation techniques, along with today's

computational power, enable the proper handling of collected measurements and estimation of more accurate fracture parameters. Data assimilation techniques will be discussed in the next subsection.

1.2.4 Inverse Theory

An inverse problem is defined as the determination of plausible values of model parameters given inexact (uncertain) data and an assumed theoretical model that relates the observed data to the model (Oliver et al, 2008).In this context, a theoretical model is an approximation to the true physical relation between physical and/or geometric properties of the reservoir and state variables. In petroleum sciences, a reservoir simulator holds these relationships and it is capable of generating reservoir performance predictions based on input model parameters.

In this study, the observed measurements are a combination of production data and most importantly temperature data collected via DTS. The goal is to estimate fracture parameters using a combination of data sets. The approach to solve the inverse problem is founded on a Bayesian viewpoint of probability and assumes that some information on model parameters is available. This prior information could be a simple estimate of reservoir permeability or in this case a range of possible fracture half-length values. In order to have a mathematically manageable inverse problem, the prior information needs to be expressed as a prior probability density function (PDF). The objective is to modify this PDF using prior information of some model parameters, inexact measurements of some observable parameters and the relation between the observed data and model

parameters. This modified PDF is referred to as the a posteriori probability density function. The construction of the same is in a sense the solution to the inverse problem.

Many techniques can be used in order to generate the final PDF that would estimate the parameters in question. When selecting a particular data assimilation technique, one must consider the type of data is being collected and the level of linearity between the model and the data. In petroleum engineering, the dynamical relationships for flow and temperature in porous media are highly non-linear. These non-linearities complicate further the inverse problem and hence eliminate a number of techniques non-suitable to handle such complexities.

In the context of this work, a useful data assimilation techniquewould be one capable of sequentially filter and enforce constraints at each integration step, ensuring that the resulting estimations are representative of the conditional PDF.The sequential EnKF is a suitable technique for applications to such non-linear assimilation problems and is, by nature, an appropriate approach for monitoring.

1.2.4.1 Ensemble Kalman Filter (ENKF)

The Ensemble Kalman filter is an adaptation of the simpler Kalman filter for non-linear problems. The Kalman filter is an efficient recursive filter that estimates the state of a linear dynamical system from a series of noisy measurements (Aanonsen et al, 2009). The Kalman filter is founded on a model equation, where the current state of the system is associated with an uncertainty expressed by a covariance matrix(Aanonsen et al,

2009), and an observation equation that relates the state variable to the measurements through a linear relationship.

The Kalman filter method consists of two sequential steps: (1) forecast and (2)analysis. In the forecast stage, the model equation is used to compute a forward step with the current estimate of the state as initial condition. In the analysis stage, the measured data is assimilated and used to condition the preliminary estimate. The updated state of the system is computed by adding the estimate computed in step (1) to the product of the Kalman gain and the difference between the observed data and model prediction. The Kalman gain is obtained through a series of matrix calculations involving the covariance matrix of the states and observed data. The issue often lies in this particular step given that the covariance matrix for reservoir flow problems is typically very large and computationally expensive for history matching purposes.

Alternatively, the EnKF overcomes several limitations of the Kalman filter, particularly the need to linearize the dynamical equations or the relationship between the state variable and the data (Oliver et al, 2008) and the need to compute and update the estimate of the covariance matrix. These factors make the EnKF a suitable method for very large models.

Similar to the Kalman filter, the EnKF consists of two sequential stages. The EnKF starts with an ensemble of N_e initial models (usually 40-100 ensembles) which are used to generate a forecast forward in time of the dynamical equations of flow in porous media (f_t). The second step is the data assimilation step where the variables describing the state of the system (m) are updated to honor the measurements (Oliver et al, 2008).

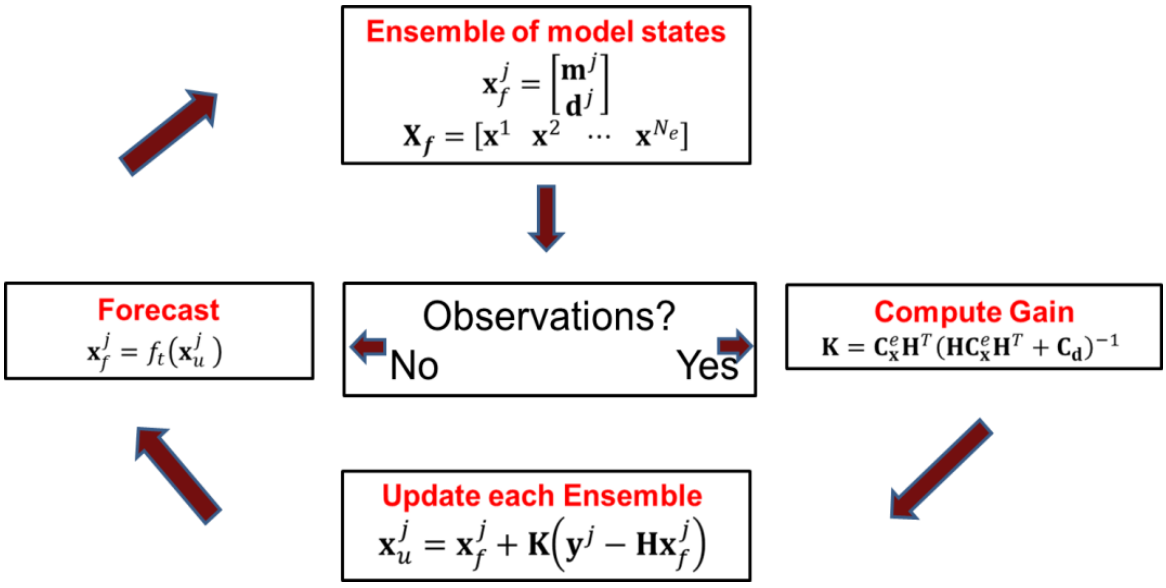

Fig. 1.3—Flow chart of EnKF's implementation. Here m is defined as the model states and parameters, while d represents simulated measurement.

In petroleum reservoir applications, the determination of the current state of the system is as important as the determination of model parameter values such as permeability and porosity. In a sense, the determination of model variables has more relevance since the determination of these variables is sufficient to demine the state of the system. In hydraulically fractured reservoirs, operators today are interested not only on characterizing the formation but also the induced hydraulic fractures. Information collected via DTS is already being used to describe qualitative aspects of HFTs however; the implementation of the EnKF in the assimilation of DTS data will enable this technology to have more quantitative applications. By determining accurate estimates of fracture geometrical parameters, operators are able to verify or correct the models used to develop a particular field and thus optimize the productive and economic life of wells.

2. NON-ISOTHERMAL RESERVOIR MODELING

2.1 Shale-Gas Reservoir Model

The complex nature of hydraulic-fracture growth in shale-gas reservoirs, along with the implementation of horizontal completions ,has made reservoir numerical simulation the preferred method when evaluating and/or predicting well performance(Cipolla et al, 2010).

Several semi analytical and analytical solutions for hydraulically fractured horizontal wells have been proposed. However, these have difficulties capturing the long transient behavior of shale's matrix blocks caused by their very low permeability(Cipolla et al, 2010). Other methods combine these solutions to numerical reservoir simulators with the goal of reducing computing time, but again, they lack the ability to model transient flow in the matrix blocks. Due to these issues, gridding the entire reservoir discretely (fracture network, hydraulic fracture, matrix blocks) though rigorous and computationally expensive, is the most accurate way to generate reservoir performance predictions.

In this study, reservoirs were modeled using a commercial reservoir simulator ECLIPSE (Bequest, S., 2010). Local grid refining (LGR) is used to represent the propped fracture's width. When modeled, fracture width is in fact orders of magnitude larger than the actual propped width. To this end, fracture permeability is calibrated accordingly as to preserve fracture conductivity values. In addition, the spacing perpendicular to the length of the propped fracture is logarithmic. Previous work by

Cipolla et al (2010)showed the effectiveness of using logarithmically spaced LGR rather than using very-fine-grid that would enable to represent actual fracture width.**Fig**. 2.1shows Cipolla et al (2010)comparison of flowing bottomhole pressure (BHP) behavior with this grid design versus a very finely gridded single porosity reference model as well as Gringarten's infinity conductivity type curve solutions.

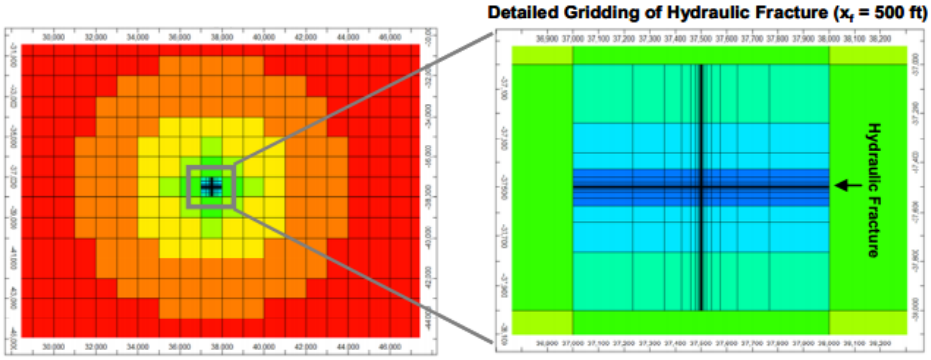

a) Detailed gridding of hydraulic fracture using Local Grid Refinement.

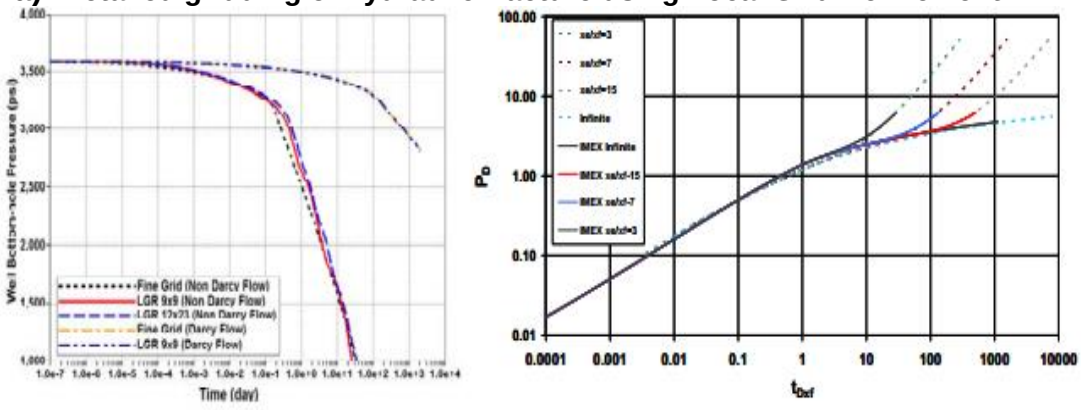

b) Flowing bottomhole pressure comparison between Figure 3-a grid design and a very-finely gridded single porosity reference model (left) and Gringarten's infinity conductivity type curve analytical solution.

Fig. 2.1—Comparison between LGR grid and very-finely grid design (Cipolla et al, 2010).

In this work, the LGR scheme divided the fracture blocks in 9 local gridblocks in the y direction and 7 local gridblocks in the z direction. In the $x$direction, the number of local gridblocks is obtained through a relationship 4 $\frac{xf}{D_X}$where x_f is fracture half-length and D_X is the gridblock size in the X direction. **Fig.** 2.3 shows an example of the LGR design used in this study to model hydraulic fractures.

In addition to the main hydraulic fractures, a network of secondary fractures is created in the vicinity of the induced primary fractures. This network can be expressed as an enhanced permeability area (EPA). The EPA is defined depending on fracture spacing and geometry, and it takes permeability values smaller than the primary fracture values and higher than the matrix block. A schematic of the reservoir and wellbore geometry with its corresponding stimulated reservoir volume is presented in **Fig. 2.2**.

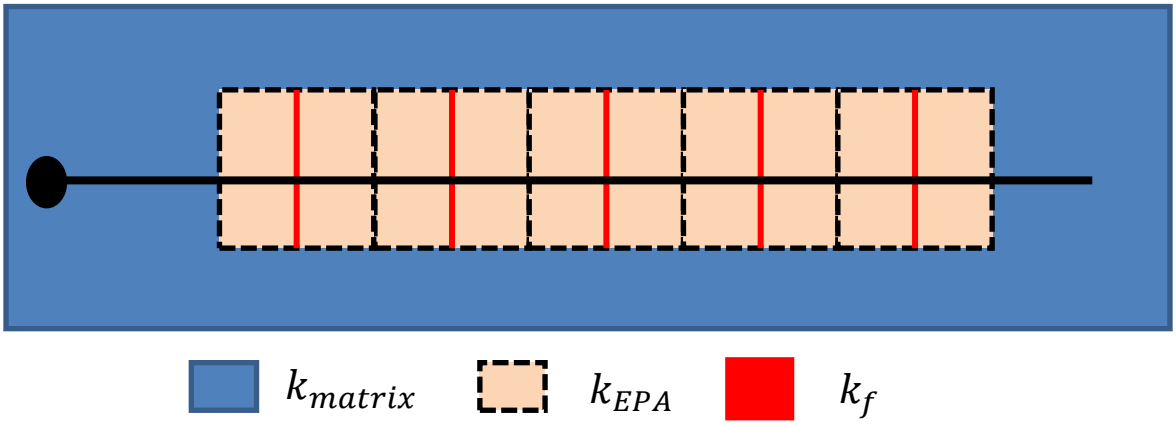

Fig. 2.2—Schematic of reservoir and wellbore geometry illustrating the different permeability zones.

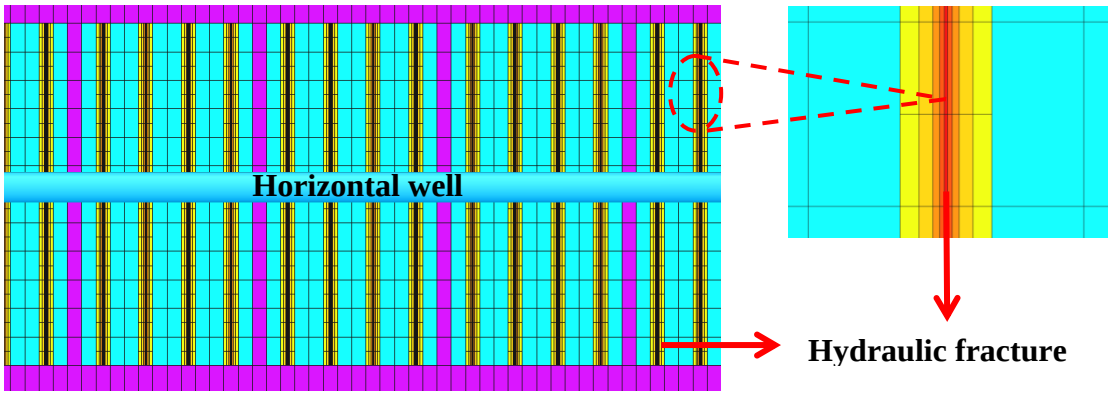

Fig. 2.3—Example of LGR scheme used to model hydraulic fractures.

2.2 Non-Isothermal Reservoir Model

A commercial reservoir simulator is used in order to simulate a shale gas reservoir's pressure and temperature responses. ECLIPSE(GeoQuest, S., 2010) reservoir simulator (E300 along with temperature option) by Schlumberger is used to construct a non-isothermal forward reservoir model that generates temperature readings as outputs. The model is executed with both, ECLIPSE 100 as a blackoil model and ECLIPSE 300 as a compositional model. Accuracy is significantly improved by running the simulation in ECLIPSE 300 where bothflow and energy conservation equations are calculated and solved simultaneously (coupled pressure and temperature equations). The improved accuracy is associated with additional computational time.

2.2.1 Reservoir Flow Model

The continuity equation for a multi-phase system is defined as follows,

$$\frac{\partial(\phi\, \rho_\alpha\, S_\alpha)}{\partial t} = -\nabla.(\rho_\alpha \boldsymbol{u}_\alpha) + q_\alpha, \qquad \alpha = w, o, g \quad \text{..... (2.1)}$$

where α represents all phases present in the reservoir, ϕ porosity, ρ phase density, S phase saturation, $\boldsymbol{u}$ Darcy velocity and q represents sink/source terms from injection or production wells respectively. Each phase has its own Darcy velocity $\boldsymbol{u}_\alpha$ and mass flow rate q_α. For a 3D two-phase flow system with gravitational force, the Darcy velocity term takes the following form,

$$\boldsymbol{u}_\alpha = -\frac{1}{\mu_\alpha} k_j \left(\nabla p_j - \rho_j \, g \, \nabla Z\right) \qquad j = w, o, g \quad \text{..... (2.2)}$$

In a fluid-porous medium, multiphase flow causes all phases to interact with each other. This results in a decrease of the effective permeability, $k_{r\alpha}$, which is related to the absolute permeability, $\boldsymbol{k}$, as follows,

$$\boldsymbol{k_\alpha} = k_{r\alpha}\boldsymbol{k} \qquad j = w, o, g \quad \text{..... (2.3)}$$

Finally, since phases are considered completely immiscible, the multi-phase flow equation in porous medium is defined as,

$$\frac{\partial\left(\phi \, \rho_j \, S_j\right)}{\partial t} = \nabla . \left(\frac{1}{\mu_j} \boldsymbol{k}_j \left(\nabla p_j - \rho_j \, g \, \nabla Z\right)\right) + q_j$$

$$S_o + S_w + S_g = 1, \; j = w, o, g \quad \text{..... (2.4)}$$

The relationships presented above describe the elemental concepts of fluid flow in porous medium. For this study, these relationships are hold by a commercial reservoir simulator ECLIPSE (GeoQuest, S., 2010) that solves for reservoir state parameters (e.g. pressure, saturation, temperature) in discrete time steps by dividing the reservoir model into discrete grid blocks, given some initial and boundary conditions.

When considering non-isothermal effects, a specialized version of ECLIPSE is implemented. ECLIPSE 300 (GeoQuest, S., 2010) enables the modelling of thermal

effects in the reservoir by solving both flow and energy conservation equations. Energy conservation equations are presented in the next sub-section.

2.2.2 Reservoir Thermal Model

In this study, DTS data will be assimilated with the objective of characterizing reservoir and fracture parameters. For this reason, thermal effects in the reservoir need to be considered, despite being disregarded in most petroleum reservoir applications.

The thermal behavior of a reservoir is accurately explained in the work developed byLi et al (2010). These relationships are implemented in ECLIPSE 300 and enable temperature modelling by simultaneously solving flow and energy conservation equations.

For a given reservoir volume V, energy is conserved as follows (Lake, 2010):

$$\begin{Bmatrix}\text{Accumulation}\\ \text{rate of energy}\\ \text{in V}\end{Bmatrix} = \begin{Bmatrix}\text{Net rate of}\\ \text{energy transport}\\ \text{into V}\end{Bmatrix} + \begin{Bmatrix}\text{Rate of}\\ \text{energy production}\\ \text{in V}\end{Bmatrix} \quad \text{..... (2.5)}$$

The energy accumulation term in the control volume V, without considering kinetic energy changes, can be expressed as

$$\begin{Bmatrix}\text{Energy}\\ \text{accumulation}\\ \text{in V}\end{Bmatrix} = \left[\phi \sum_{j=1}^{N_p} \rho_j S_j \left(U_j + gD\right) + (1-\phi)\rho_s U_s\right]_t^{t+dt} V \quad \text{..... (2.6)}$$

where the subscript j denotes the fluid phase, s is the solid rock, U is the internal energy, and D is the depth. Here ϕ, S_j and g have the same definition as in the flow equations.

Next, the energy transport in the reservoir occurs either by heat convection or conduction. These are expressed as follows:

$$\left\{\begin{matrix}\text{Energy transport}\\ \text{convection}\end{matrix}\right\} = \sum_{j=1}^{N_p} \rho_j \boldsymbol{u}_j \left(H_j + gD\right) A \quad \text{..... (2.7)}$$

$$\left\{\begin{matrix}\text{Energy transport}\\ \text{conduction}\end{matrix}\right\} = \left(-K_{T_t} \nabla T\right) A \quad \text{..... (2.8)}$$

where H is the enthalpy of fluid, K_{T_t} is the total heat conductivity and A is the surface area of the control volume V.

When an injecting or producing well is present in the reservoir, heat transfer between the reservoir and the wellbore occurs. This phenomenon is represented as $\dot{Q}$ in the energy balance equation, and represents the heat transfer term per unit time per unit area.

$$\dot{Q} = -K_{Tt} \frac{\partial T}{\partial r}|_{r=rw} + \sum_{j=1}^{N_p} \rho_j \boldsymbol{u}_j C_{p,j} \left(T_i - T_w\right) \quad \text{..... (2.9)}$$

The first terms in Eq. 2.9represents the heat conduction between wellbore and formation, while the second term denotes the heat convection of the same. In the heat convection term, $C_{p,j}$ is the heat capacity of the phase j , T_i is the reservoir temperature at the contact betweenreservoir and wellbore (also known as arriving temperature) while T_w is the wellbore flowingtemperature. Combining all terms and ignoring any energy production on the control volume V, the energy balance expression is obtained by combining Eq. 2.6 through Eq.2.9 into Eq.2.5:

$$\frac{d}{dt}\left[\, \phi \sum_{j=1}^{N_p} \rho_j S_j \left(U_j + gD\right) + (1-\phi)\rho_s U_s V \,\right] = \nabla \cdot \left[\sum_{j=1}^{N_p} \rho_j \boldsymbol{u}_j \left(H_j + gD\right) A \,\right] - \nabla \cdot \left(K_{T_t} \nabla T\right) \quad \text{..... (2.10)}$$

Further expansion of this expression is possible if enthalpy, thermal expansion coefficient and internal energy are defined. These terms are expressed as

$$dH = C_p\, dT + \frac{1}{\rho}(1 - \beta\, T)dp \quad \text{..... (2.11)}$$

$$\beta = -\frac{1}{\rho}\left(\frac{\partial p}{\partial T}\right)_p = \frac{1}{V}\left(\frac{\partial p}{\partial T}\right)_p \quad \text{..... (2.12)}$$

$$U = H - \frac{p}{\rho} \quad \text{..... (2.13)}$$

In addition, the internal energy of the formation rock is defined as,

$$dU_s \approx C_{p,s}\, dT \quad \text{..... (2.14)}$$

These definitions enable the energy balance equation to be expressed in terms of reservoir temperature. Combining Eq.2.10 through Eq.2.14 into Eq.2.10, the following expression for energy conservation is obtained:

$$-[\sum_{j=1}^{N_p} \phi\, \rho_j S_j C_{p,j} + (1-\phi)\rho_s C_{p,j}\,]\frac{dT}{dt} + \sum_{j=1}^{N_p} \phi\, S_j \beta_j\, T \frac{dp_j}{dt} = \sum_{j=1}^{N_p} \phi\, \rho_j \boldsymbol{u}_j C_{p,j}\, \nabla T -$$

$$\nabla \cdot \left(K_{T_t} \nabla T\right) + \sum_{j=1}^{N_p} \left(\boldsymbol{u}_j \cdot \nabla p_j\right) - \sum_{j=1}^{N_p} \beta_j T \left(\boldsymbol{u}_j \cdot \nabla p_j\right) + \sum_{j=1}^{N_p} p_j \boldsymbol{u}_j \nabla(gD) \quad \text{..... (2.15)}$$

The terms on the left hand side of the equation are the accumulation term and thermal expansion due to pressure change with respect to time respectively. On the right side, the first element denotes the change in temperature due to convection, the second one represents the change in temperature due to conduction, the third term describes viscous dissipation heating, the fourth one denotes the thermal expansion caused by pressure change in space, while the fifth one represents the contribution of elevation effects.

In the next subsection, synthetic reservoirs will be modeled using ECLIPSE300 to study the thermal behavior of shale gas formations when hydraulically fractured. The

findings of this preliminary assessment will contribute to the calibration of the model that will be used to history match field data.

2.3 Synthetic Models

Based on the aforementioned modeling techniques, synthetic examples are simulated in order to study the temperature behavior of ultra-tight gas reservoirs with induced multiple transverse fractures. Two base cases are used in order to study the effect of different fracture parameters on the reservoir's temperature response. The first case is a horizontal well with homogenous fractures while the second one has heterogeneous fractures. The first part of this exercise sets both cases to produce under constant rate. Next, the effect of the fracture network around primary hydraulic fracture (represented by an EPA) is studied under both production conditions.

Note that this study does not consider wellbore temperature due to the lack of a wellbore thermal model. The arriving temperature, T_i, is the closest parameter to the wellbore temperature, T_w, since it is in fact the temperature at the wellbore-reservoir contact(Yoshida et al, 2013). In this study, the temperature of gridblocks containing a wellbore section will serve as the arriving temperature.

2.3.1 Input Parameters

The ultimate goal of this work is to history match production field data from a horizontal gas well in the Marcellus shale. For this reason, the parameters used in these synthetic

cases attempt to resemble properties commonly found in this formation. Reservoir geometrical properties, along with fluid/thermal and rock properties are specified next.

2.3.1.1 Reservoir Geometrical Properties

A "box-shaped" rectangular shape is assumed for the reservoir**(Table 2.1).** Reservoir parameters are selected based on values commonly found in petroleum literature describing the Marcellus shale. Reservoir length and depth are determined based on relevant literature (Soeder, 1988) as well as field data.

Table 2.1 Reservoir geometrical properties.

Parameter	Description	Value [unit]
-	Reservoir Shape	Rectangular
L	Reservoir Length	3500 [ft]
h	Reservoir Thickness	90 [ft]
w	Reservoir Width	600 [ft]

2.3.1.2 Fluid Properties

Initial reservoir pressure and temperature **(Table 2.2)** need to be specified in order to determine fluid properties. These will change accordingly as the well starts producing and the reservoir starts depleting. The geothermal temperature gradient is approximated from real DTS data presented in Section 6. Fluid properties of gas are summarized in **Fig. 2.4**.

Table 2.2 Pressure and temperature data.		
Parameter	Description	Value [unit]
P_{res}	Initial reservoir pressure	6000 [psi]
$T_{R,ini}$	Initial reservoir temperature	115 [F]
T_G	Geothermal temperature gradient	0.02 [F/ft]

2.3.1.3 Rock Properties

Petrophysical and thermal properties of the rock **(Table 2.3)** are also obtained from relevant petroleum literature on the Marcellus shale (Soeder, 1988).

Table 2.3 Rock properties.		
Parameter	Description	Value [unit]
ρ_R	Matrix Density	148 [$\mathrm{lbm/ft^3}$]
ϕ	Matrix Porosity	8.0[%]
k_T	Thermal Conductivity	24 [Btu/ft/day/°R]
c_{p_R}	Rock Heat Capacity	30 [BTU/lbm F]

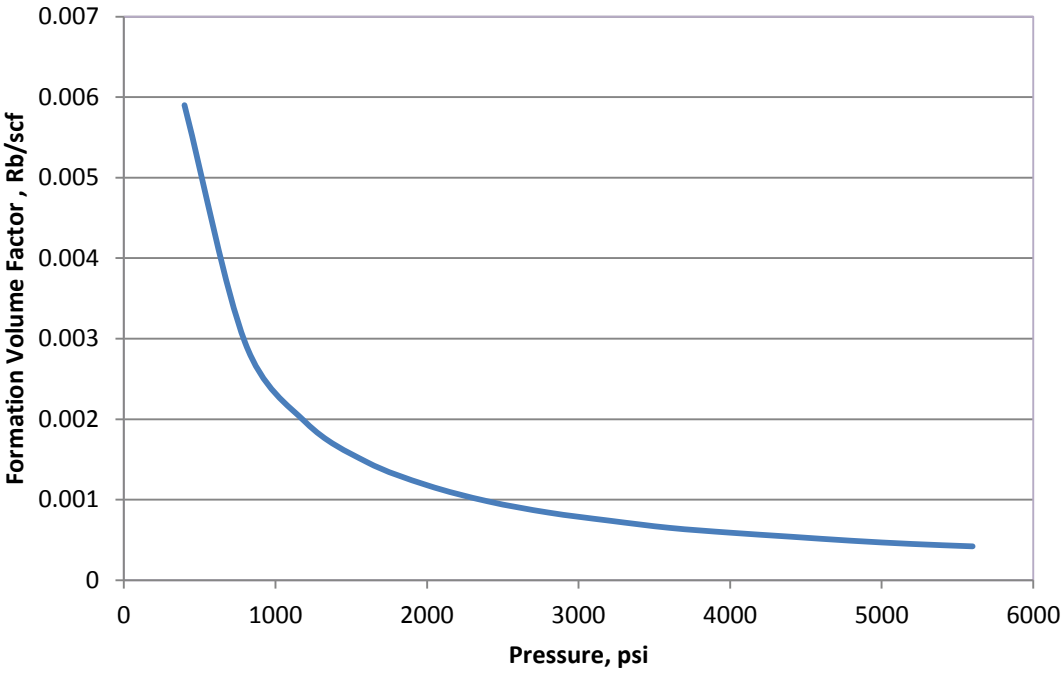

a) Gas formation volume factor

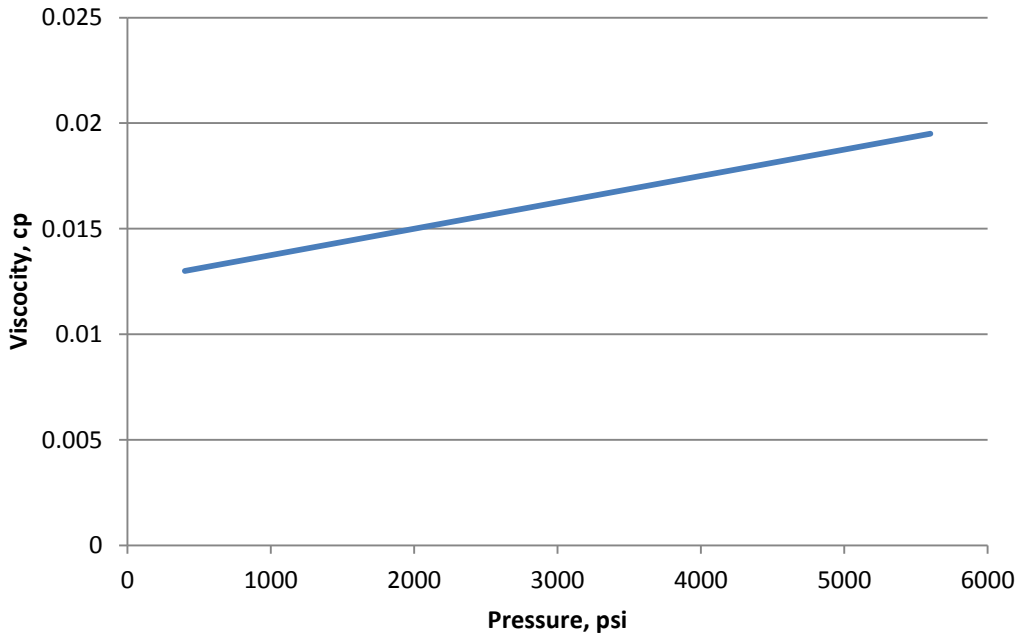

b) Gas viscosity

Fig. 2.4—Gas properties: formation volume factor and viscosity.

2.3.2 Forward Model

The number of hydraulic fractures for both case studies is five. In addition to fracture parameters, the effect of the area around the primary fractures is also studied. Rock and fracture properties used for the homogenous case are summarized in **Table 2.4** As specified before, for the first case study all fractures share the same properties. For the heterogeneous case, the parameters vary by a factor of 0.5, 1.5, 1, 2 and 0.25 at each fracture respectively. **Fig.** 2.5 shows a schematic of the reservoir geometry as well as a cross section of the horizontal well with its corresponding fractures and SRV.

Table 2.4 Rock and hydraulic fracture parameters

Parameter	Description	Value [unit]
k_{matrix}	Matrix permeability	10^{-4} [md]
k_{EPA}	EPA permeability	0.005 [md]
k_f	Fracture permeability	500 [md]
ϕ_{matrix}	Matrix porosity	0.08[%]
ϕ_{EPA}	EPA porosity	0.081 [%]
ϕ_f	Fracture porosity	0.33 [%]
x_f	Fracture half length	150[ft]
h_f	Fracture height	90[ft]

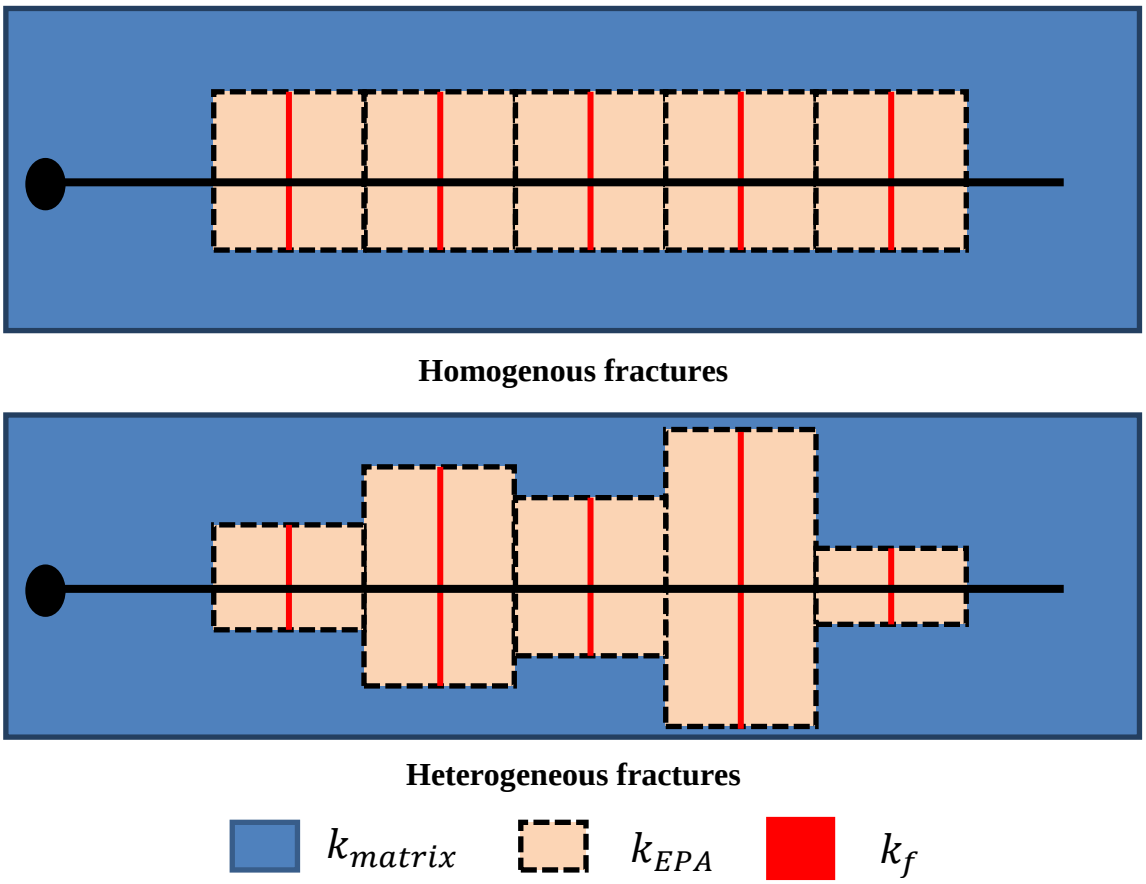

Fig. 2.5—Schematic of reservoir-fracture configuration for homogenous (top) and heterogeneous case (bottom).

2.4 Results

2.4.1 Homogenous Hydraulic Fractures

A horizontal well with five identical transverse hydraulic fractures is simulated using the parameters specified in **Table 2.4**. This well is under production for 30 days at a rate of 500Mscf/day. **Fig. 2.6** through **Fig. 2.7** show the resulting arriving temperature, pressure and inflow distribution along the wellbore after 30 days.

The reservoir temperature at the well level is shown in **Fig. 2.6**. The lowest temperature reading is identified at the gridblock where the fracture is located making the fracture location very noticeable. This substantial drop in temperature is caused by pressure variations in the reservoir, making the temperature of the incoming reservoir fluid a lot cooler than the original reservoir temperature.

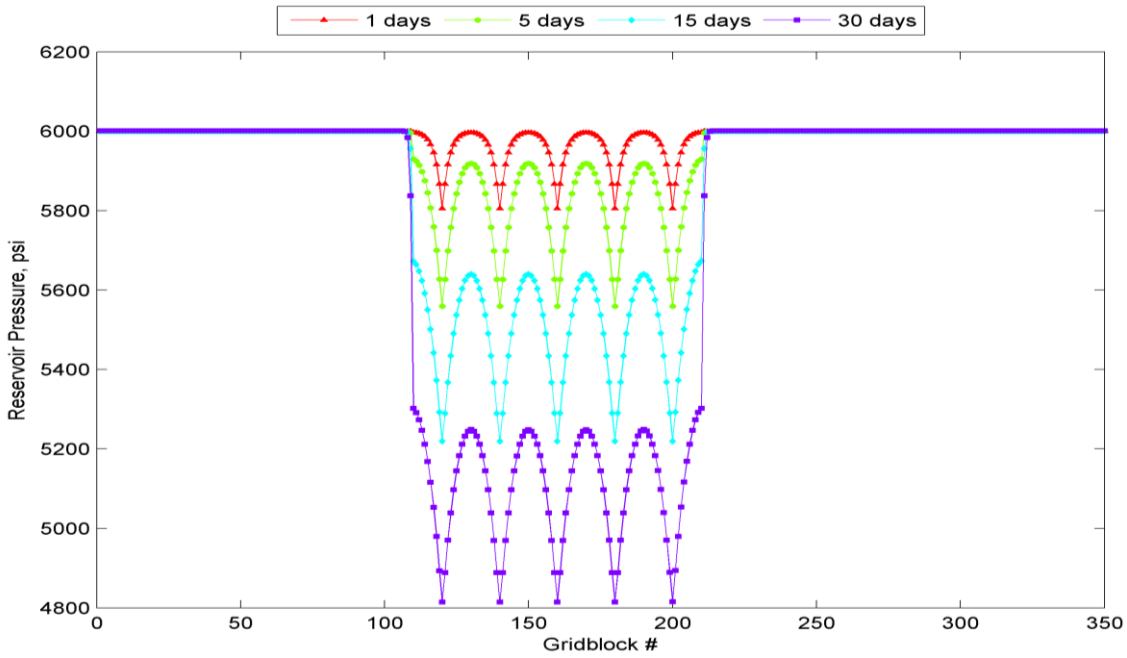

Fig. 2.6—Pressure distribution (Homogenous fracture case, constant rate).

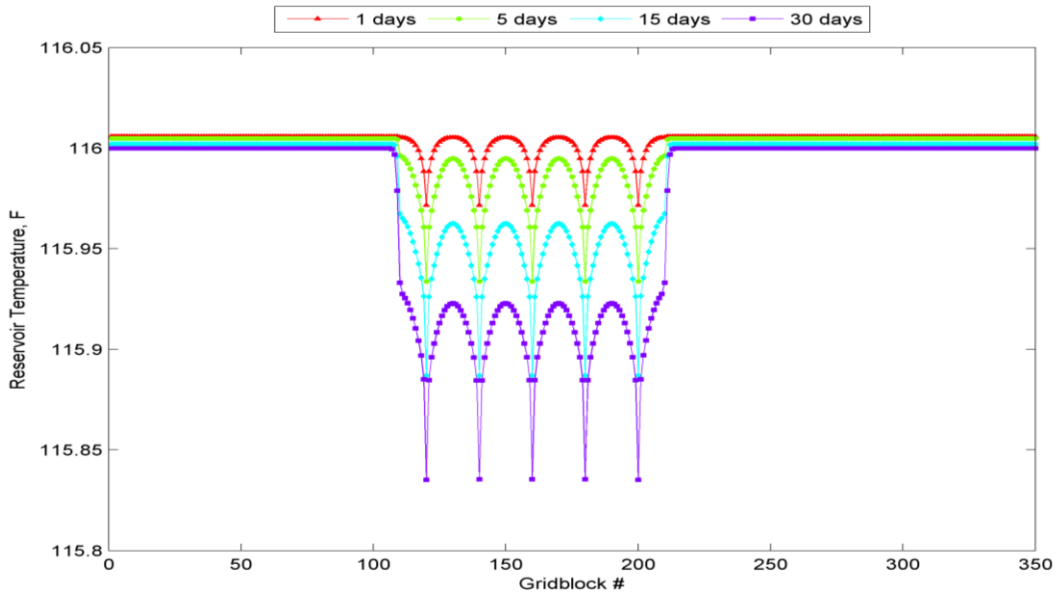

Fig. 2.6—Temperature distribution (Homogenous fracture case, constant rate).

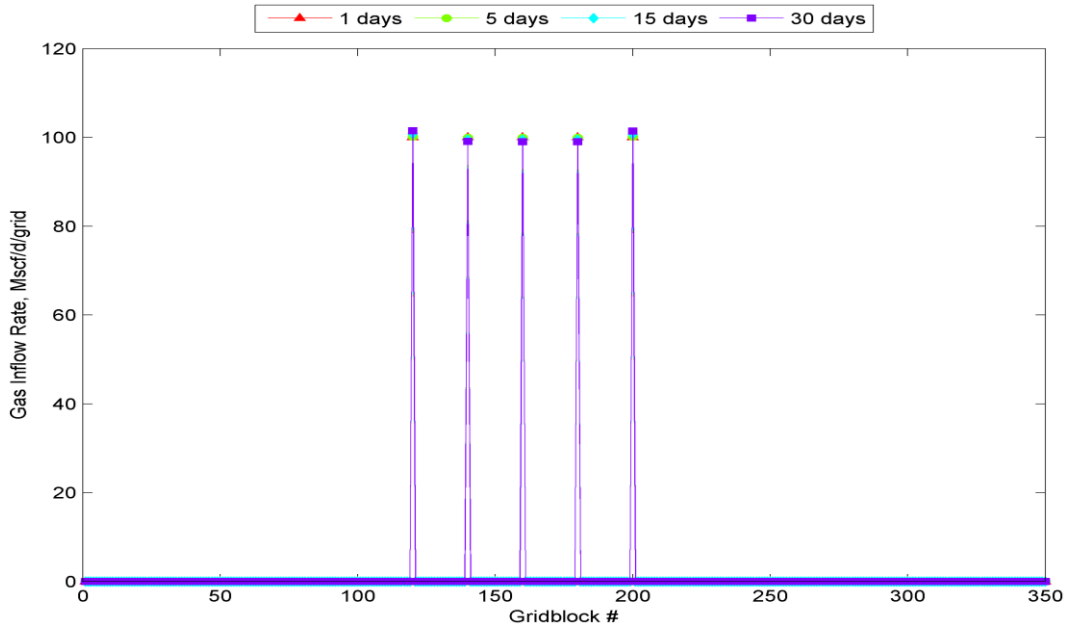

Fig. 2.7—Gas inflow rate. (Homogenous fracture case, constant rate).

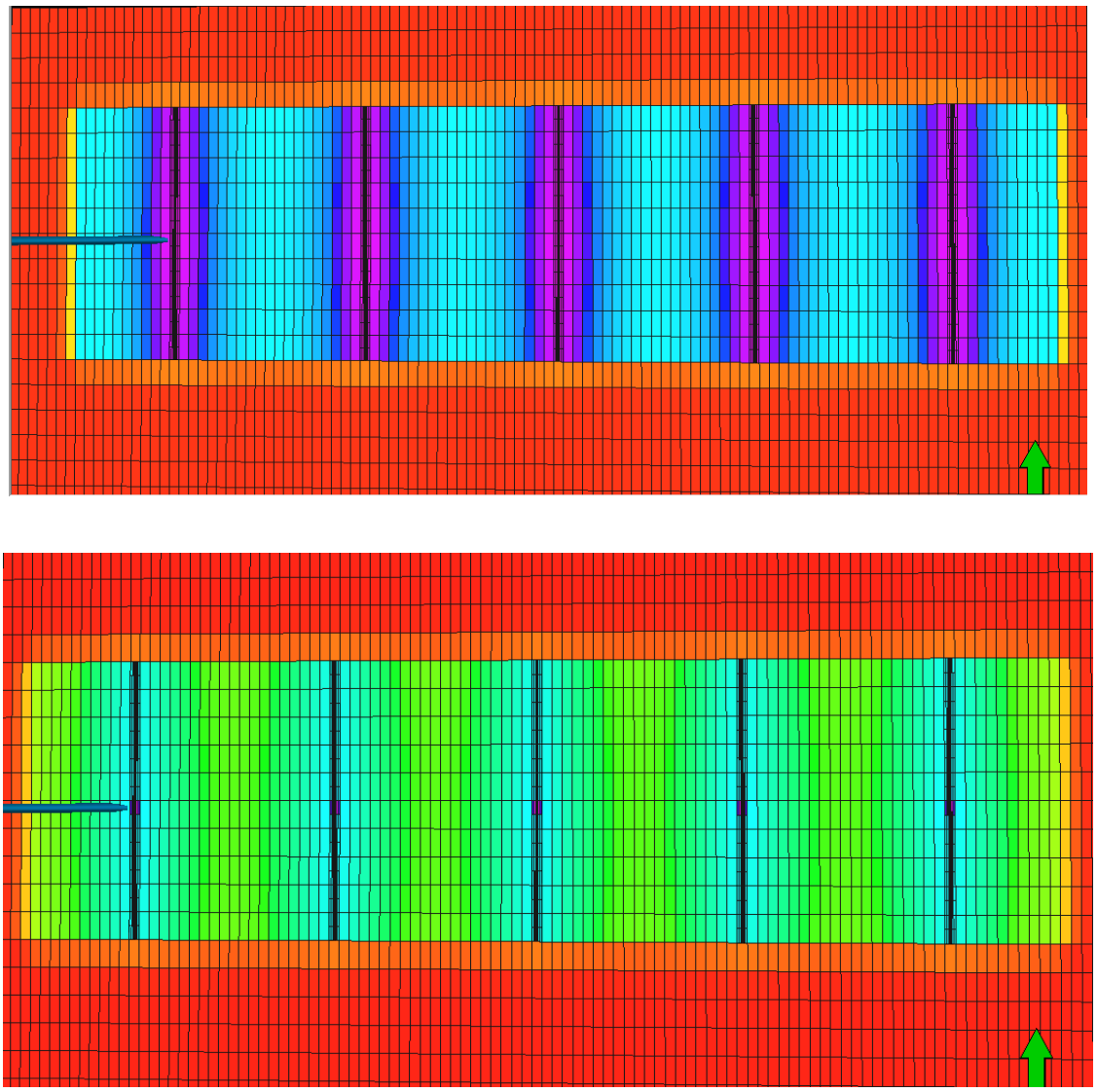

Fig. 2.8—Pressure and temperature distribution (Homogenous fracture case, constant rate, t= 30 days)

2.4.1.1 Heterogeneous Hydraulic Fractures

Next, different parameter values are assigned to each hydraulic fracture in the reservoir model. For each fracture, original parameters are varied by a factor of 0.5, 1.5, 1, 2 and 0.25 respectively. In this way, a horizontal well with five different fractures is simulated in order to assess the effect of fracture heterogeneity in both pressure and temperature distribution.

As in the homogenous case, the cooling effect at the fracture location is very noticeable however; the increase/decrease of parameters' values causes the temperature difference to vary as well. **Fig. 2.9** through **Fig. 2.11** shows the resulting arriving temperature, pressure and inflow distribution along the wellbore.

According to **Fig. 2.11**, the distribution of gas inflow rate corresponds to the level of heterogeneity of the fractures. Fractures with higher fracture properties have a greater gas inflow. In addition, points of higher inflow rate also correspond to points of greater temperature drop.

From these results, it is observed that when pressure change is similar across fractures, the inflow gas rate is in fact the determinant factor in the temperature behavior. From Eq.2.15, it is observed that the convection and viscous dissipation terms depend on gas flow rate. Based on **Fig. 2.10** and **Fig. 2.11** the cooling effect caused by convective heat transfer becomes predominant when pressure behavior across fractures is similar yet differences in gas inflow rate exist.

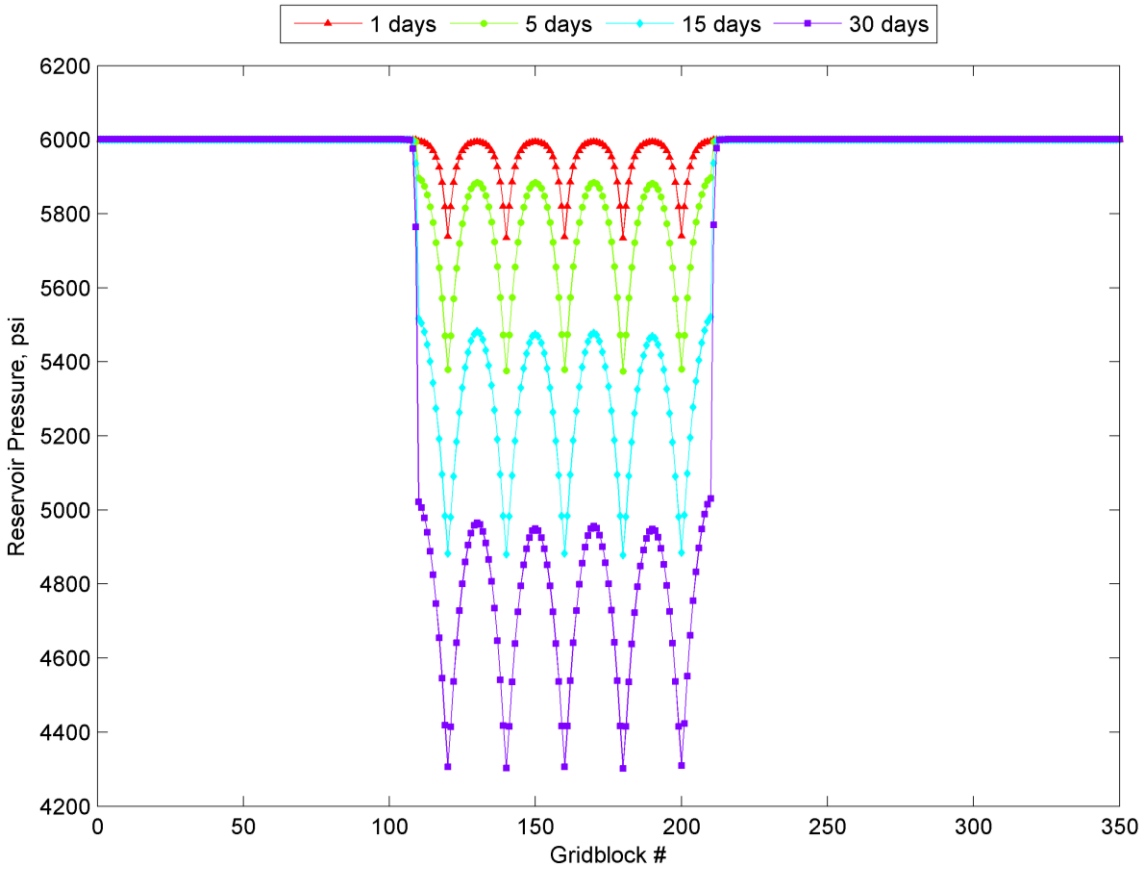

Fig. 2.9—Pressure distribution (Heterogeneous fractures case, constant rate).

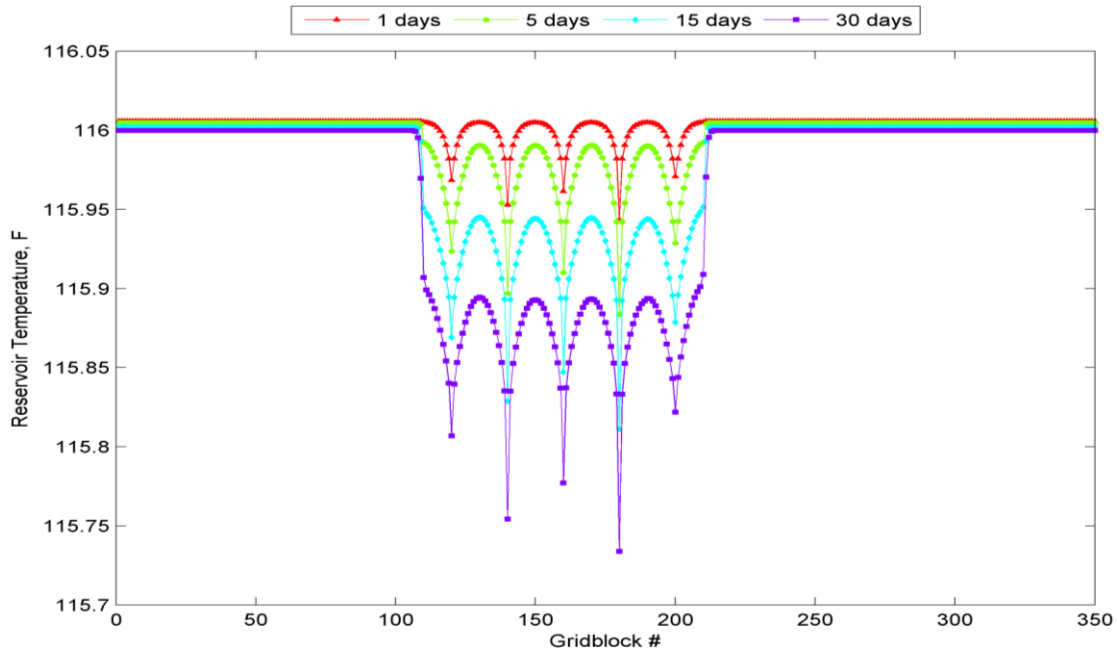

Fig. 2.10—Temperature distribution (Heterogeneous fractures case, constant rate).

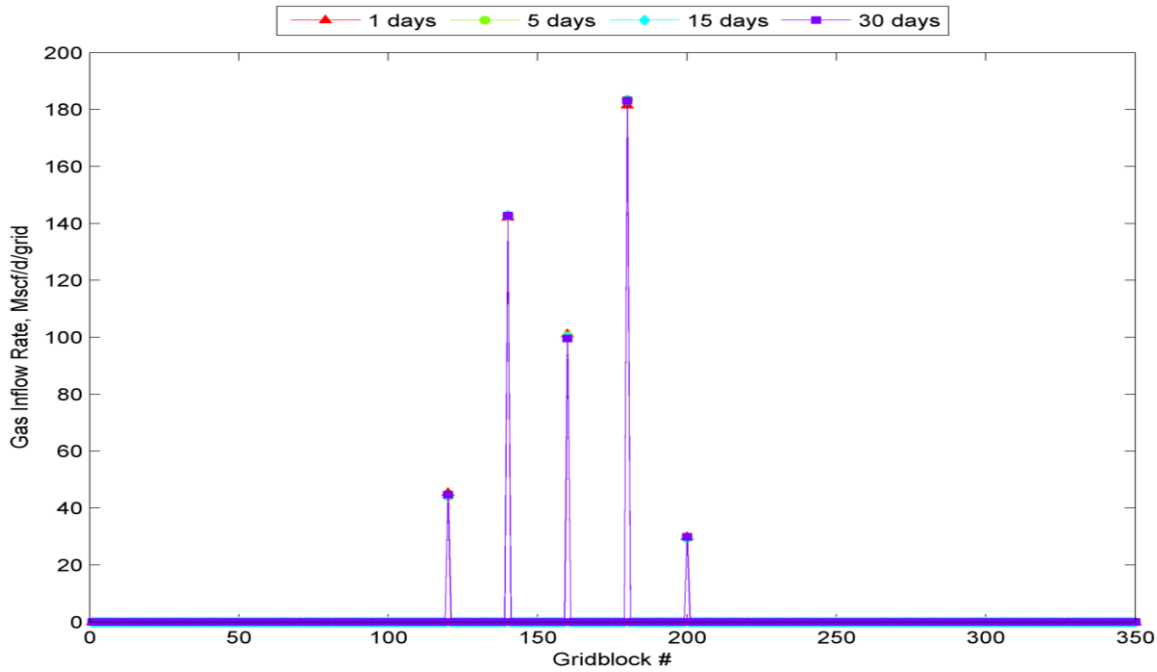

Fig. 2.11—Gas inflow rate distribution (Heterogeneous fractures case, constant rate).

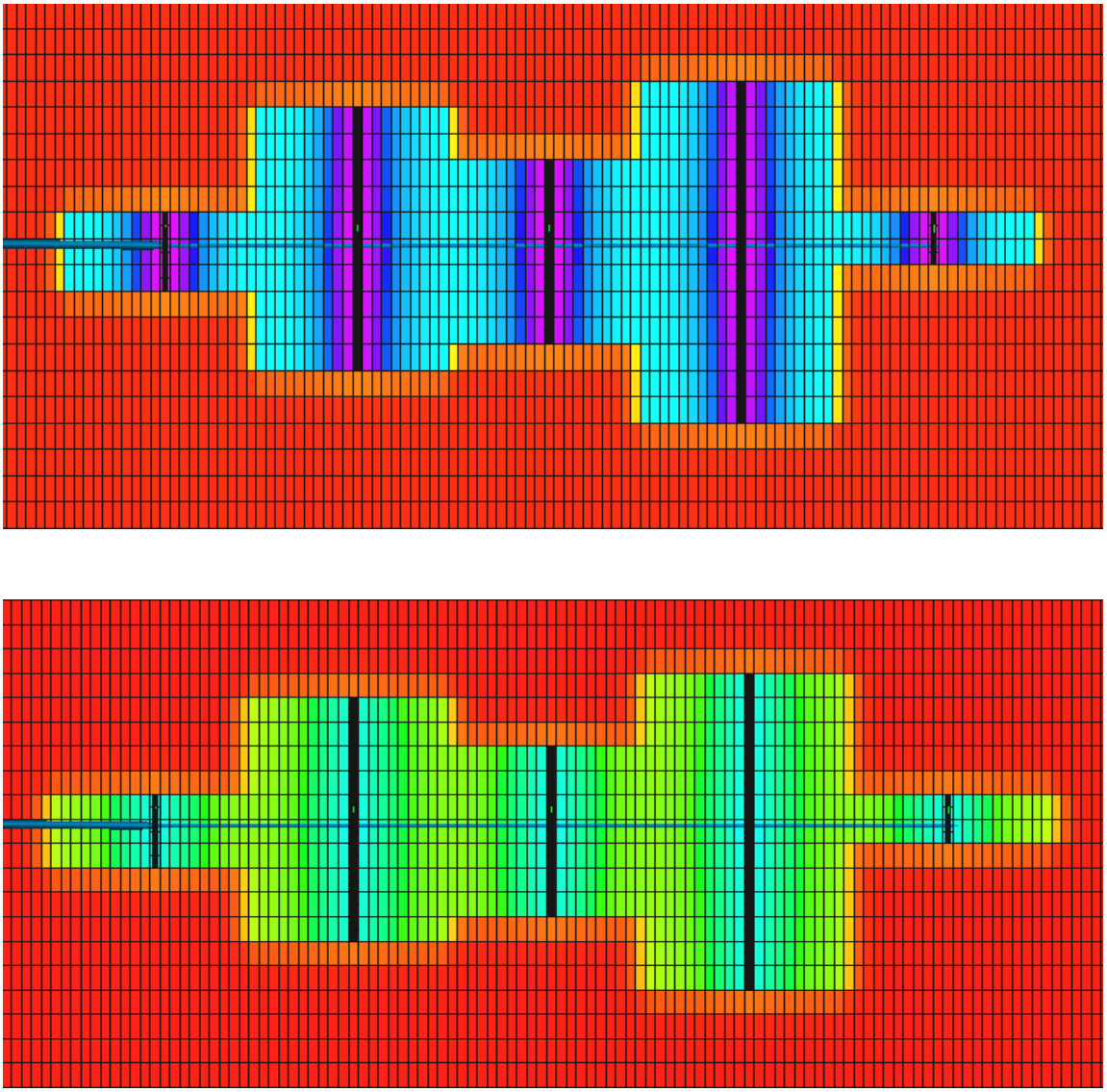

Fig. 2.12—Pressure and temperature distribution (Heterogeneous fracture case, constant rate, t= 30 days).

2.5 Effect of Fracture Networks

The stimulated area around the primary fractures can be represented through a network of secondary fractures. In this study, such network is modeled as an area with an

enhanced permeability. This network plays an important role on the pressure and temperature distribution around the primary hydraulic fractures.

Two cases are analyzed, one with a complete fracture network and one with a reduced network. In both cases, hydraulic fractures are homogeneous. **Fig. 2.14** shows a schematic of the two case studies. In addition, both case studies are set to flow under constant rate and constant BHP.

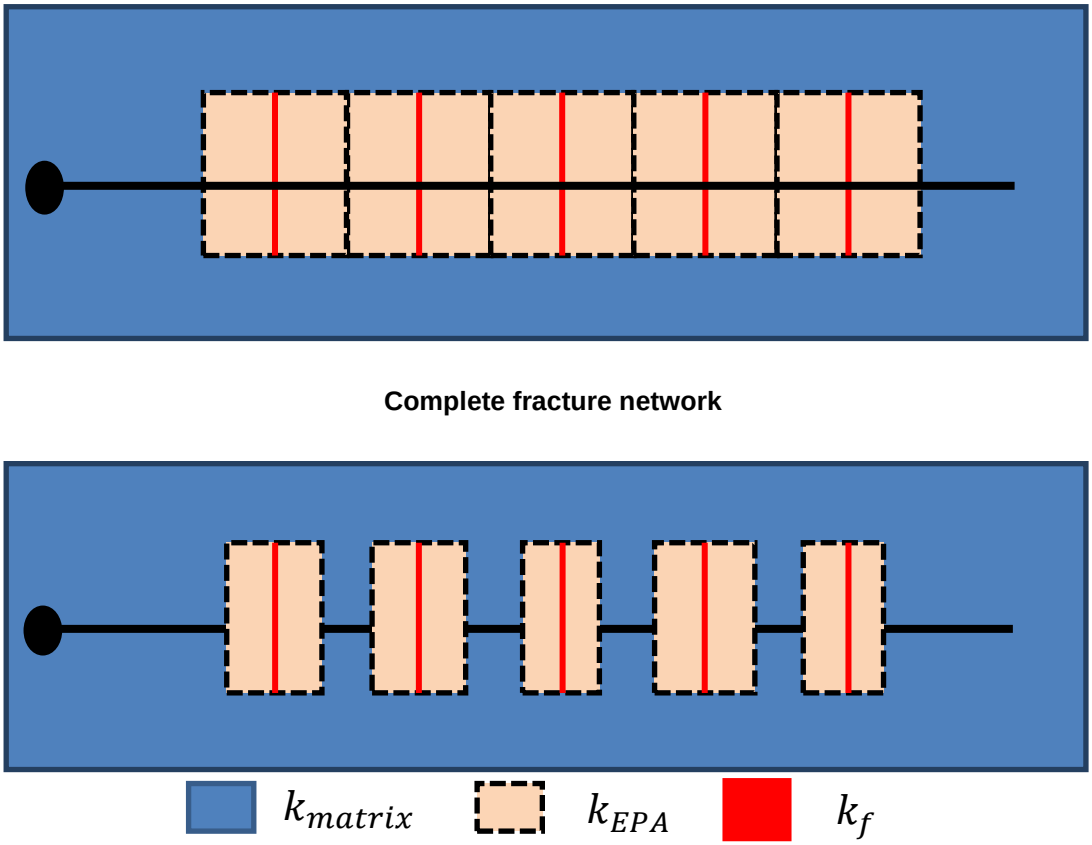

Fig. 2.13—Schematic of hydraulic fractures with complete (top) and reduced fractured network (bottom).

2.5.1 Network Effect Under Constant Rate Production

Reducing the fracture network has noticeable effects on the pressure and temperature distribution. **Fig. 2.15** through **Fig. 2.16** show pressure, temperature and inflow gas rate of the full fracture network and reduced fracture network case. Both cases are bounded to a $\mathbf{500\ Mscf/day}$ production rate for 30 days. In addition, both configurations are plotted on the same scale in order to highlight differences in the absence of a fracture network.

Fig. 2.14 shows the pressure response for both cases. The pressure behavior between the two cases is substantially different. The reservoir with a reduced fracture network experiences a greater pressure drop. With less stimulated area, the well has difficulty reaching the established production rate and thus more pressure drawdown is required. The additional pressure drops translates into a greater gas expansion cooling effect and subsequently into a higher temperature drop (see **Fig. 2.15**). Finally, Fig. 2.16 shows the corresponding gas inflow distribution at each perforation.

Having to produce $500\ Mscf/day$ for 30 days, each fracture is supposed to produce approximately$100\ Mscf/day$; however, the reduced fracture network case is not able to maintain this production level for 30 days straight. A lower gas rate has an effect in the cooling caused by convective heat transfer. In this case, however, the gas expansion cooling effect (caused by the high pressure drop) is the predominant heat transfer mechanism and the temperature drop is not heavily affected by the reduction in flow rate.

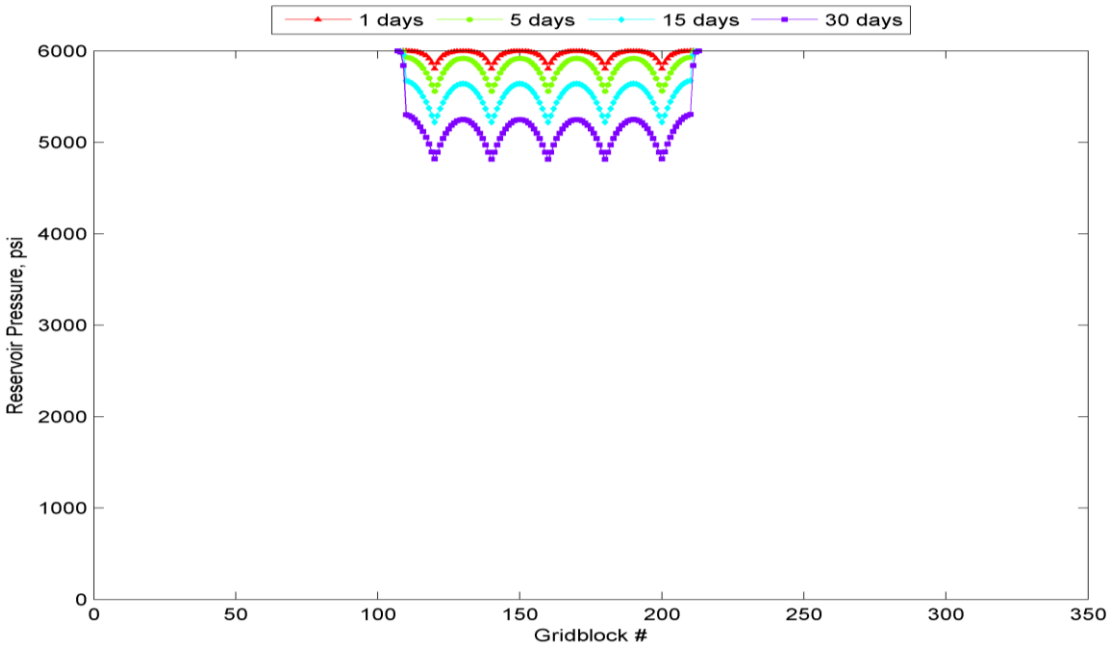

Fig. 2.14—Pressure distribution of hydraulically fractured reservoir with complete and reduced fracture network. (Homogenous fractures, constant rate production).

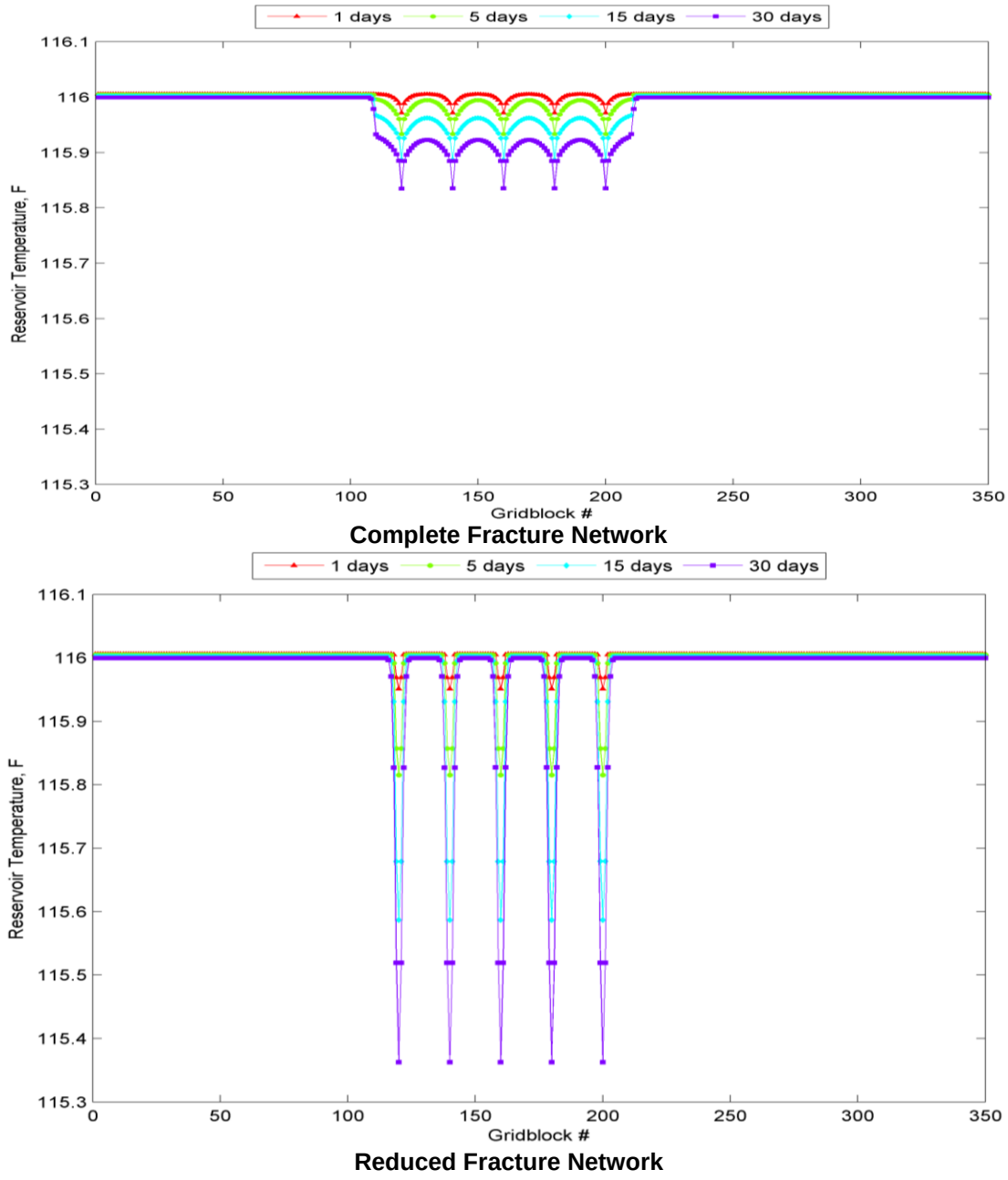

Fig. 2.15—Temperature distribution of hydraulically fractured reservoir with complete and reduced fracture network. (Homogenous fractures, constant rate production).

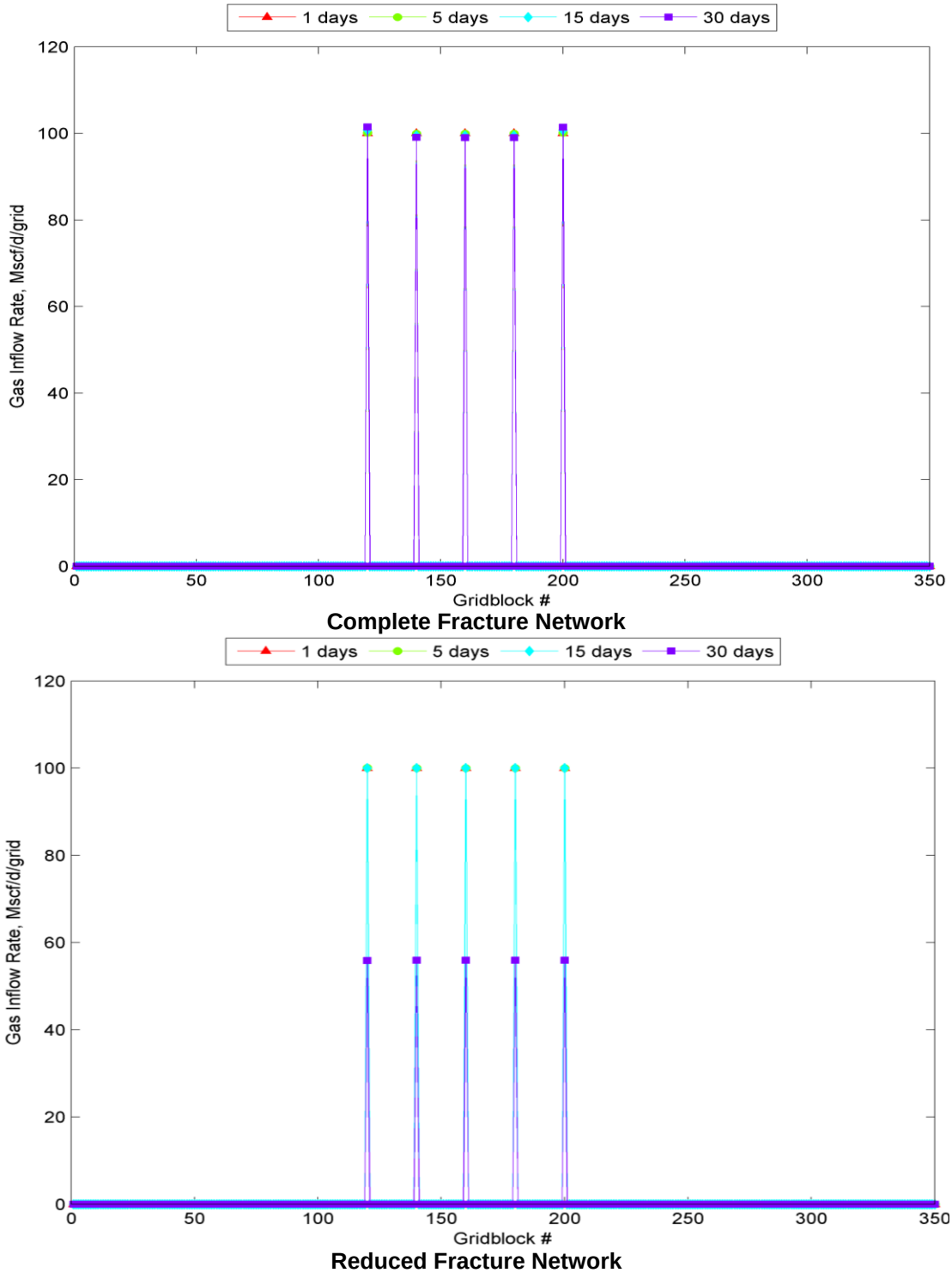

Fig. 2.16—Gas inflow rate of hydraulically fractured reservoir with complete and reduced fracture network. (Homogenous fractures, constant rate production).

2.5.2 Network Effect Under Constant BHP Production

Next, the constant production condition is changed to a constant BHP of 1000 psi. In the previous case, since the well was bounded to meet a specific rate, the contribution of the EPA was necessary in order to meet the established rate, and so the EPA was reduced rather than eliminated. For the constant BHP case, the EPA is completely eliminated in order to make any differences in pressure or temperature more noticeable. **Fig. 2.17** through **Fig. 2.19**show the pressure, temperature and inflow gas distribution of both fracture configurations.

The differences in pressure, temperature and flow rate are very noticeable between the two cases. When an EPA is present, opposite to the constant rate case, the reservoir experiences a greater temperature drop corresponding to a greater pressure drop and gas inflow. This is reflected in the difference in temperature drop shown in **Fig. 2.18.**

Without an EPA, the reservoir produces a very small amount of gas given that is harder to produce directly from the matrix blocks. As a results, the reservoir pressure changes abruptly only at the vicinity of the fracture, leaving the rest of reservoir almost unchanged.

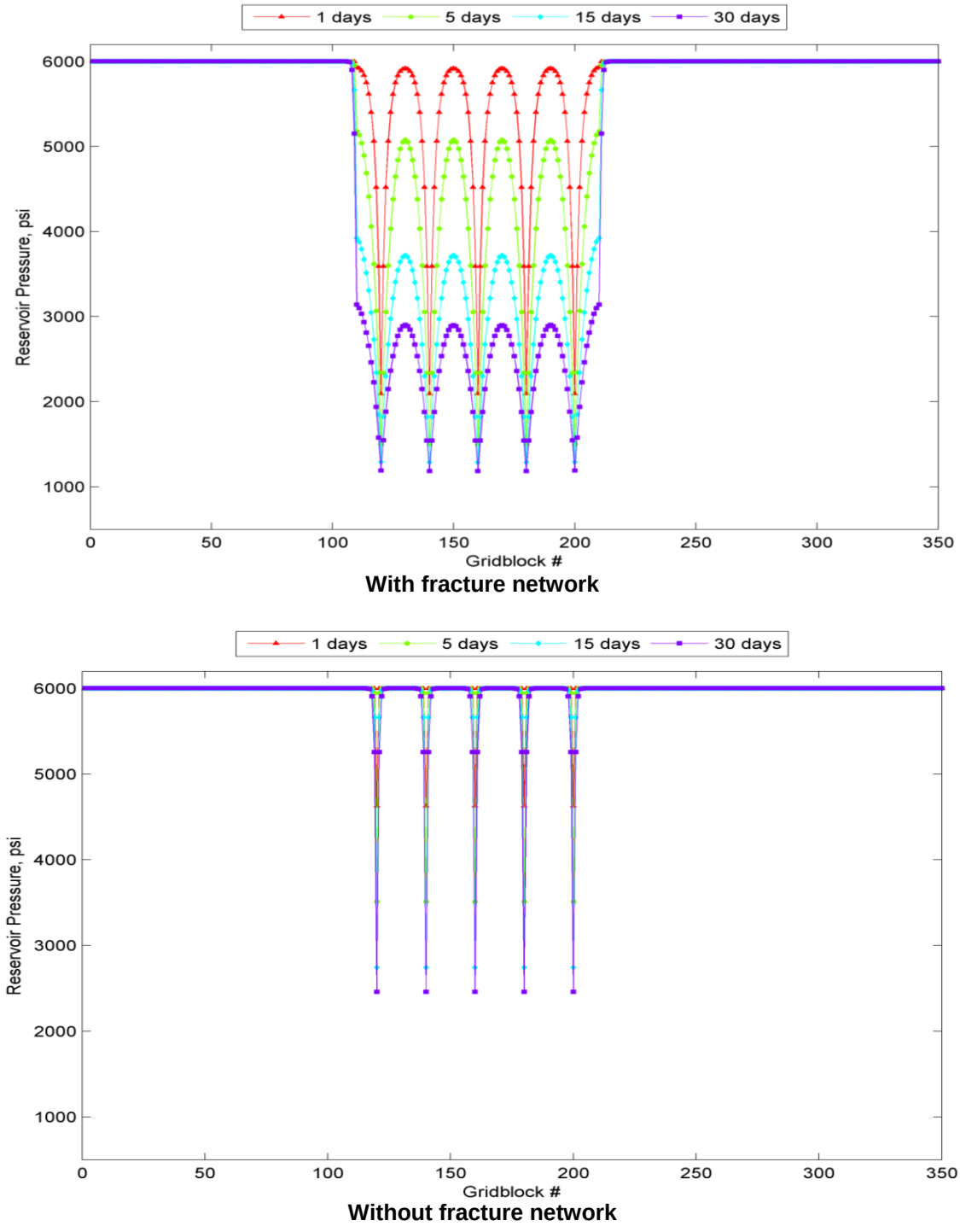

Fig. 2.17—Pressure distribution of hydraulically fractured reservoir with and without fracture network. (Homogenous fractures, constant BHP production).

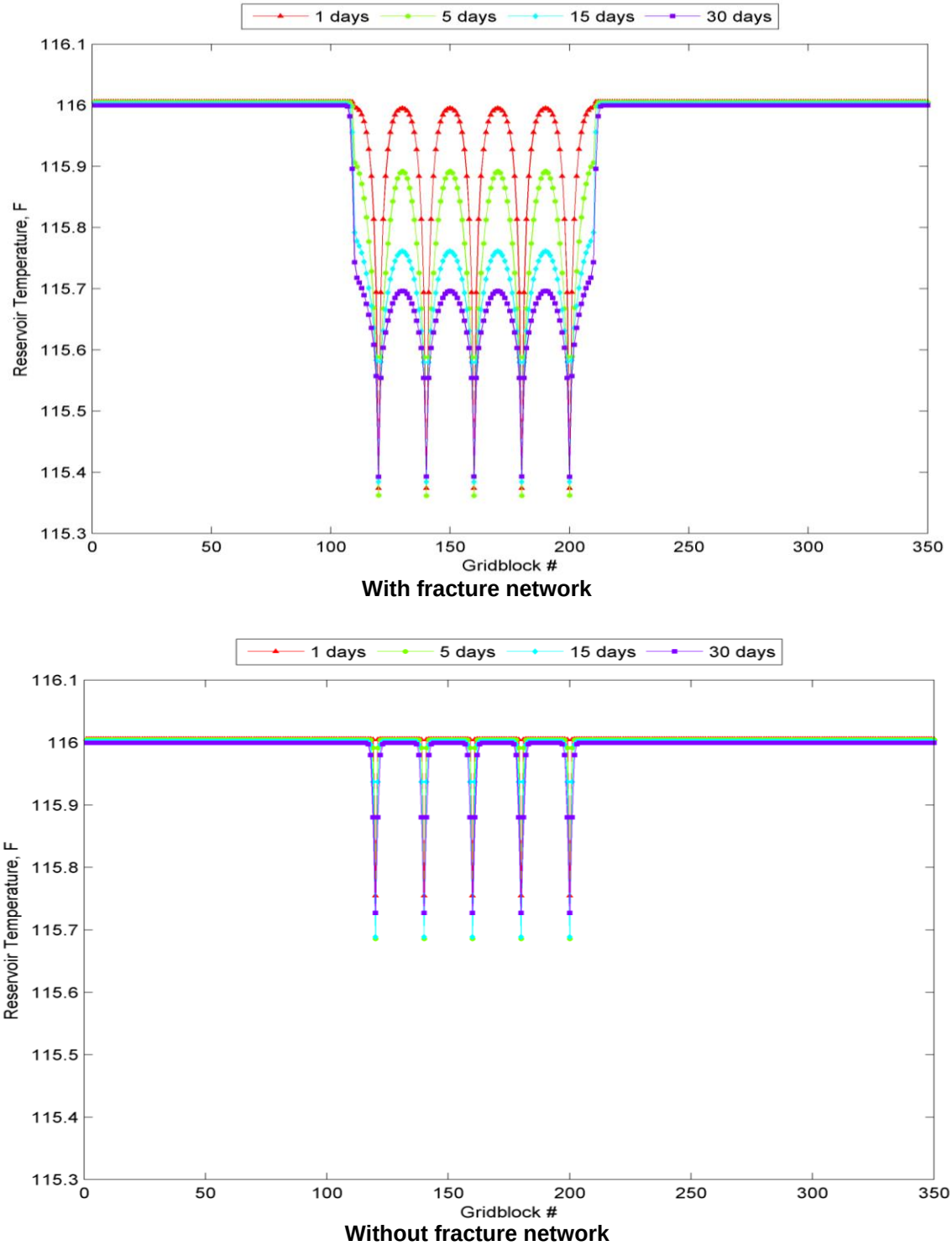

Fig. 2.18—Temperature distribution of hydraulically fractured reservoir with and without fracture network. (Homogenous fractures, constant BHP production).

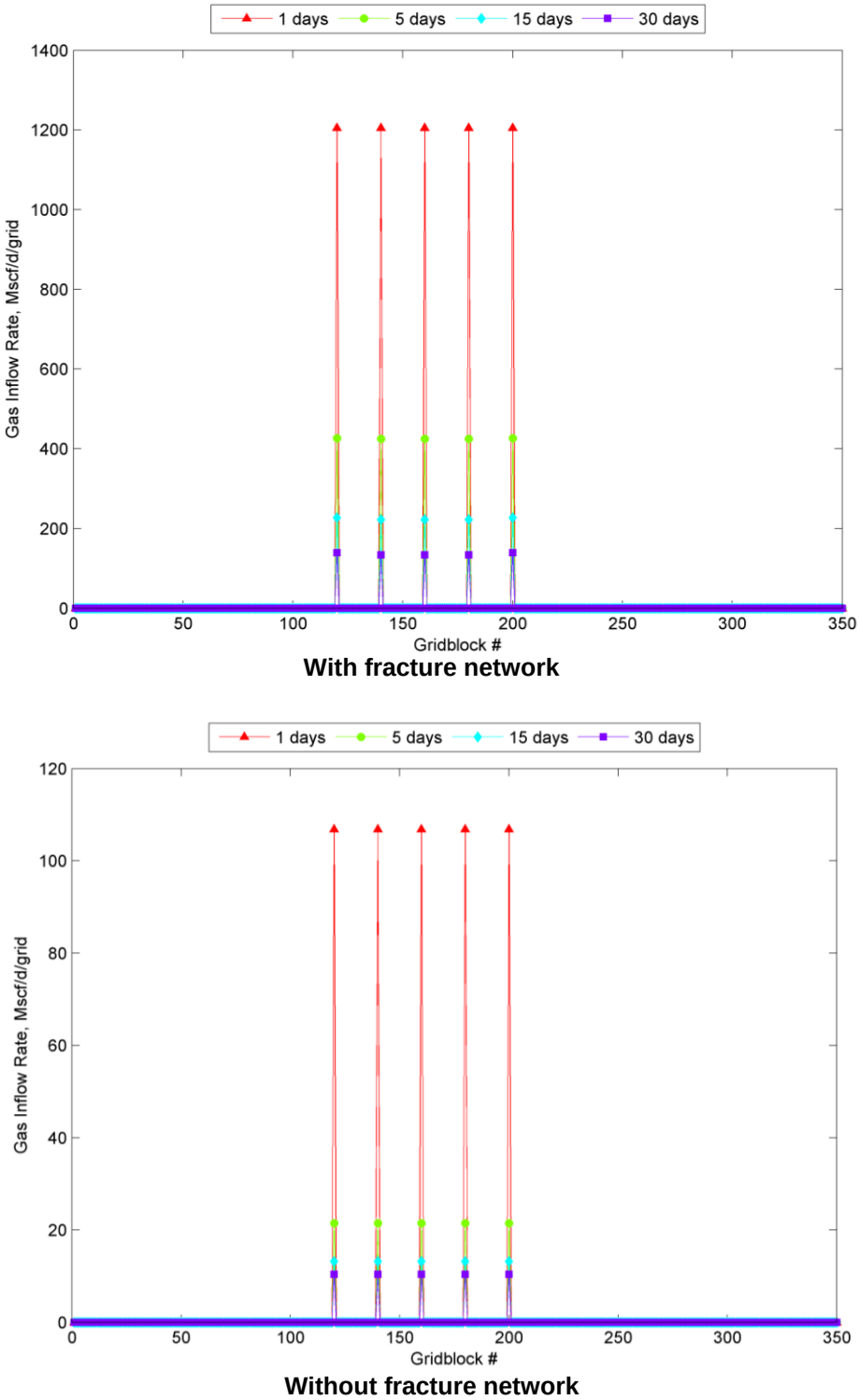

Fig. 2.19—Gas inflow rate of hydraulically fractured reservoir with and without fracture network. (Homogenous fractures, constant BHP production).

2.6 Discussion

From the results obtained in the previous synthetic cases, two predominant cooling mechanisms are identified: gas expansion and convective cooling effects. The gas expansion cooling effect is caused by the so called Joule-Thompson effect, JTE. This phenomenon describes the effect of a fluid subjected to a change in the pressure environment and the temperature change associated with this environment change (Reyes et al, 2011). Tight-gas wells produce with high drawdown pressure drop and the JTE can be noticed clearly, thus making gas wells excellent candidates to implement DTS technology. The second cooling mechanism is associated with the inflow rate through the fluid velocity terms specified in Eq. 2.13. Convective cooling effects depend on the velocity of the fluid and the heat capacity of the fluid phase.

A relevant conclusion from this assessment is the importance of accurately modelling the area around the primary hydraulic fracture. It was observed how the extension and the permeability of this area influenced the pressure response in the vicinity of the fracture. Under constant rate, the JTE proves to be the main cooling mechanism. A reduced EPA requires a high pressure drawdown to meet the established rate, which at points is not met since the BHP reaches its lower limit. A reduction in gas inflow is not sufficient however to diminish the cooling effect associated with the pressure variation. Under constant BHP, the presence of an EPA allows the drainage of additional reservoir volume, reducing the reservoir pressure significantly. In addition to the change in reservoir pressure, a higher inflow rate is experienced and more cooling is felt at the fracture location in comparison to the case with a reduced EPA.

After identifying the main heat transfer mechanisms, the next step is to determine which parameters affect these phenomena the most and quantify their effect on the thermal behavior of the reservoir. This is achieved through a sensitivity analysis which is carried out in the next section.

3. SENSITIVITY STUDY

3.1 Introduction

The previous chapter showed the effect of different model parameters on the reservoir's pressure and temperature response. In this section, a sensitivity analysis is performed in order to quantify and compare the effect each parameter has on the dynamics of the reservoir. The goal is to identify which parameters are more influential and use these results in the eventual implementation of the EnKF.

The parameters to be studied are fracture permeability, fracture porosity, fracture half-length, fracture height, EPA permeability, EPA porosity, reservoir permeability and reservoir porosity. A horizontal well with a single fracture will be modeled along with different EPA and fracture permeability configurations bounded to both constant production and constant BHP.

As described in Section 3, the main heat transfer mechanisms responsible for cooling effects are thermal expansion caused by pressure change along with convective heat transfer related to the inflow rate. Similarly, the inflow rate is also responsible for heating effects caused by viscous dissipation. The system is indeed a complex one and so the estimation of the sensitivity is complicated in an analytical sense. Due to the complexity of the system, both temperature drop and gas inflow rate are monitored in an attempt to better understand the reservoir's thermal behavior.

3.2 Procedure

A horizontal well with a single hydraulic fracture serves as the forward model. Furthermore, two reservoir fracture configurations will be used as base cases. One has a highly permeable EPA with a low permeability hydraulic fracture while the other one has a low permeable EPA with a highly permeable hydraulic fracture. In addition, the cases will be bounded to both a constant production rate of 250 Mscf/dayand a constant bottomhole pressure of 1000 psi.Fracture and reservoir parameters are varied by a factor of ± 45% and ±75 %. Five simulations will be run in total, including the base case which will be used as reference for comparison. **Fig 3.1** shows a schematic of how the sensitivity analysis is done for one parameter. The same procedure is carried out for all parameters specified in **Table 3.1.**

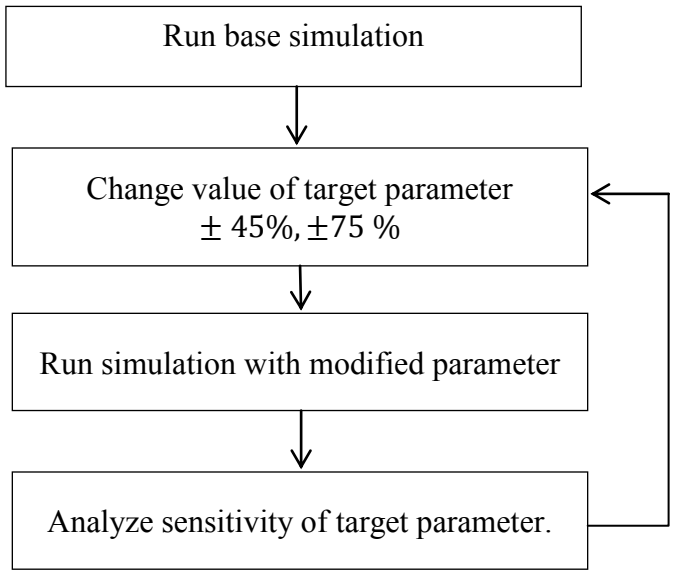

Fig. 3.1—Flow chart of sensitivity analysis.

Table 3.1 Parameters of base cases for sensitivity analysis.				
Parameter	Description	Units	Base Case 1 Low k_{EPA} - High k_f	Base Case 1 Low k_{EPA} - High k_f
k_{matrix}	Matrix permeability	[md]	10^{-4}	10^{-4}
k_{EPA}	EPA permeability	[md]	0.005	0.05
k_f	Fracture permeability	[md]	500	50
ϕ_{matrix}	Matrix porosity	[%]	0.08	0.08
ϕ_{EPA}	EPA porosity	[%]	0.081	0.081
ϕ_{EPA}	Fracture porosity	[%]	0.33	0.33
x_f	Fracture half length	[ft]	150	150
h_f	Fracture height	[ft]	90	90

3.3 Sensitivity Analysis Results

3.3.1 Constant Rate – Case I: Low Permeability EPA/ High Permeability Fracture

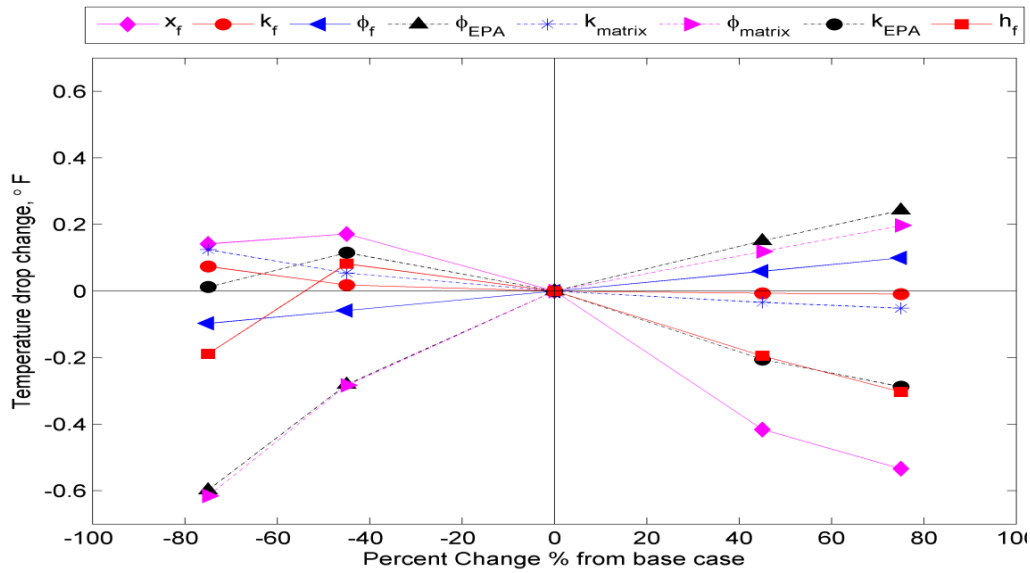

Fig. 3.2—Temperature drop sensitivity (Constant rate, low permeability EPA/ high permeability fracture).

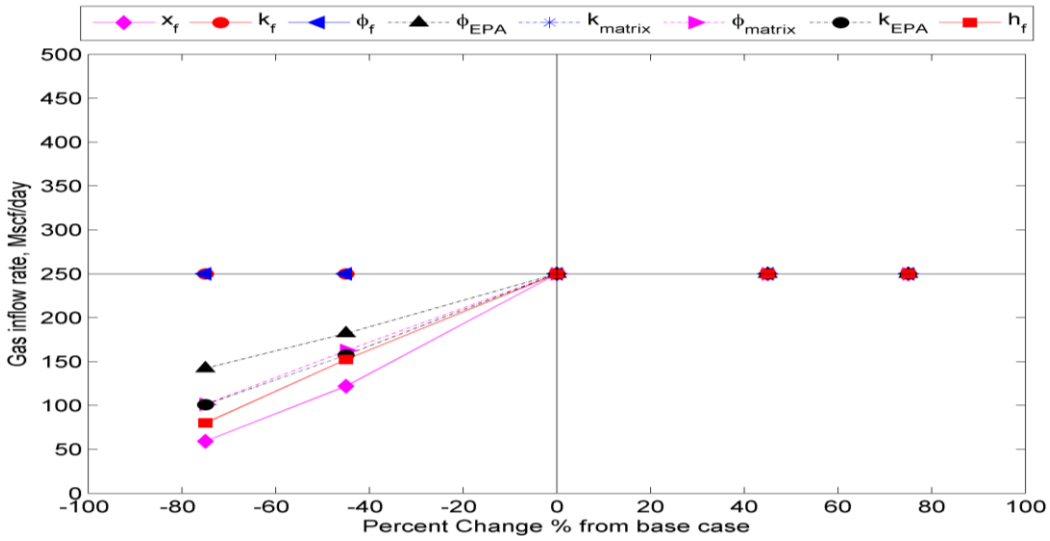

Fig. 3.3—Gas inflow rate sensitivity (Constant rate, low permeability EPA/ high permeability fracture).

3.3.2 Constant Rate – Case II: High Permeability EPA/Low Permeability Fracture

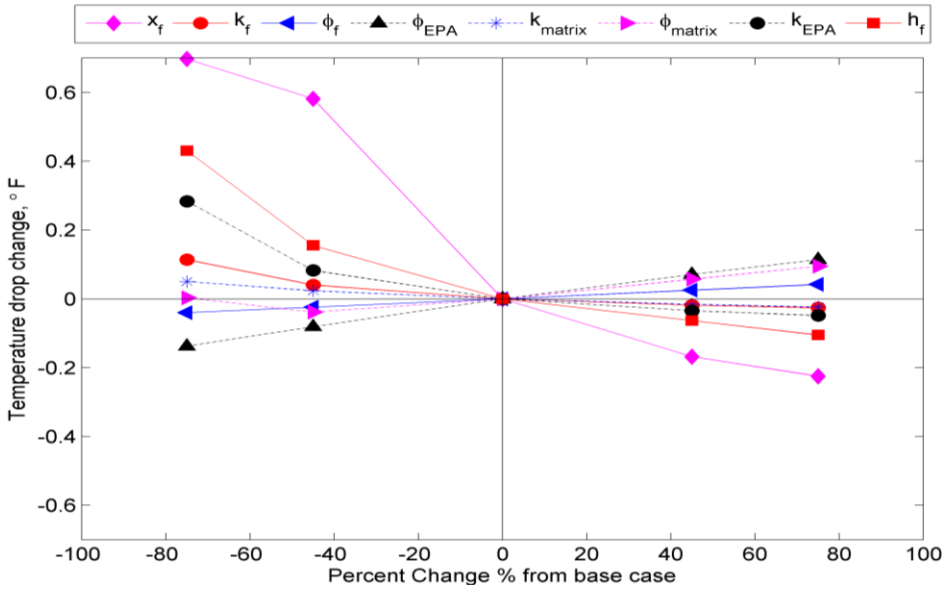

Fig. 3.4—Temperature drop sensitivity (Constant rate, high permeability EPA/ low permeability fracture).

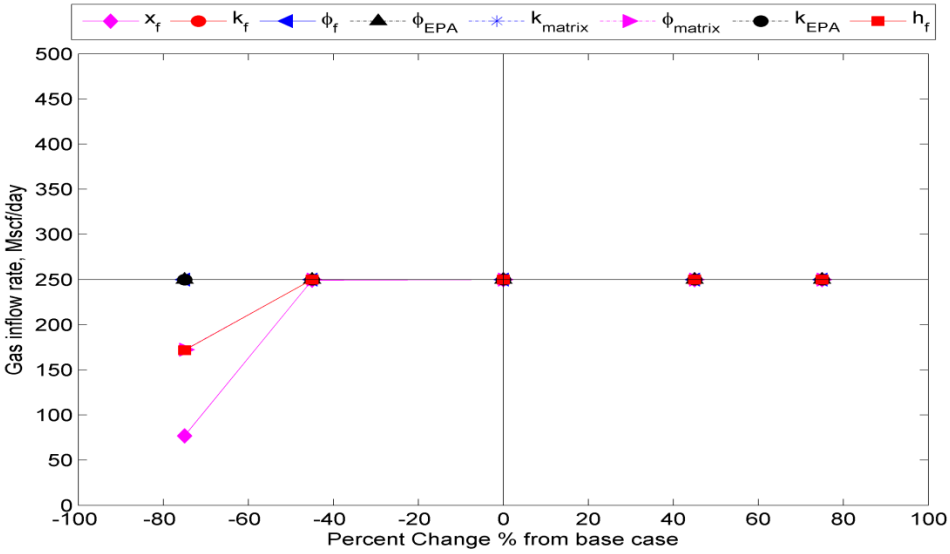

Fig. 3.5—Gas inflow rate sensitivity (Constant rate, high permeability EPA/ low permeability fracture).

3.3.3 Constant BHP – Case III: Low Permeability EPA/High Permeability Fracture

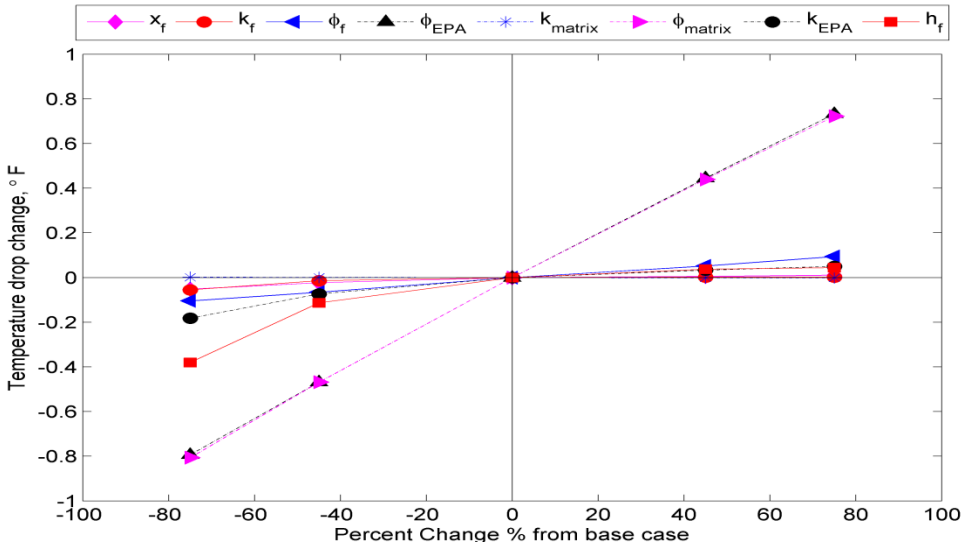

Fig. 3.6—Temperature drop sensitivity (Constant rate, low permeability EPA/ high permeability fracture).

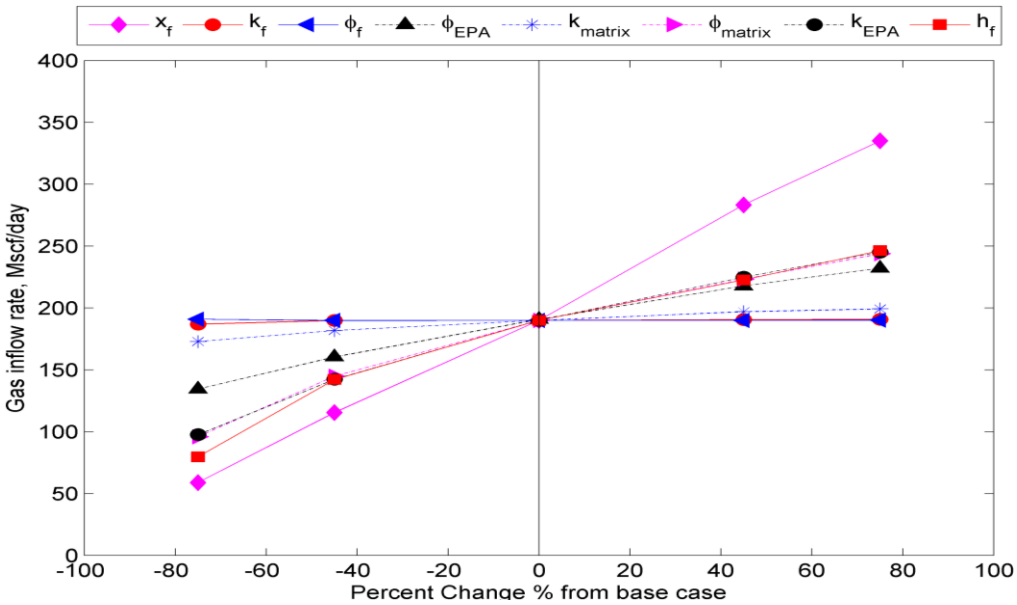

Fig. 3.7—Gas inflow rate sensitivity (Constant BHP, low permeability EPA/ high permeability fracture).

3.3.4 Constant BHP – Case IV: High Permeability EPA/Low Permeability Fracture

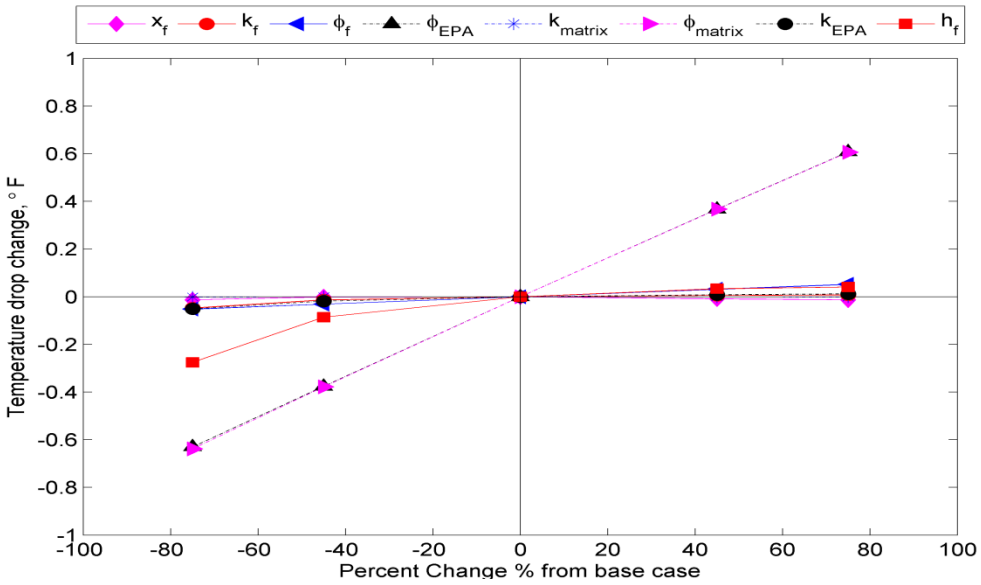

Fig. 3.8—Temperature drop sensitivity (Constant rate, high permeability EPA/ low permeability fracture).

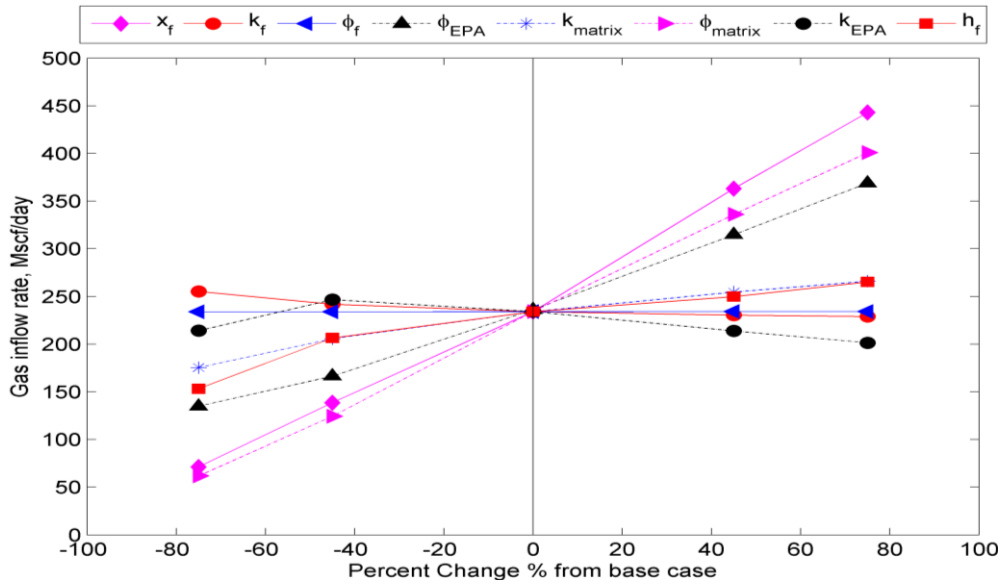

Fig. 3.9—Gas inflow rate sensitivity (Constant BHP, low permeability EPA/ high permeability fracture).

3.4 Discussion

Under the constant rate condition, the increase of EPA porosity, matrix porosity and fracture porosity causes the increase of temperature drop difference. The opposite occurs when these three parameters are decreased. Porosity terms control the pore volume of the reservoir and change the pressure behavior of the reservoir. Note that due to the constant rate condition, an increase in flow rate is not observed. With higher pore volume, an increase in temperature drop is observed.

Furthermore, when the remaining parameters are increased, less pressure drawdown is necessary to meet the established rate. As result, the cooling effect caused by gas expansion is reduced. Regarding fracture half-length and fracture height, reducing these terms decreases the stimulated reservoir volume which increases the pressure drawdown. Despite experiencing a reduction of gas inflow when reducing these terms, the temperature drop increases which means that thermal expansion effects (caused by pressure drop variations) are predominant. However, if the flow rate is significantly reduced, as a result of a drastic reduction of fracture half-length and/or height, gas inflow becomes relevant and convective cooling effects become predominant.

Furthermore, changes in fracture permeability do not have a major impact on the temperature distribution in Case I or Case II. Fracture permeability, however, is slightly more sensitive in Case II. A different response is observed when the EPA's permeability is changed. Note that in the EPA, a significant pressure drop occurs; therefore the cooling effect caused by gas expansion is highly influenced by the pressure response in this area. Similarly, the pressure drop depends on the EPA's permeability. When

maintaining a constant inflow rate, decreasing the permeability of the EPA leads to an additional pressure reduction that translates into additional cooling. Further reduction of the EPA's permeability leads to a similar reduction in pressure drop but the inflow rate starts to affect the temperature behavior. At this point, convective effects become predominant and with a lower inflow rate less temperature drop is observed.

Similar results are observed in Case II. In this case, fracture half-length, fracture height, EPA permeability and fracture permeability are more influential in the temperature response than the porosity terms. As also observed in the previous case, the temperature continues to be more sensitive to permeability in the EPA than the one in the fracture. In addition, no reduction in flow rate is observed when the parameters are decreased. In a way, this facilitates the analysis since only gas expansion effects are relevant.

In the constant BHP cases, the increase of all parameters corresponds to the increase of temperature drop, which also corresponds to the increase of gas inflow.

In Case 3 and Case 4, when fracture half-length is increased a similar increase in inflow rate is observed. Despite this, temperature drop at the fracture location is not significantly higher. The opposite is observed when porosity terms are increased. Less inflow rate is observed when compared to fracture half-length variations, yet the temperature drop is higher for the porosity cases. Once again, gas expansion effects are predominant due to the increase of pressure differential.

In the end, the sensitivity of reservoir temperature to fracture parameters was demonstrated. Highly sensitive fracture parameters are fracture half-length and EPA

permeability. Fracture permeability's sensitivity changes depending on the hydraulic fracture-network configuration. These results serve as a guideline for the set-up of the inverse problem, where sensitive variables serve as the objective parameter. In the next section, it will be explained how to setup the inverse model problem using the EnKF as the data assimilation technique.

4. INVERSE MODELING WITH ENSEMBLE KALMAN FILTER

4.1 ENKF Implementation

In this section, the goal is to integrate DTS data as observations for the inverse problem to estimate hydraulic fracture geometry and conductivity. The EnKF is the chosen technique to assimilate the temperature data collected by DTS.

The EnKF has been successfully applied in different fields such as hydrology, meteorology, oceanography, groundwater and oil reservoir model calibration (Evensen, 2007, 2009; Aanonsen et al., 2009; Naevdal et al., 2005). Like the original Kalman filter, the EnKF consists of two sequential steps: forecast and analysis.

In the forecast stage, the reservoir model equation is used to compute a forward step with the current estimate of the state as initial condition. An ensemble of reservoir parameters, N_e, is generated for an unknown reservoir parameter, for instance fracture half-length. A Monte Carlo simulation is then executed, running the reservoir simulator for all N_e values and generating N_e sets of simulated data. In the analysis stage, the simulated DTS data is compared with the observed DTS data. This comparison follows the EnKF analysis equation and the ensemble of reservoir parameters (e.g. fracture half-length) is updated. In this way, state and observation predictions for the ensemble of model realizations is obtained,

$$\mathbf{x}_{t|t-1}^{j} = f_t\left(\mathbf{x}_{t-1|t-1}^{j}, \mathbf{z}_{t-1}, \mathbf{w}_{t-1}^{j}\right) \qquad j = 1, \dots, N_e \quad \text{(4.1)}$$

where. $|t$ represents conditioning on observations up to time t; $\mathbf{z}_{t-1}$ is a vector of known (nonrandom) time-dependent boundary conditions and controls (such as injection rate);

and $\mathbf{w}_{t-1}^{j}$ is a vector of random variables that accounts for modeling errors. The function $f_t(.,.,.)$ represents the state propagation equation from time $t-1$ to time t. In this application,Eq.4.1 represents the solution of the coupled mass and energy balance equations (non-isothermal reservoir simulation results using ECLIPSE E300) that describes the time evolution of pressure, saturation and temperature distributions for each individual realization j of the ensemble reservoir model parameter

To make the initial ensemble of reservoir parameters (e.g. fracture half-length), a uniform probability density function (PDF) is used. The augmented state vector for this case is of the form,

$$\mathbf{x}^j = \begin{bmatrix} \mathbf{m}^j \\ \mathbf{d}^j \end{bmatrix}; \qquad j = 1, \dots, N_e \Rightarrow \mathbf{X} = [\mathbf{x}^1 \mathbf{x}^2 \quad \cdots \quad \mathbf{x}^{N_e}] \quad \text{..... (4.2)}$$

where $\mathbf{m}^j$ is the reservoir parameter realization and $\mathbf{d}^j$ is the observation obtained from running the simulation using$\mathbf{m}^j$. When estimating a single parameter, the reservoir parameter realization $\mathbf{m}^j$ is a scalar. On the other hand, when executing a joint estimation (e.g. fracture half-length and fracture permeability) the realization $\mathbf{m}^j$ is a 2×1 vector.

The corresponding simulated DTS data is depicted by$\mathbf{d}^j$. Its dimension corresponds to the number of sample points indicated in the forward model. For instance, if the reservoir model has 100 grid blocks along the horizontal well from which temperature values are recorded and reported as DTS data, then the dimension of $\mathbf{d}^j$ is 100×1. In the case of estimating a single parameter the dimension of the state vector $\mathbf{x}^j$ would be 101×1.

At time steps when DTS data is available, the EnKF analysis equation is applied to update the reservoir parameter realizations. After each update, a confirmation step is used to derive the future state predictions from the initial time step using the updated parameters. We repeat the sequence of prediction and update steps until all DTS measurements are integrated. The EnKF analysis equation can be expressed as

$$\mathrm{x}_u^j = \mathrm{x}_f^j + \mathrm{K}\left(\mathrm{y}^j - \mathrm{H}\mathrm{x}_f^j\right), \quad \mathrm{K} = \mathrm{C}_\mathrm{x}^e\mathrm{H}^T(\mathrm{H}\mathrm{C}_\mathrm{x}^e\mathrm{H}^T + \mathrm{C}_\mathrm{d})^{-1} \quad \text{..... (4.3)}$$

where $\mathbf{K}$ is the Kalman gain matrix and the subscripts u and f denote updated and forecast quantities while the superscript e indicates ensemble calculated statistics. The notations $\mathbf{C}_\mathbf{x}^e$ and $\mathbf{C}_\mathbf{d}$ represent the states sample covariance and observation covariance matrices respectively.

For the case of estimating a single parameter, the measurement matrix$\mathbf{H}_{100\times101} = [\mathbf{0}_{100\times1}|\mathbf{I}_{100\times100}]$, where $\mathbf{0}_{100\times1}$ and $\mathbf{I}_{100\times100}$are zero and identity matrices of the specified dimensions, respectively, acts as a selection operator that extracts the predicted DTS measurement components from the augmented state vector. The notation $\mathbf{y}^j$ is used to represent the jth realization of the perturbed DTS observations. To perturb the DTS observations, an uncorrelated realization from a Gaussian random noise, with a specified observation covariance matrix C_d, is added to the value of the observed quantities. The perturbed observations are made as follows:

$$\mathbf{y}^j = \mathbf{y} + \boldsymbol{\varepsilon}^j; \qquad j = 1, \dots, N_e \;;\; \boldsymbol{\varepsilon}^j \sim N(\mathbf{0}_{100\times1}, \mathbf{C}_\mathbf{d}) \quad \text{..... (4.4)}$$

where $\mathbf{y}$ is the true observed DTS data. The states sample covariance $\mathbf{C}_\mathbf{x}^e$ can be computed from the ensemble of state vectors

$$\mathbf{C}_{\mathbf{x}}^{e} = \frac{1}{N_e-1}\sum_{j=1}^{N_e}\left(\mathbf{x}_f^j - \bar{\mathbf{x}}_f^j\right)\left(\mathbf{x}_f^j - \bar{\mathbf{x}}_f^j\right)^T \; ; \quad \bar{\mathbf{x}}_f^j = \frac{1}{N_e}\sum_{j=1}^{N_e}\mathbf{x}_f^j \quad \text{..... (4.5)}$$

where $\bar{\mathbf{x}}_{\mathbf{f}}^{\mathbf{j}}$ is used to denote the ensemble mean of the forecast states, meaning the reservoir model property from the previous step and the corresponding DTS response forecasts. Finally, the EnKF update equation uses the Kalman gain matrix to linearly combine the predicted and observed DTS data for each realization.

4.2 Synthetic Examples

In these examples, the EnKF algorithm is implemented with$\mathrm{N_e} = 100$. To speed up the inversion procedure, specifically the Monte Carlo simulation in the forecast step, the EnKF is executed using MATLAB's parallel computing toolbox (MATLAB, 2011). First, fracture half-length and fracture permeability will be estimated individually. Next, joint estimation of (1) fracture half-length and fracture permeability and (2) fracture half-length and EPA permeability will be executed.

4.2.1 Forward Model

For these examples, the true values of the estimated parameters are predefined. In this way, the accuracy of the resulting estimations can be evaluated at the end of the assimilation stage. The parameters used in the forward model are detailed on **Table 4.1**. Highlighted in red are the true values of the objective parameters.

For this exercise, the synthetic reservoirs are set to produce only dry gas. Fluid properties are the same used in Section 2 (see Fig. 2.4). In addition, flowing conditions,

constant rate and constant BHP, are studied to see the response of the EnKF under both production conditions.

Table 4.1 Forward model parameters used in EnKF estimation		
Parameter	Description	Value [unit]
N_{stages}	Number of stages	10
k_{matrix}	Matrix permeability	10^{-4} [md]
k_{EPA}	EPA permeability	0.05 [md]
k_f	Fracture permeability	500 [md]
ϕ_{matrix}	Matrix porosity	0.08[%]
ϕ_{EPA}	EPA porosity	0.081 [%]
ϕ_f	Fracture porosity	0.33 [%]
x_f	Fracture half length	100[ft]
h_f	Fracture height	30[ft]

4.2.2 Results

Results of all of these tests are shown in **Fig. 4.1** through **Fig. 4.20.**

4.2.2.1 Constant BHP

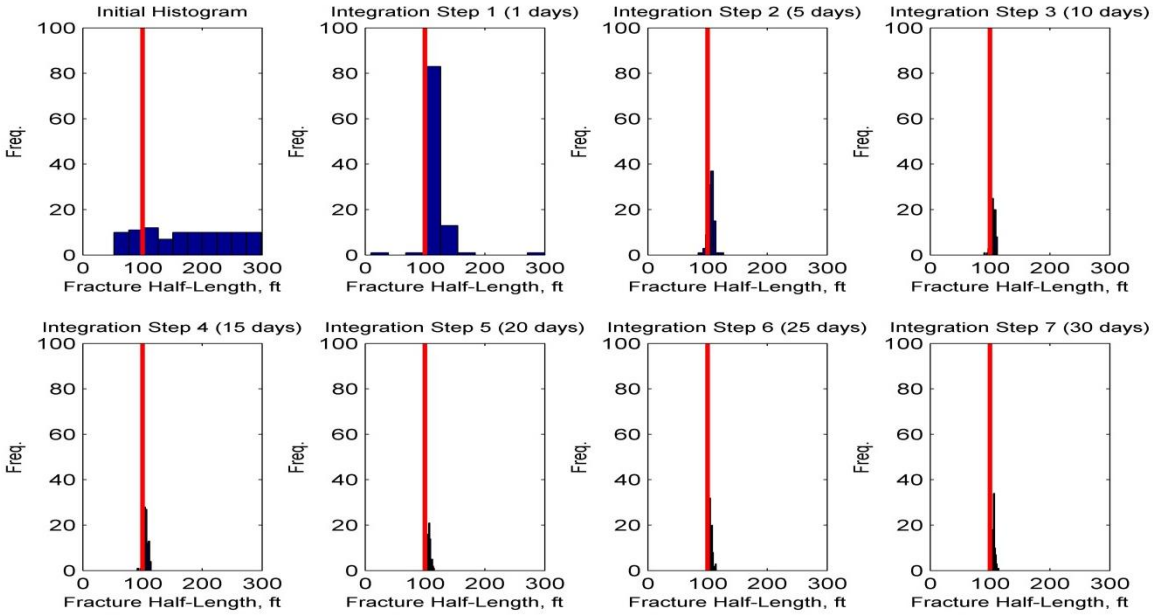

Fig. 4.1—Individual estimation of fracture half-length using EnKF (constant BHP, t=30 days). True value marked in red.

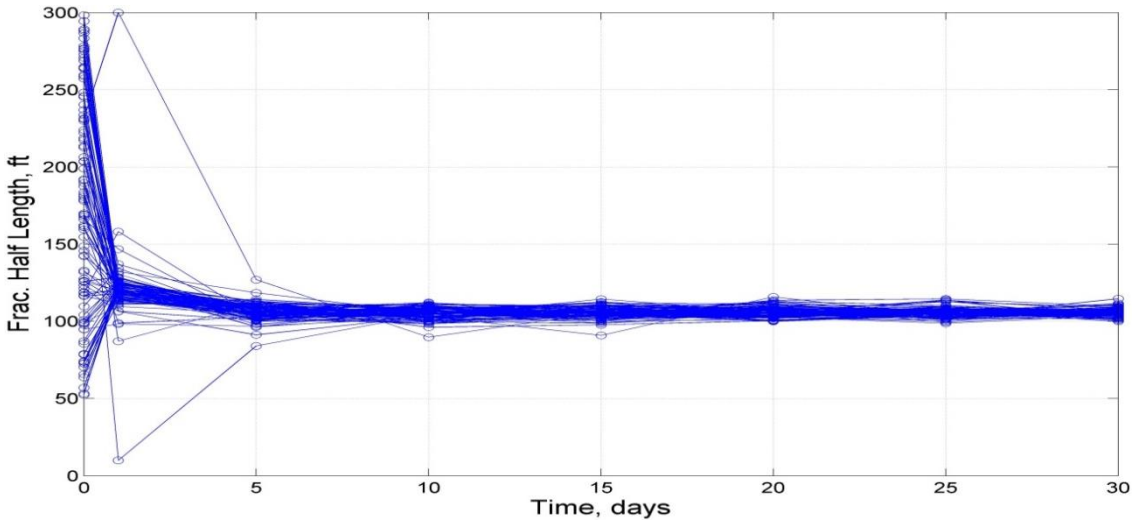

Fig. 4.2—Fracture half-length ensemble evolution by integration steps. (Constant BHP, t=30 days).

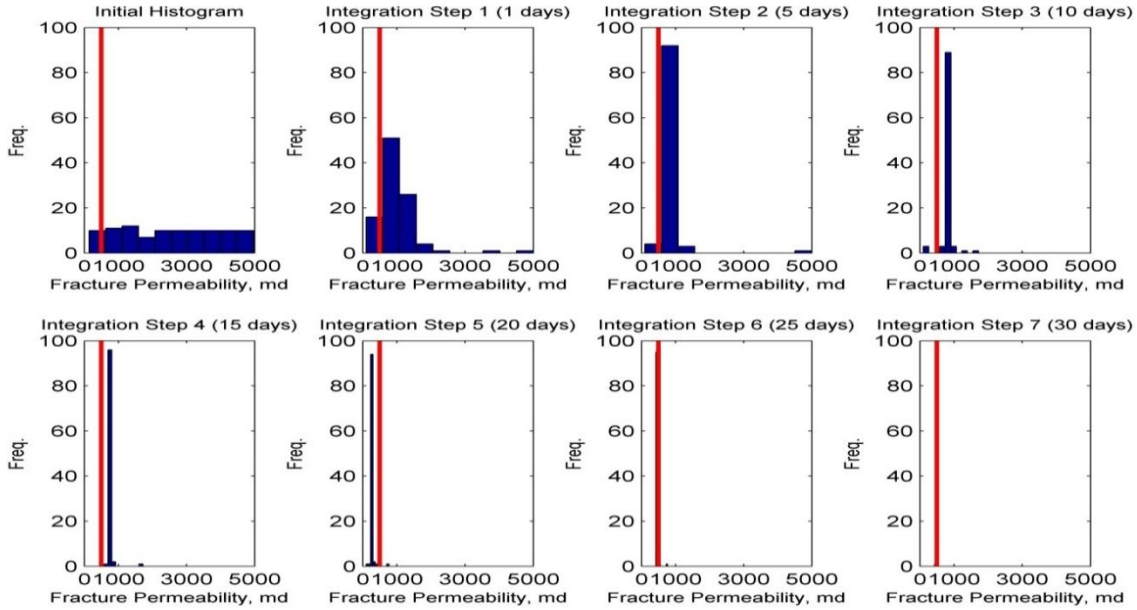

Fig. 4.3—Individual estimation of fracture permeability using EnKF (constant BHP, t=30 days). True value marked in red.

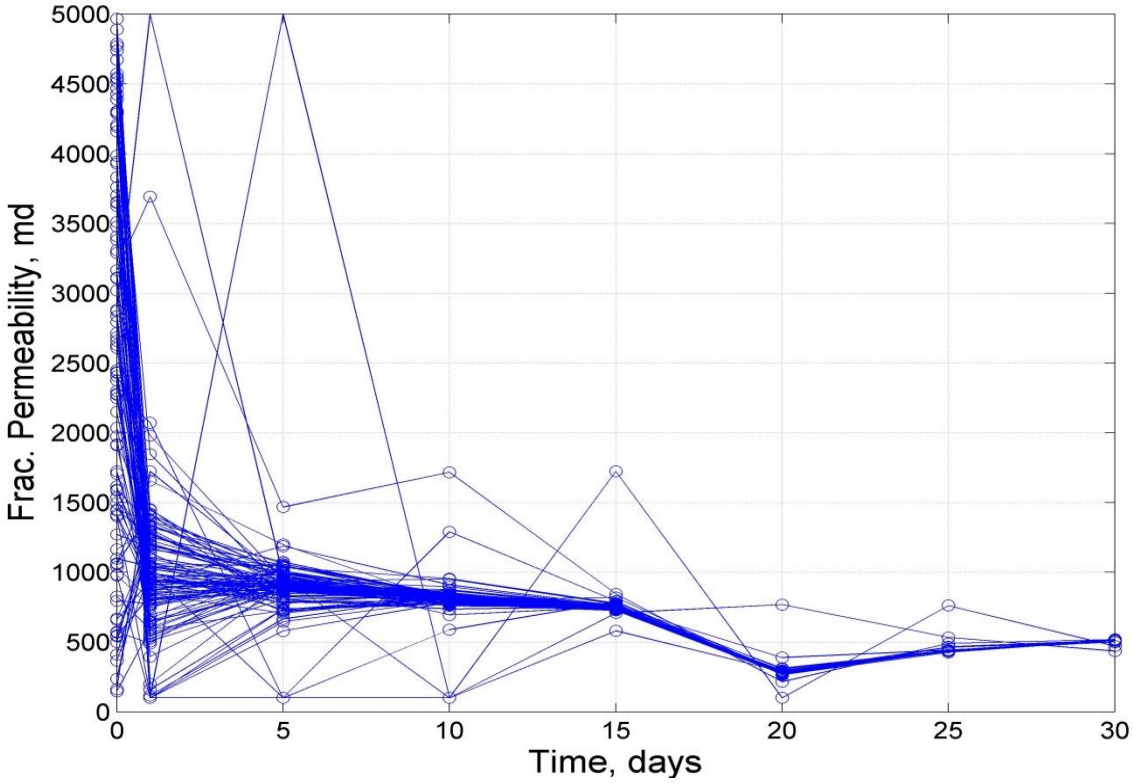

Fig. 4.4—Fracture permeability ensemble evolution by integration steps. (Constant BHP, t=30 days).

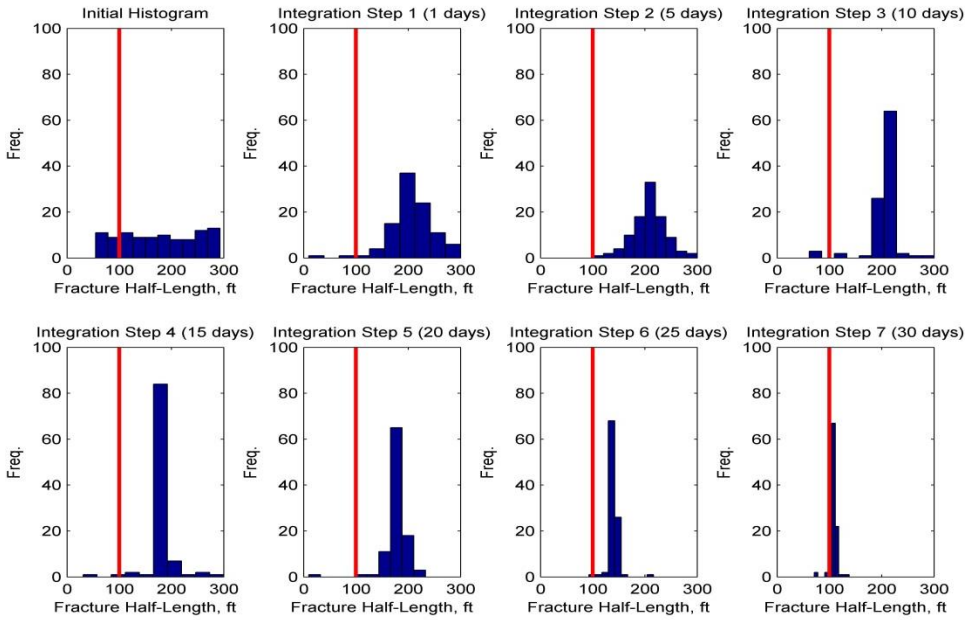

Fracture half-length

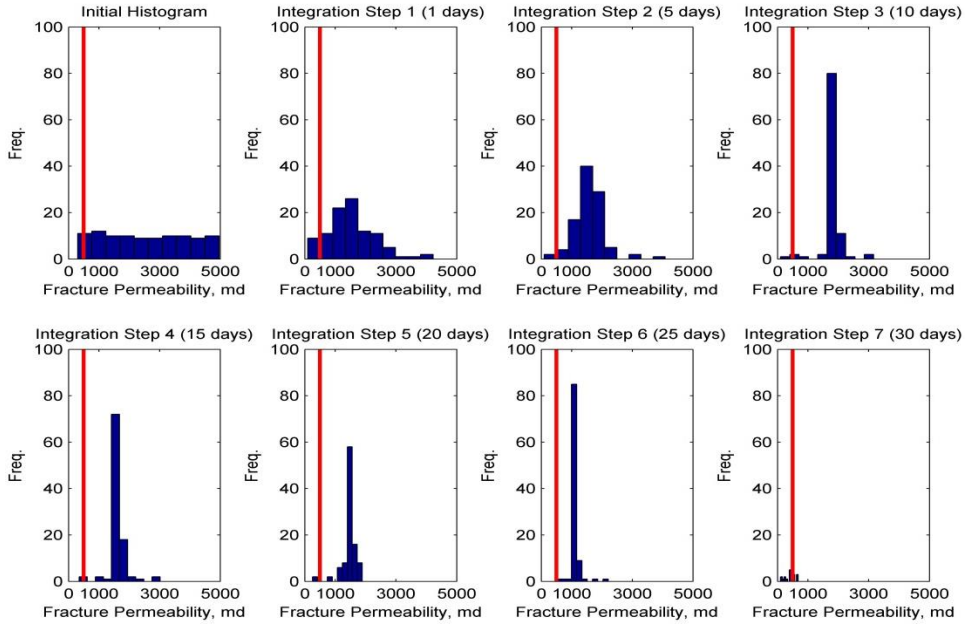

Fracture permeability

Fig. 4.5—Joint estimation of fracture half-length (top) and fracture permeability (bottom) (constant BHP, t=30 days). True values marked in red.

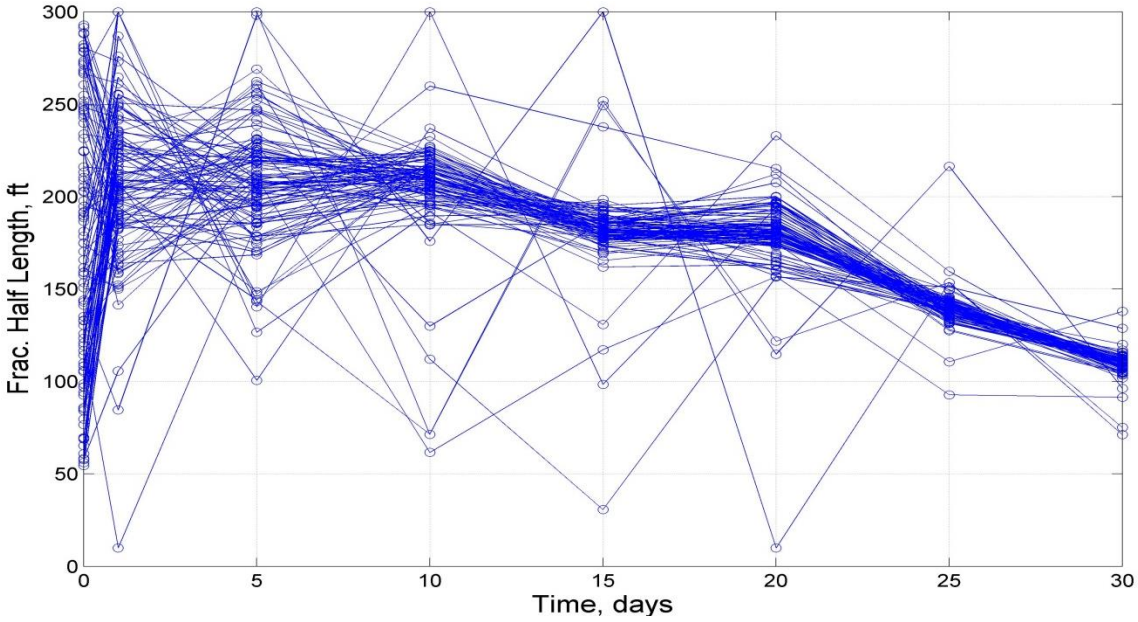

Fig. 4.6—Fracture half-length ensemble evolution by integration steps. (Constant BHP, t=30 days, joint estimation).

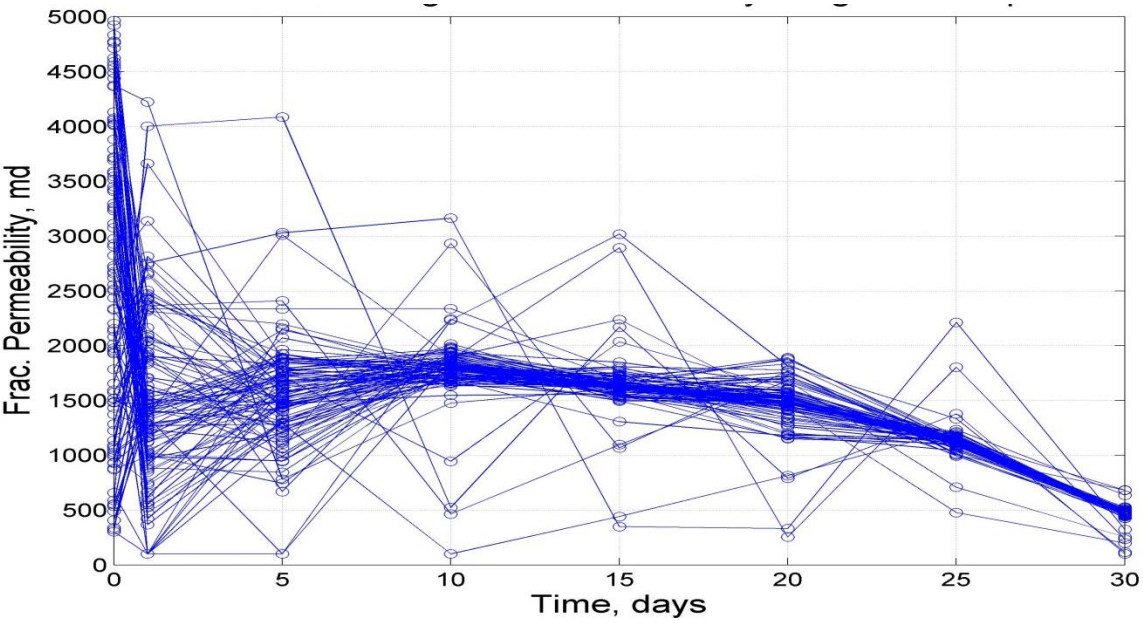

Fig. 4.7—Fracture permeability ensemble evolution by integration steps. (Constant BHP, t=30 days, joint estimation).

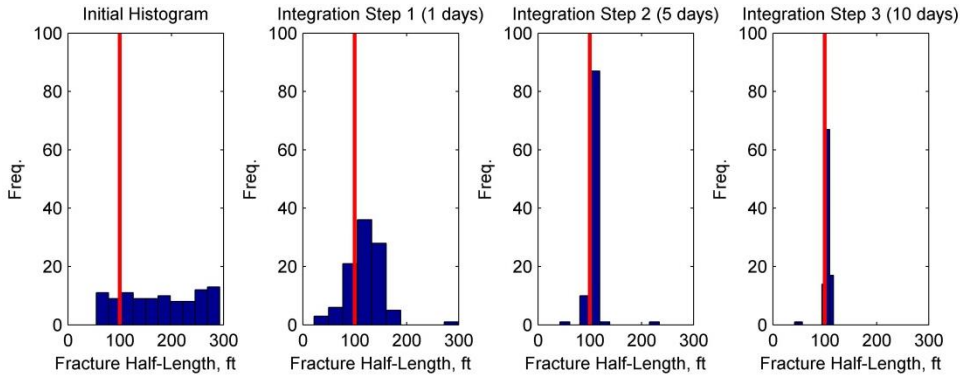

Fracture half-length.

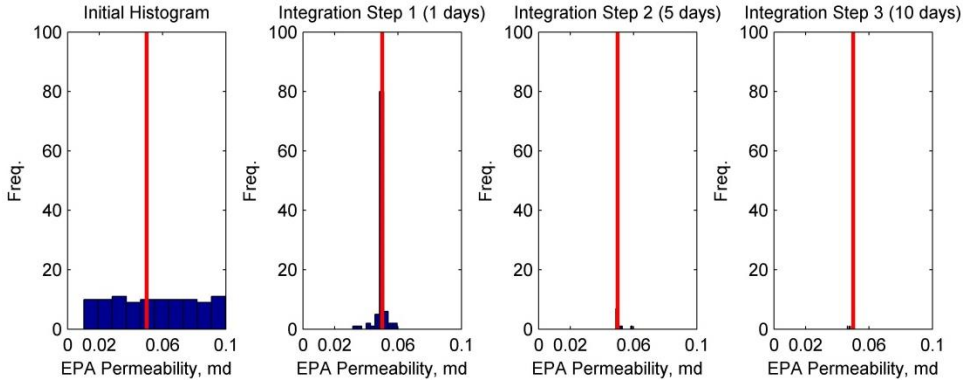

EPA permeability.

Fig. 4.8—Joint estimation of fracture half-length (top) and EPA permeability (bottom) (constant BHP, t=30 days). True values marked in red.

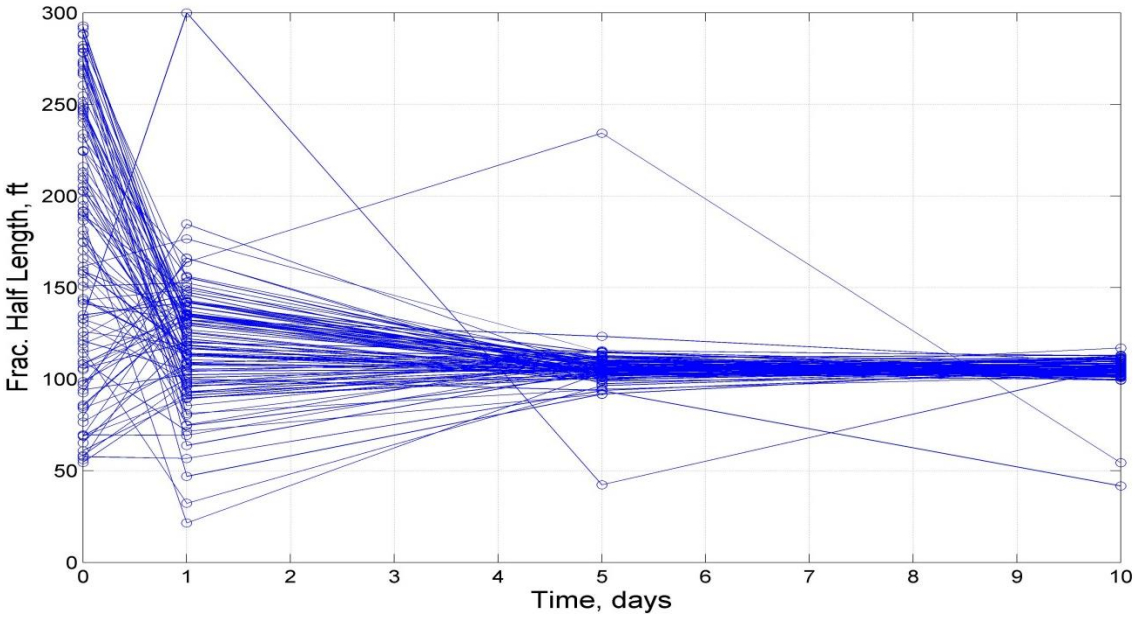

Fig. 4.9—Fracture half-length ensemble evolution by integration steps. (Constant BHP, t=30 days, joint estimation).

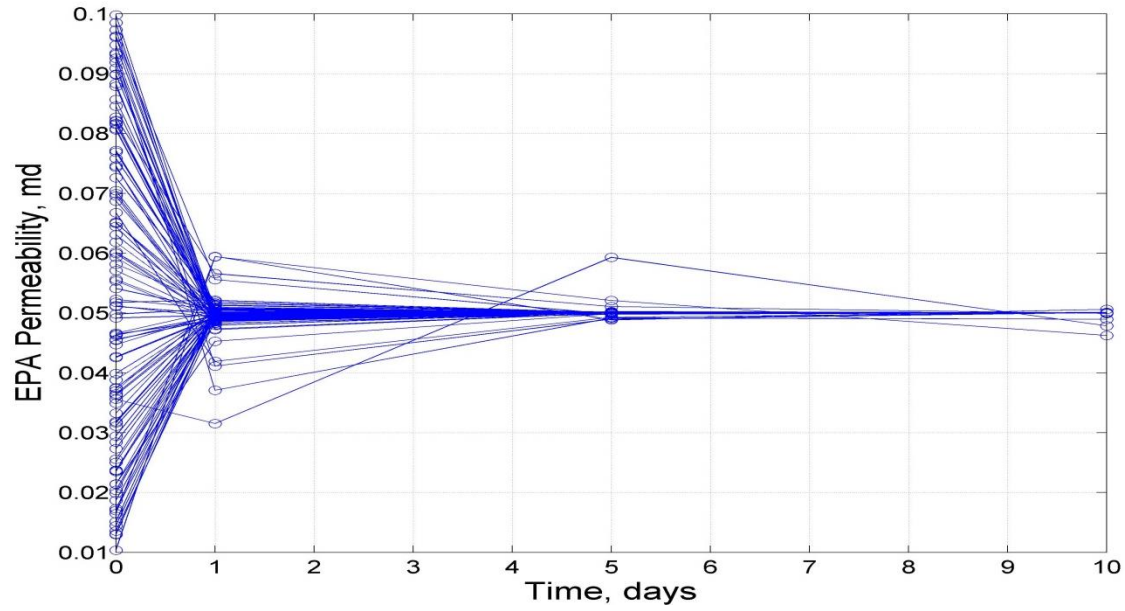

Fig. 4.10—EPA permeability ensemble evolution by integration steps. (Constant BHP, t=30 days, joint estimation).

4.2.2.2 Constant Rate

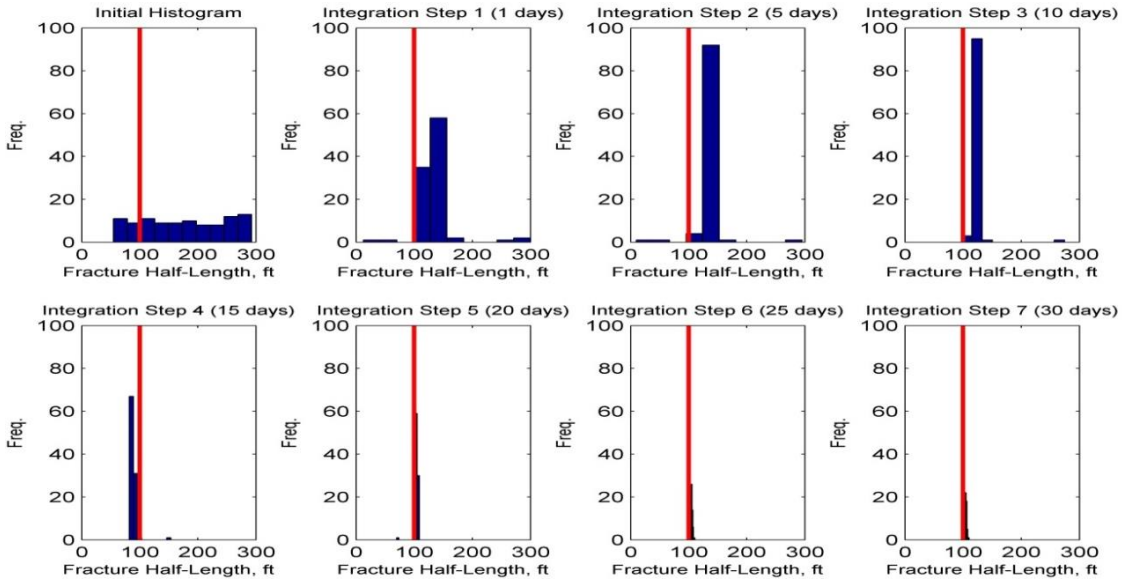

Fig. 4.11—Individual estimation of fracture half-length using EnKF (constant rate, t=30 days). True value marked in red.

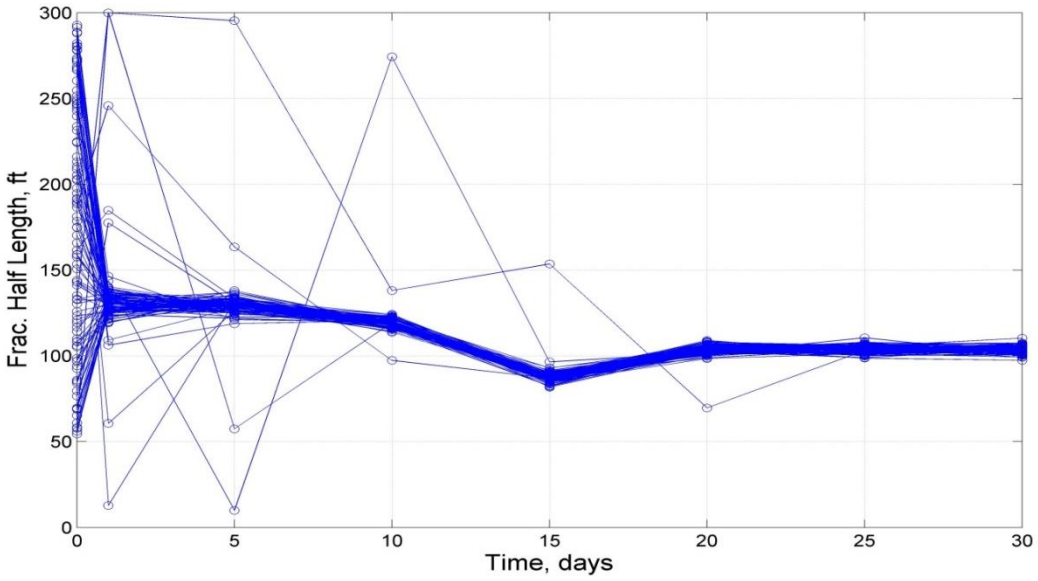

Fig. 4.12—Fracture half-length ensemble evolution by integration steps. (Constant rate, t=30 days).

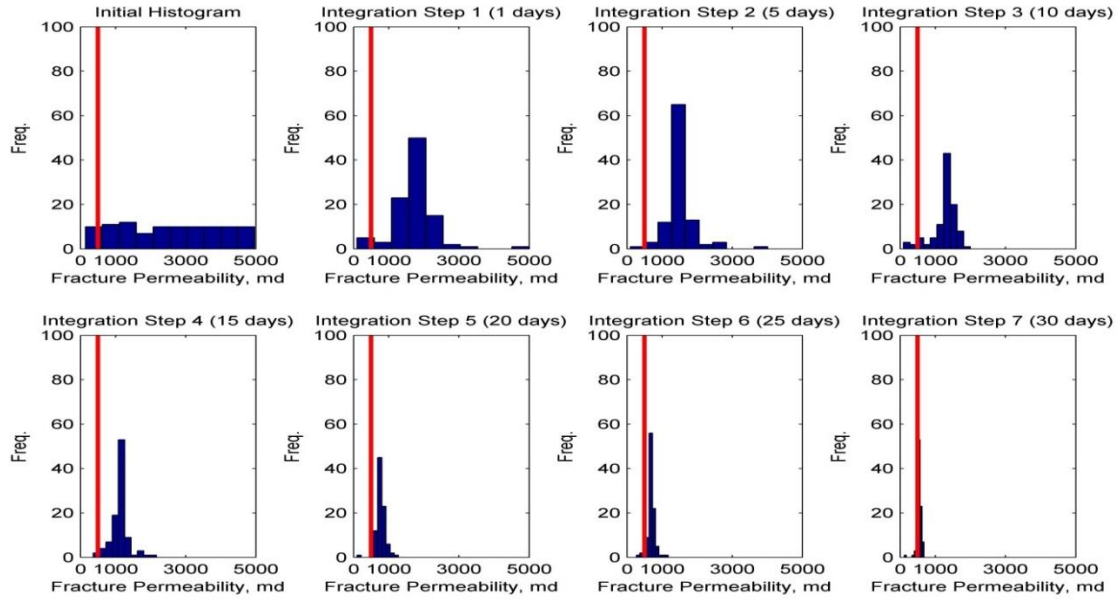

Fig. 4.13—Individual estimation of fracture permeability using EnKF (constant rate, t=30 days). True value marked in red.

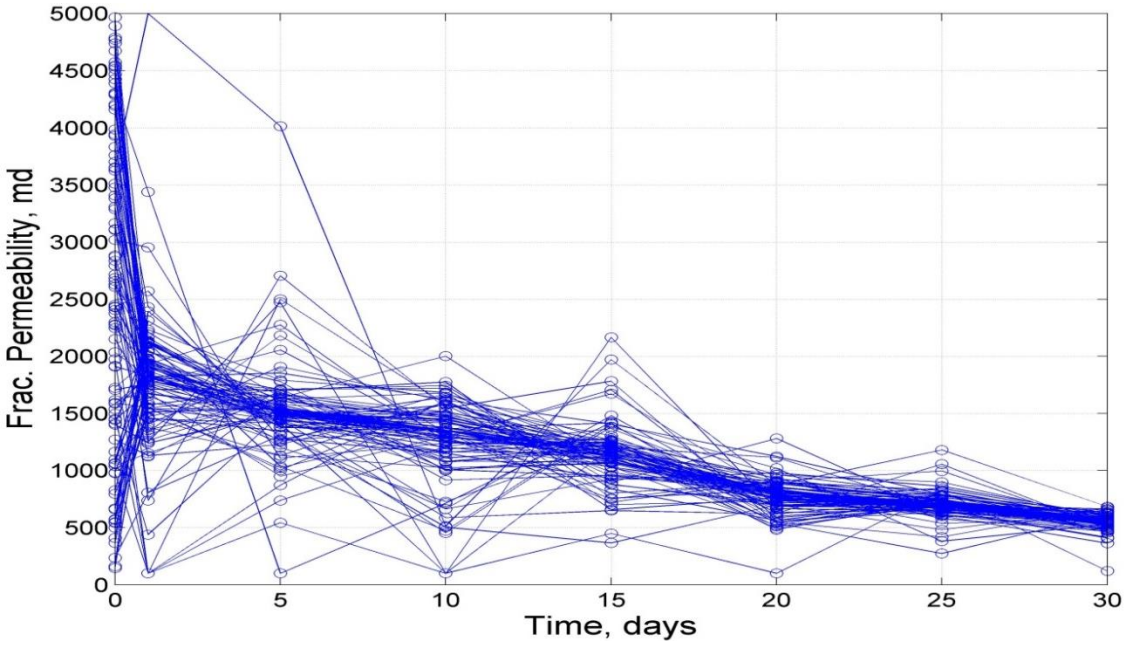

Fig. 4.14—Fracture permeability ensemble evolution by integration steps. (Constant rate, t=30 days).

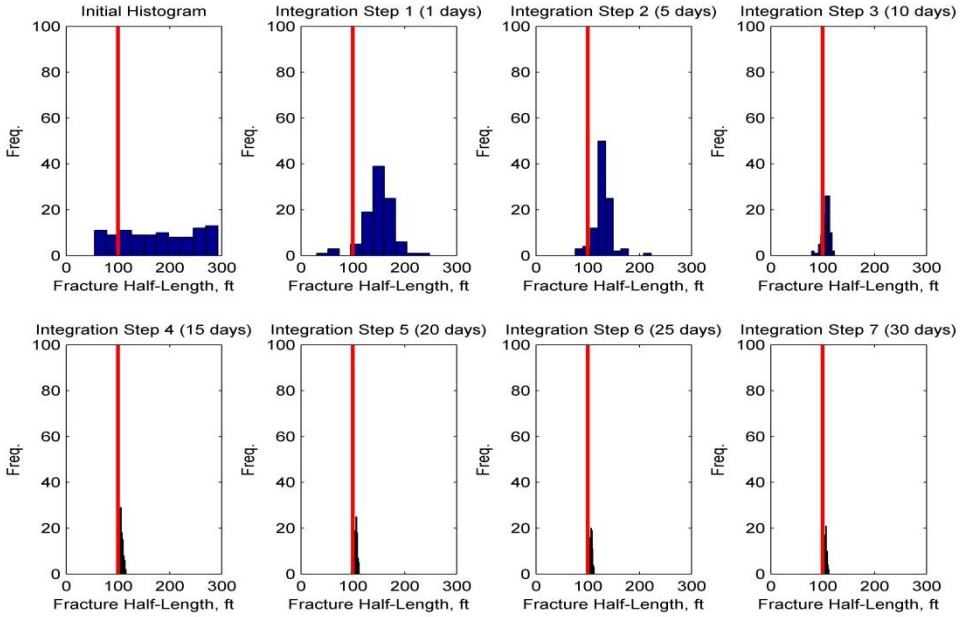

Fracture half-length.

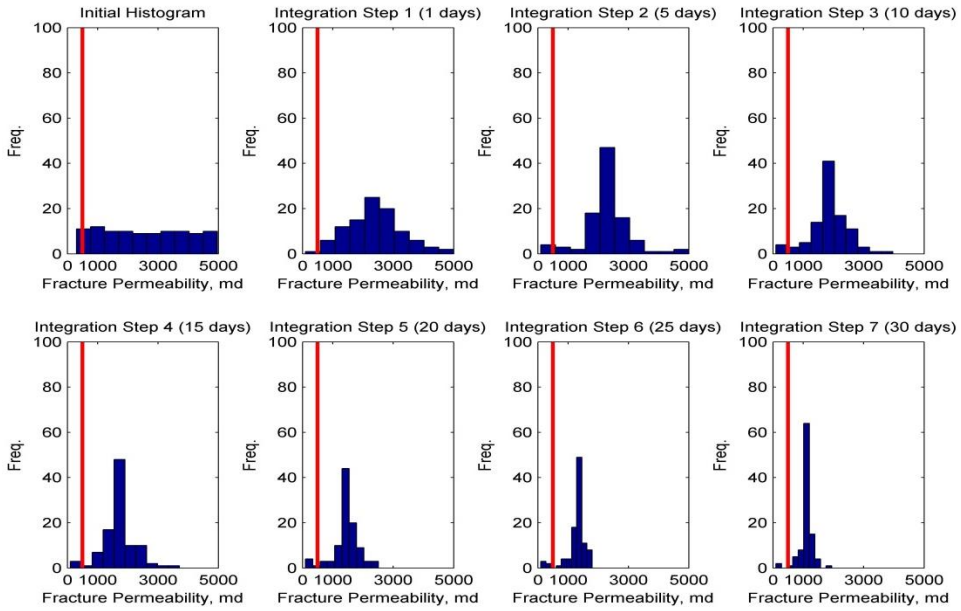

Fracture permeability.

Fig. 4.15—Joint estimation of fracture half-length (top) and fracture permeability (bottom) (constant rate, t=30 days). True values marked in red.

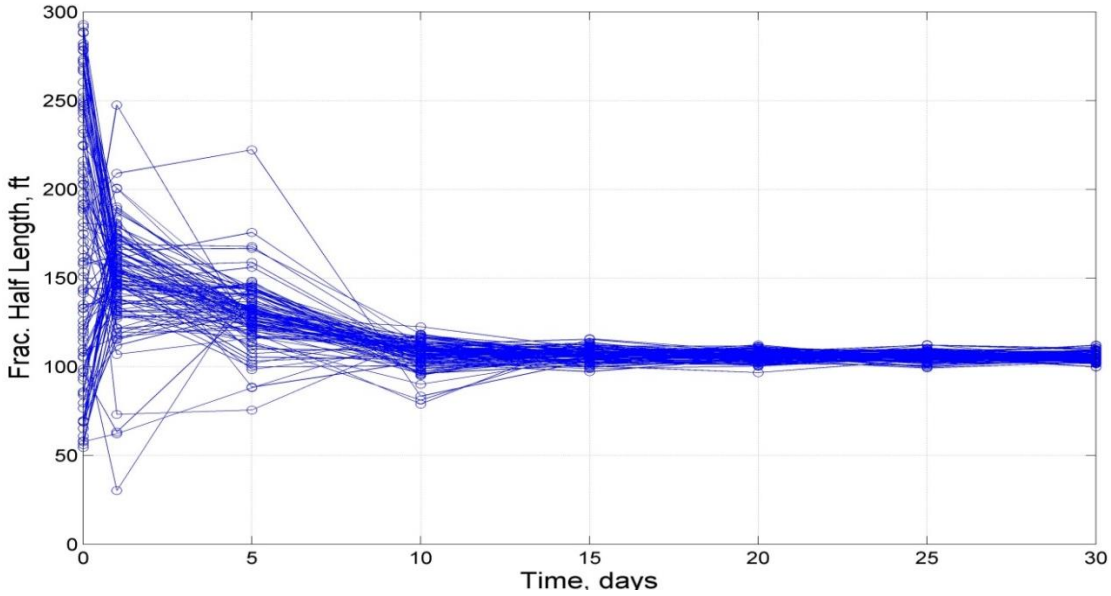

Fig. 4.16—Fracture half-length ensemble evolution by integration steps. (Constant rate, t=30 days, joint estimation).

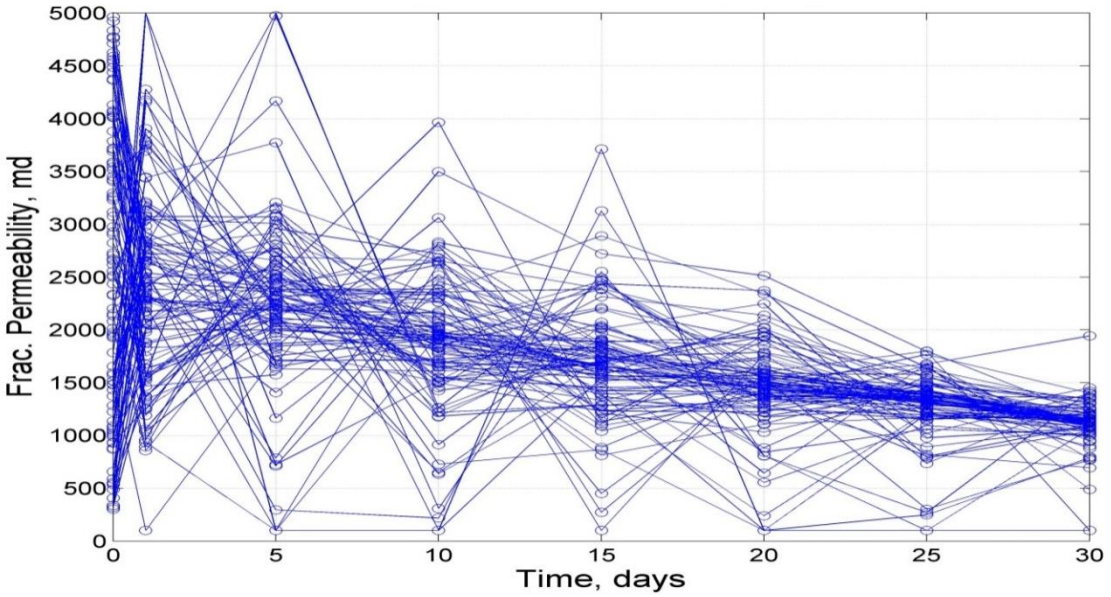

Fig. 4.17—Fracture permeability ensemble evolution by integration steps. (Constant rate, t=30 days, joint estimation).

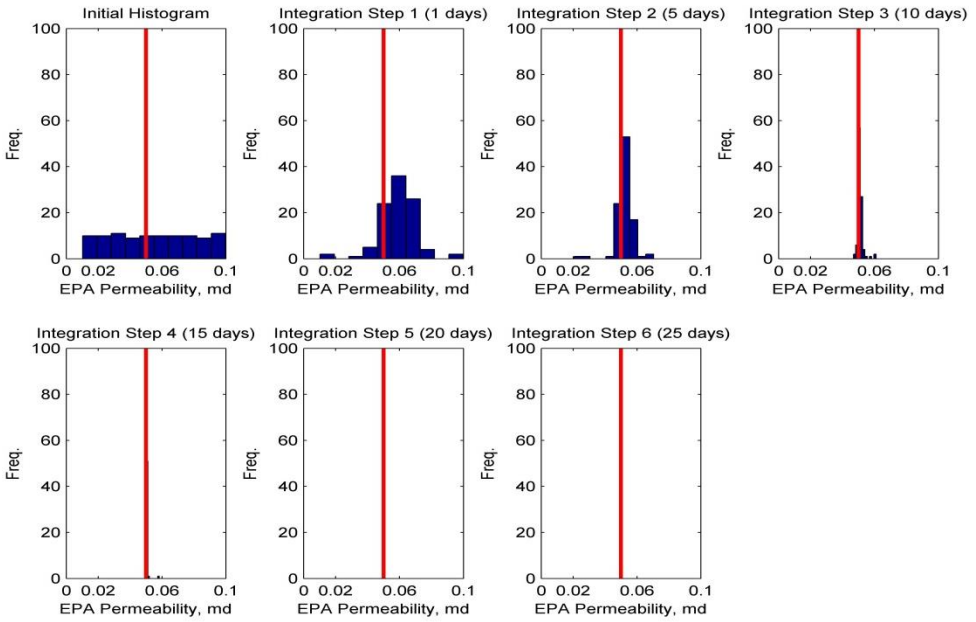

Fracture half-length.

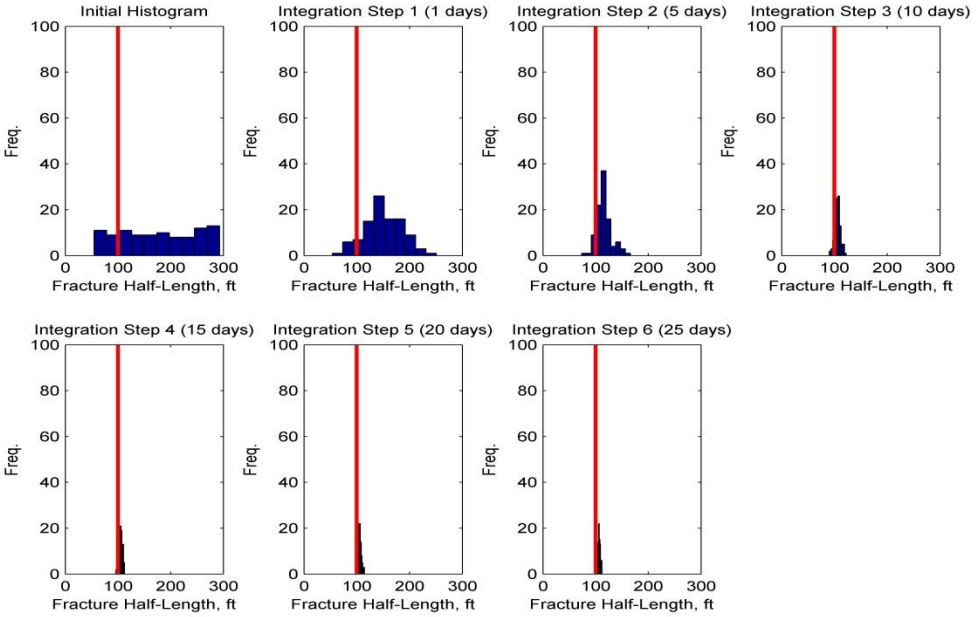

EPA permeability

Fig. 4.18—Joint estimation of fracture half-length (top) and EPA permeability (bottom) (constant rate, t=30 days). True values marked in red.

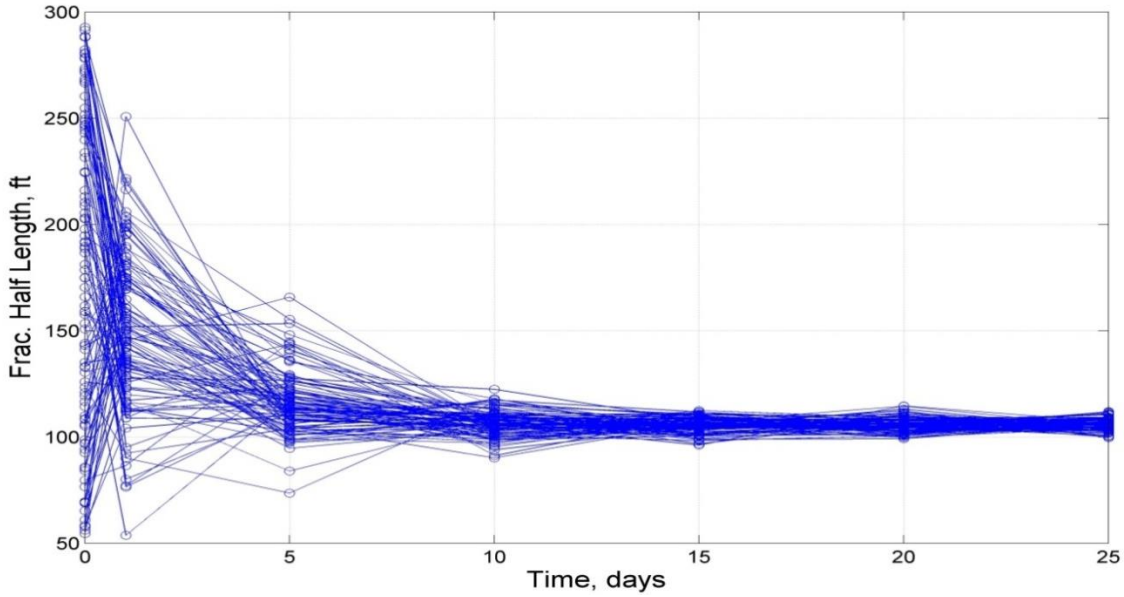

Fig. 4.19—Fracture half-length ensemble evolution by integration steps. (Constant rate, t=30 days, joint estimation).

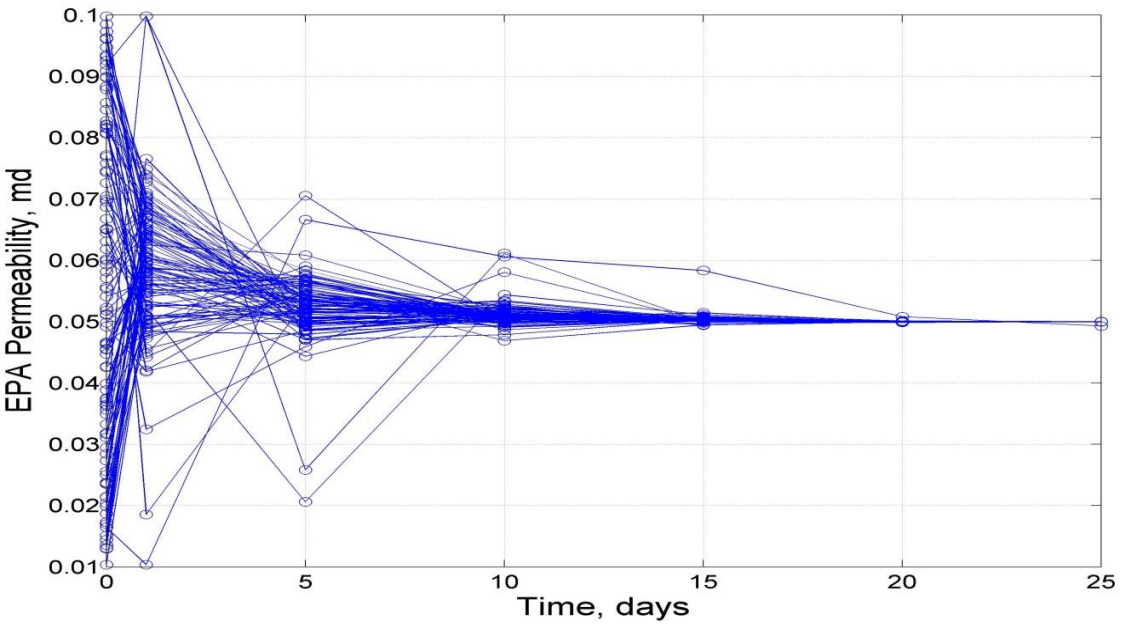

Fig. 4.20—EPA permeability ensemble evolution by integration steps. (Constant rate, t=30 days, joint estimation).

4.3 Discussion

Given the synthetic nature of the previous models, the effectiveness of the estimations is easily verified by comparing the results with the true values of the objective parameters. Fig. 4.1through Fig. 4.20 show the results of all individual and joint estimations under different production conditions. The estimation's evolution after each integration step is also plotted (e.g. Fig. 4.12) in order to illustrate the convergence of all ensembles to the true value. Increasing the number of ensembles (from 40 to 100) had a significant improvement in the evolution of EnKF even though higher computational time was associated with it.

Note that individual estimations are in essence idealistic, since in real scenarios there is always more than one unknown parameter. For individual estimations of fracture and EPA permeability, the problem tends to be over determined and a solution is reached very fast. This should not be confused with EnKF collapse, where the number of ensemble members is significantly reduced after the first assimilation step (Baker, 2007).

Joint estimations, on the other hand, provide a more realistic touch to this exercise since it attempts to estimate two parameters simultaneously. For all cases, the spread of the ensemble distribution is significantly reduced very early in the process, given the sensitivity of the system to the objective fracture parameters. The histograms show how the ensemble estimation evolves at each integration step, converging to the true value as time progresses. For fracture half-length and EPA permeability joint estimation (see Figure 5.4 and Fig 5.8), the EnKF is stopped after 10 days (15 days

under constant BHP) given that an acceptable solution is reached. All other estimations reach acceptable results after 30 days.

After seeing encouraging results in the implementation of the EnKF on synthetic models, observations are replaced with field data and the forward model is calibrated accordingly. Field data interpretation and the history match results are presented in the next section.

5. MARCELLUS SHALE FIELD CASE

After seeing favorable results on synthetic cases, the proposed method is tested using real DTS data provided by an oil and gas operator in the Marcellus shale. First, all provided data is interpreted to then set up the inverse problem is that will estimate fracture half-length and fracture permeability. The true values of these parameters are unknown so the accuracy of the resulting estimations is hard to verify. Nevertheless, acceptable ranges will be established based on data obtained from literature and other field examples.

5.1 Field Data

First, a wellbore diagram (WBD) is constructed based on the directional drilling report. **Fig. 5.1** is a vertical displacement (TVD) vs. total measured displacement (TMD) plot showing the well's "curve" and lateral section. **Fig. 5.2** shows only the lateral section as to illustrate the elevation differences in this part of the well.

Next, the location of all fracture stages is marked on the WBD. For Well A, there are 14 stages with four clusters per stage. For modelling purposes, only 14 model fractures are considered as to illustrate the combined effect of all clusters present in a stage rather than the contribution of each cluster.

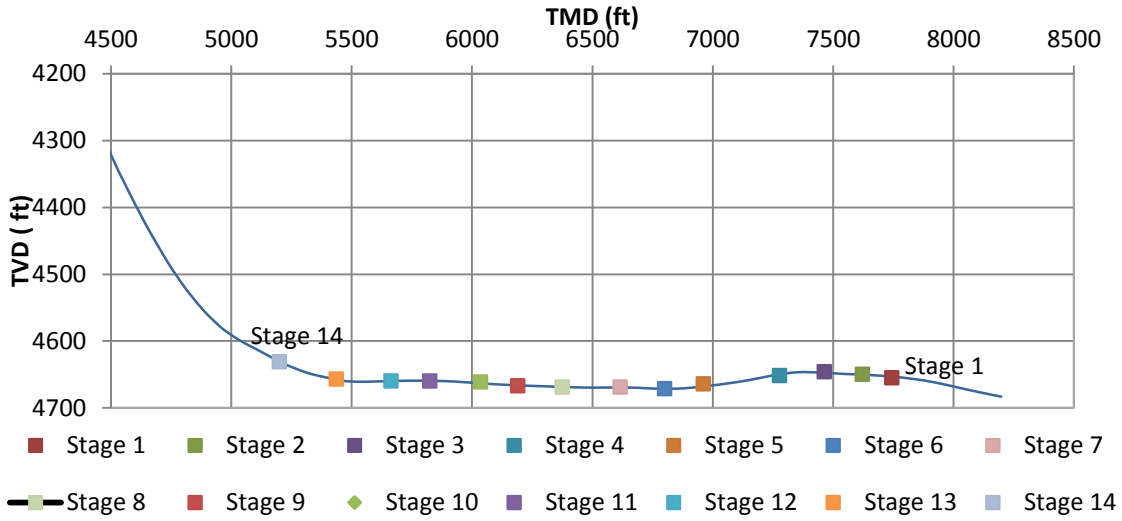

Fig. 5.1—WBD with vertical, curve and lateral section. Location of fracture stages are marked along wellbore.

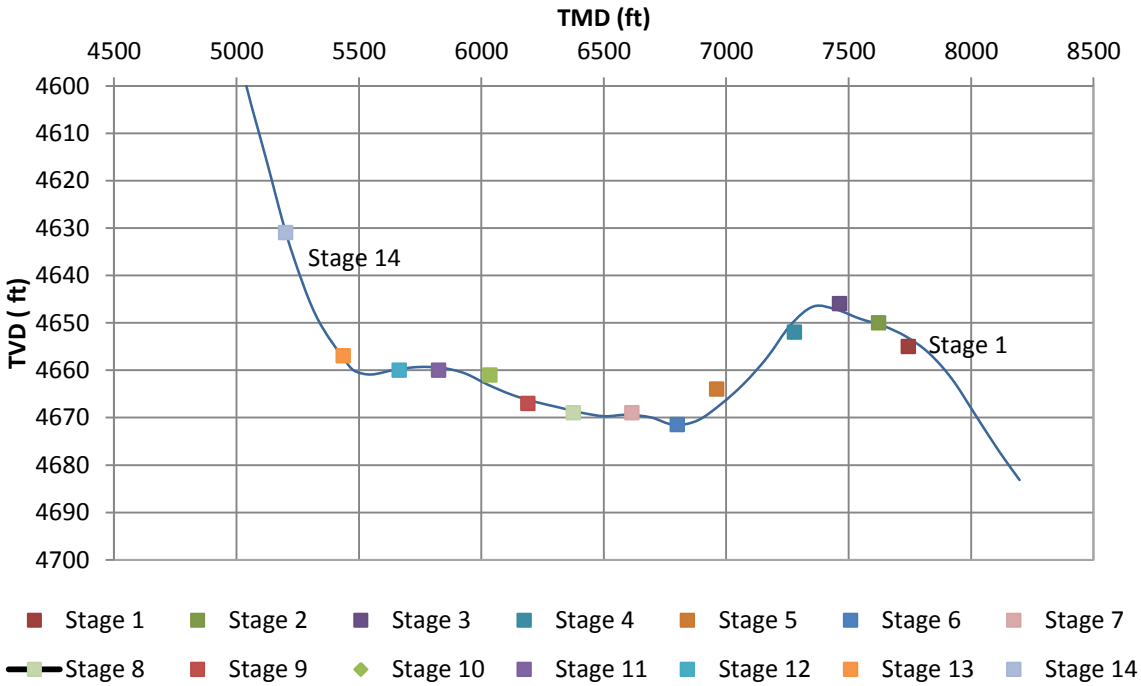

Fig. 5.2—WBD with lateral section only. Location of fracture stages are marked along wellbore.

5.1.1 Production Data

Two pieces of information are needed for the execution of the EnKF: production and DTS data. Both data sets need to have been recorded at the same time period in order to integrate them in the optimization problem.

The data provided for this study corresponds to a time of very early production. Production data specifying gas and water inflow rate are specified in **Fig. 5.3** and **Fig. 5.4.** Gas inflow data stars from 7/13/2011-8:00 to 7/14/2011-1:15. After that time, the well was shut-in. On 7/13/2011-19:00, maintenance service was performed and no data was recorded. On the other hand, DTS data is available from 7/13/2011-21:00 to 7/14/2011-7:00. The time disparity between production and DTS data reduces the time of study. As a result, the time interval is shortened to a period of four hours, between 7/13/2011-21:00 and 7/14/2011-1:15.

Next, the flowing conditions are established. Based on casing pressure readings shown in **Fig. 5.5,** it is assumed that the horizontal well was producing under constant bottomhole pressure. Furthermore, information from a production logging report corroborates this assumption and so the wellbore pressure is set to 700 psi.

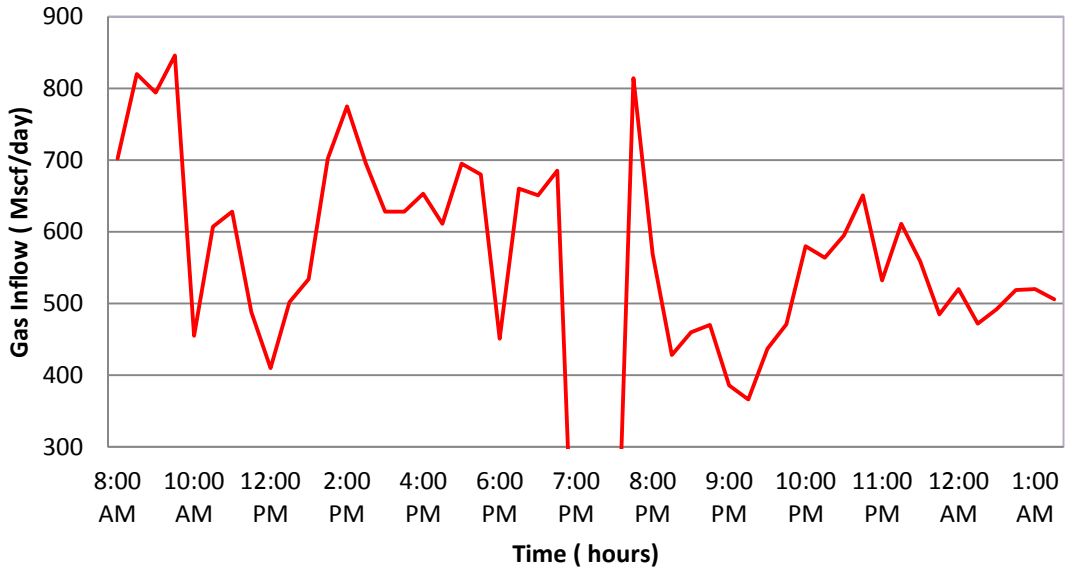

Fig. 5.3—Gas inflow rate.

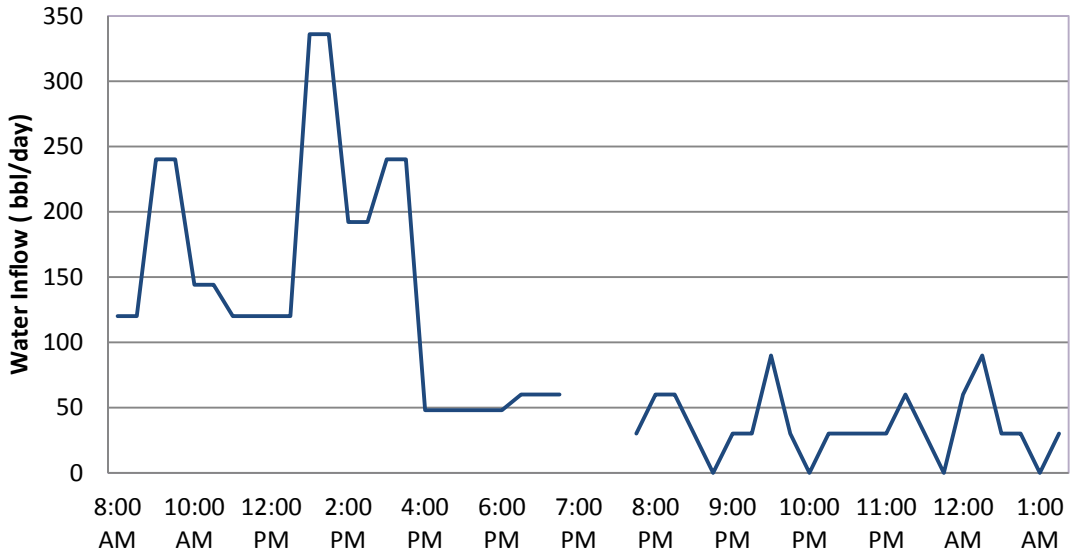

Fig. 5.4—Water inflow rate.

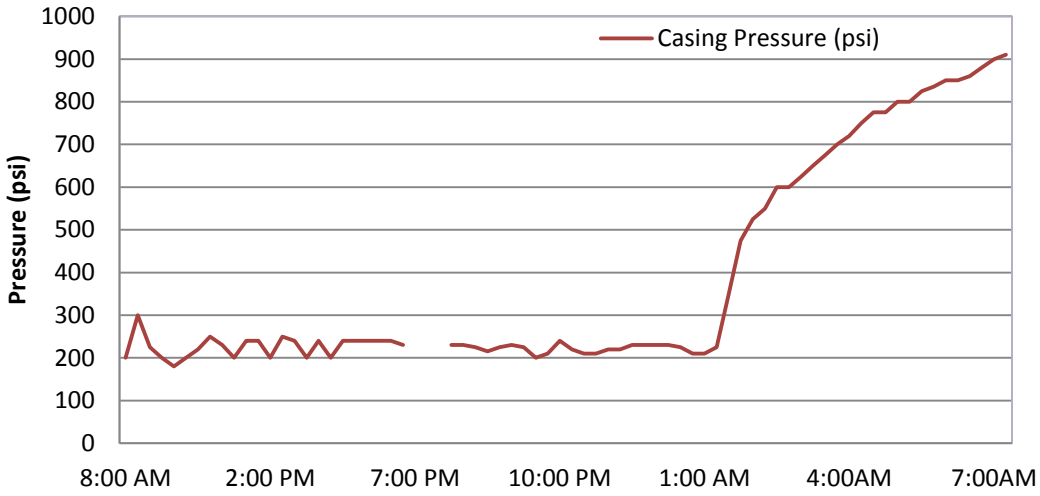

Fig. 5.5—Casing pressure.

5.1.2 DTS Field Data

The next piece of information is DTS data. The fiber optic cable of the DTS system extends from the well's toe all the way back to surface facilities. For the purposes of this study, only DTS data along the wellbore is needed. The vertical section of the well is identified by spotting the geothermal gradient's linear behavior (see **Fig. 5.6**). In this way, DTS data is correlated to the WBD. **Fig. 5.7** is a snapshot of a temperature profile with the wellbore trajectory superimposed on the secondary axis.

A quick glance at **Fig. 5.11** reveals the sharp temperature drop experienced at the location of the induced hydraulic fractures. Matching the hydraulic fracture location with the correct temperature data point affects the evolution of the EnKF estimation in the

data assimilation stage. For this reason, the appropriate selection of observation points is critical for the successful execution of the EnKF.

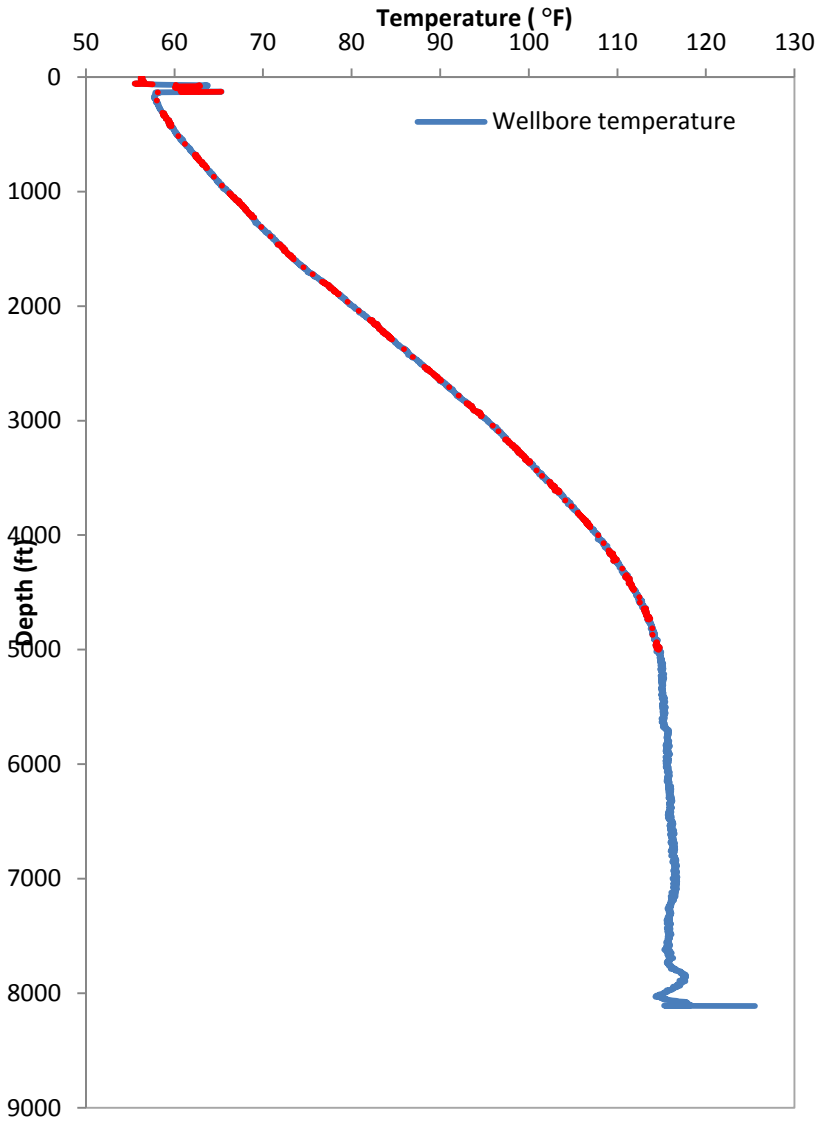

Fig. 5.6—Geothermal gradient of Well A. Vertical section of Well A is determined by identifying linear behavior of wellbore temperature.

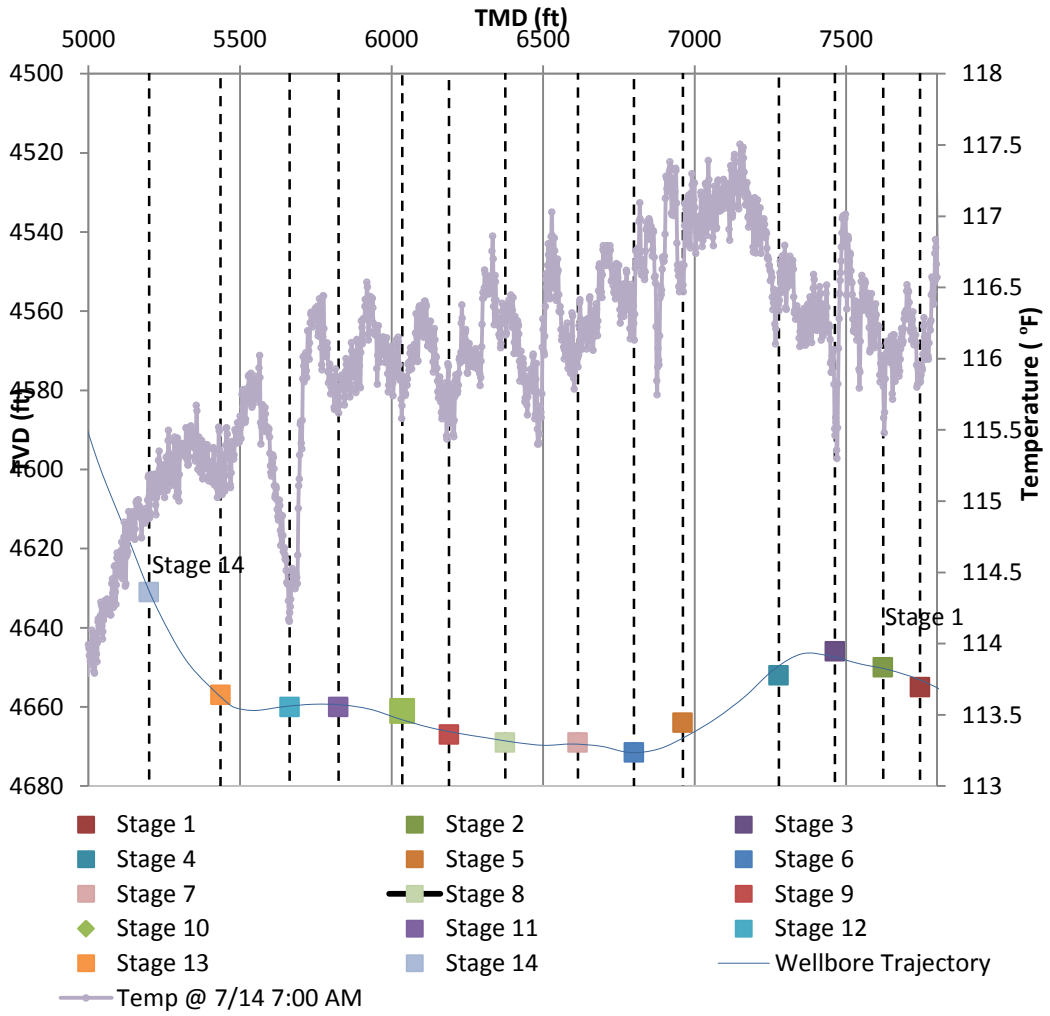

Fig. 5.7—Plot of wellbore trajectory (horizontal section only) on DTS profile. Sharp drops in temperature occur at the location of the hydraulic fractures.

5.2 Forward Model

A reservoir forward model responsible for generating pressure and temperature responses is set up next. Reservoir parameters are described in **Table 5.1**while fluid properties are specified in **Fig. 5.8** through **Fig. 5.9**. Results from data interpretation of production and DTS data (e.g. WBD, flowing condition, fracture location) are considered when calibrating the forward model.

At this point, it is important to recall that the closest parameter to the wellbore temperature, T_w, is the temperature at the wellbore-reservoir contact, also known as the arriving temperature, T_i. These are equal to each other only at the fracture nearest to the well's toe given that mixing effects inside the wellbore are not considered at this location. As a result, the history match is narrowed down to data corresponding to Stage No.1only, which will be the only stage opened to flow. Production data corresponding to Stage No.1 specifies that this stage is responsible for 3.5% of the total surface flow. **Fig. 5.10** and **Fig**. **5.11** show visual representations of the horizontal well in the rectangular-shaped reservoir used in this forward model.

Table 5.1 Forward model parameters used in EnKF estimation.		
Parameter	Description	Value [unit]
N_{stages}	Number of stages	14
k_{matrix}	Matrix permeability	10^{-4} [md]
k_{EPA}	EPA permeability	0.05 [md]
k_f	Fracture permeability	$unknown$
ϕ_{matrix}	Matrix porosity	0.08[%]
ϕ_{EPA}	EPA porosity	0.081 [%]
ϕ_f	Fracture porosity	0.33 [%]
x_f	Fracture half length	$unknown$
h_f	Fracture height	90 ft

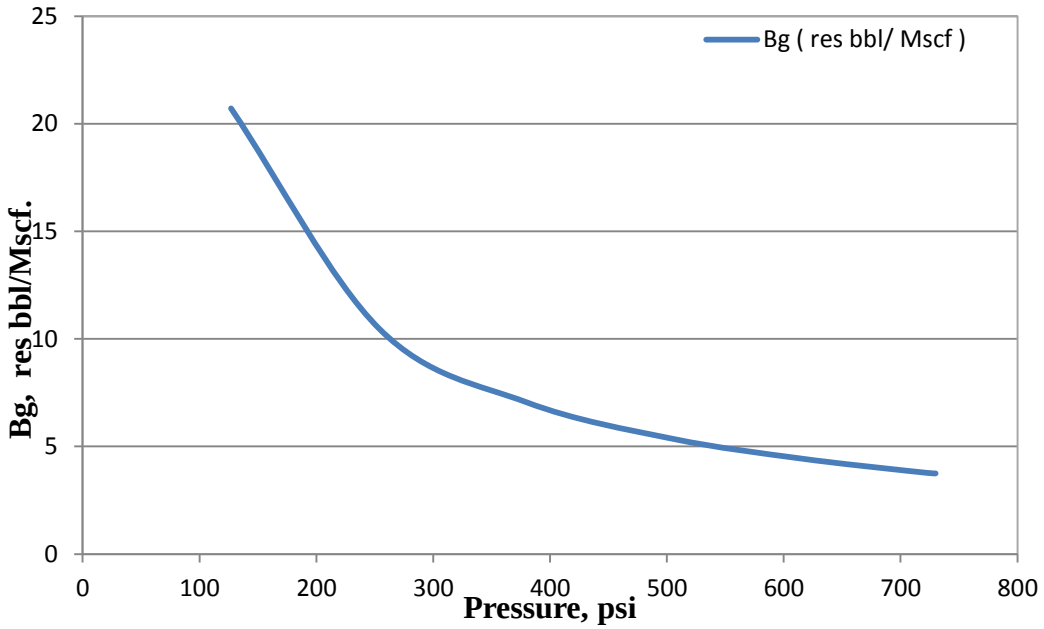

Fig. 5.8 —Gas formation volume factor.

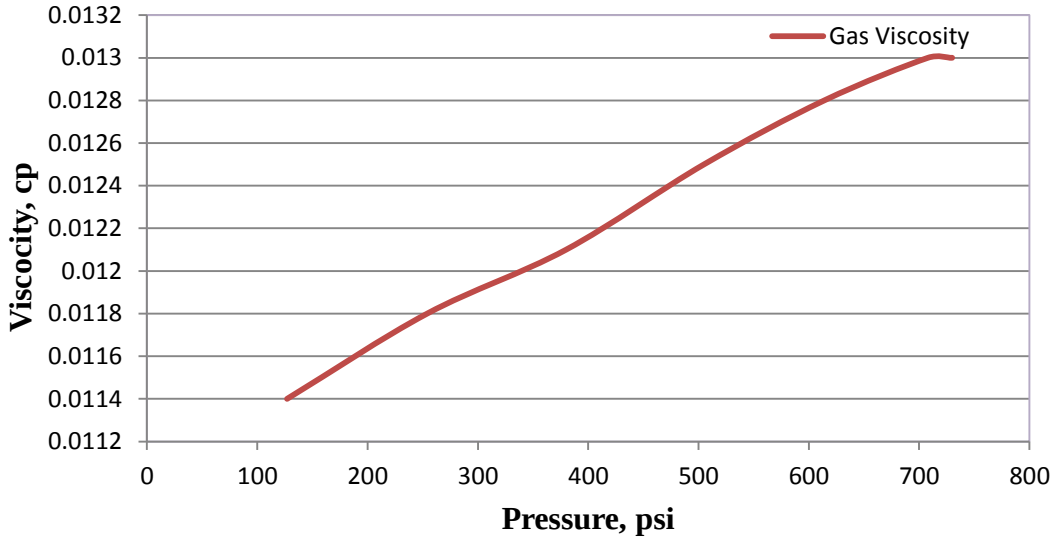

Fig. 5.9—Gas viscosity.

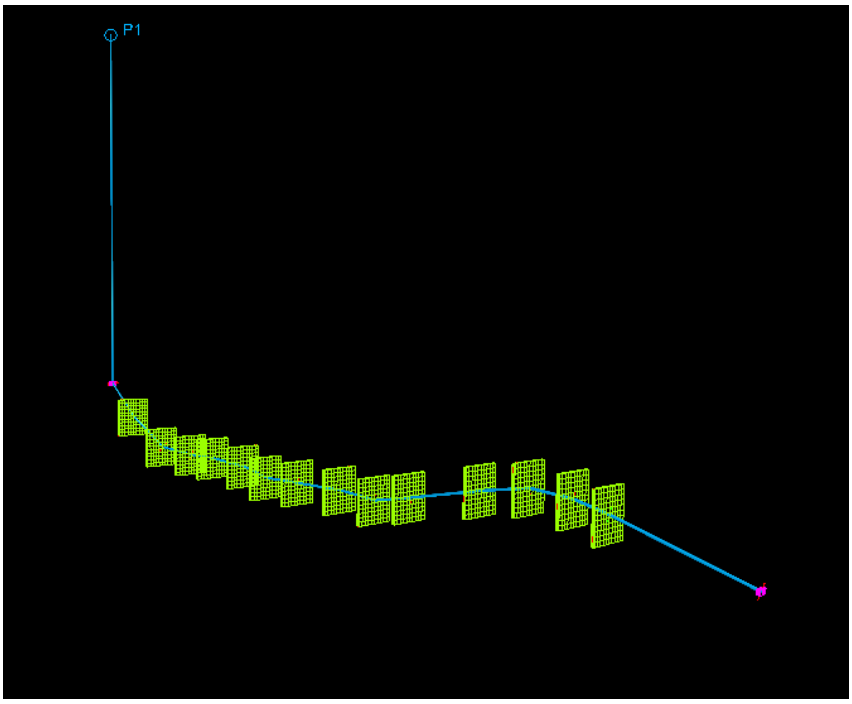

Fig. 5.10—Model of horizontal well with induced hydraulic fractures.

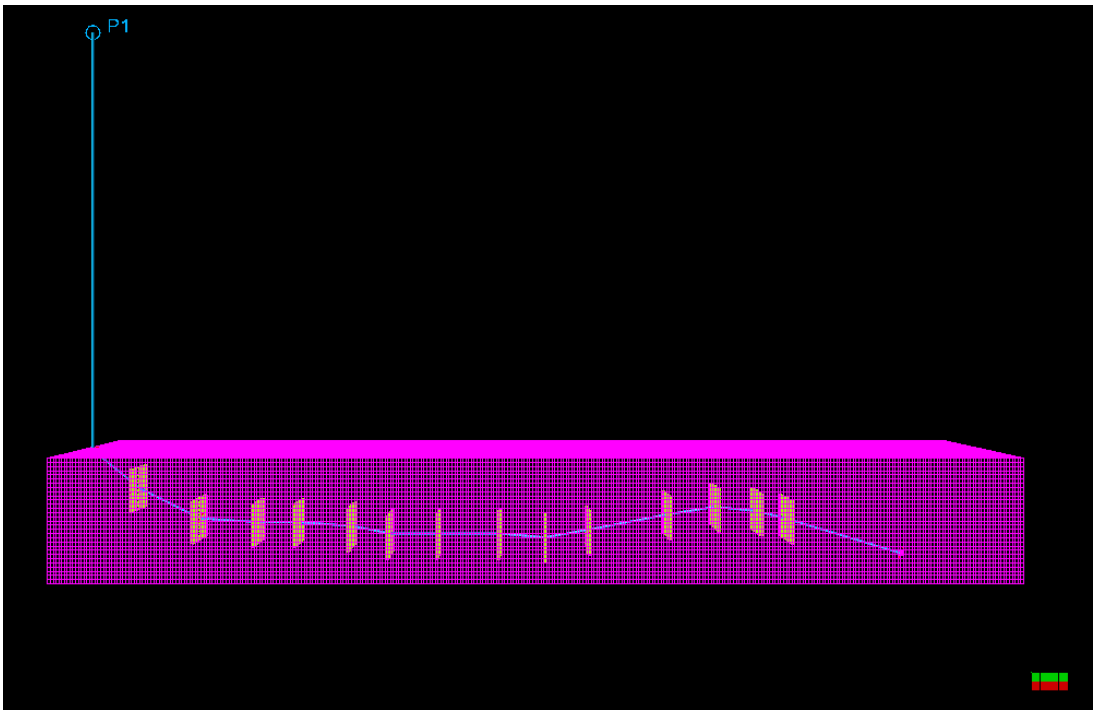

Fig. 5.11—Rectangular shaped reservoir with horizontal well and induced hydraulic fractures.

5.3 Inverse Model

For this implementation of the EnKF, the parameter used as observation is not the well's temperature profile (as was the case on all synthetic examples) but rather the temperature difference at the fracture location. **Fig. 5.12** illustrates this concept. By doing this, inaccuracies in the determination of initial conditions and geothermail gradient are avoided.

For this case, a joint estimationof fracture half-length and fracture permeability is preferred as to show the capabilites of the EnKF when handling more than one objective parameter and also to maximize computational time. As mentioned before, true values of model parameters are unknown so its hard to verify the accuracy of the estimations. Neverthless, a range of validity is established based on relevant literature information and other field examples. Results are presented in the next section **(Fig. 5.13** to **Fig. 5.18).**

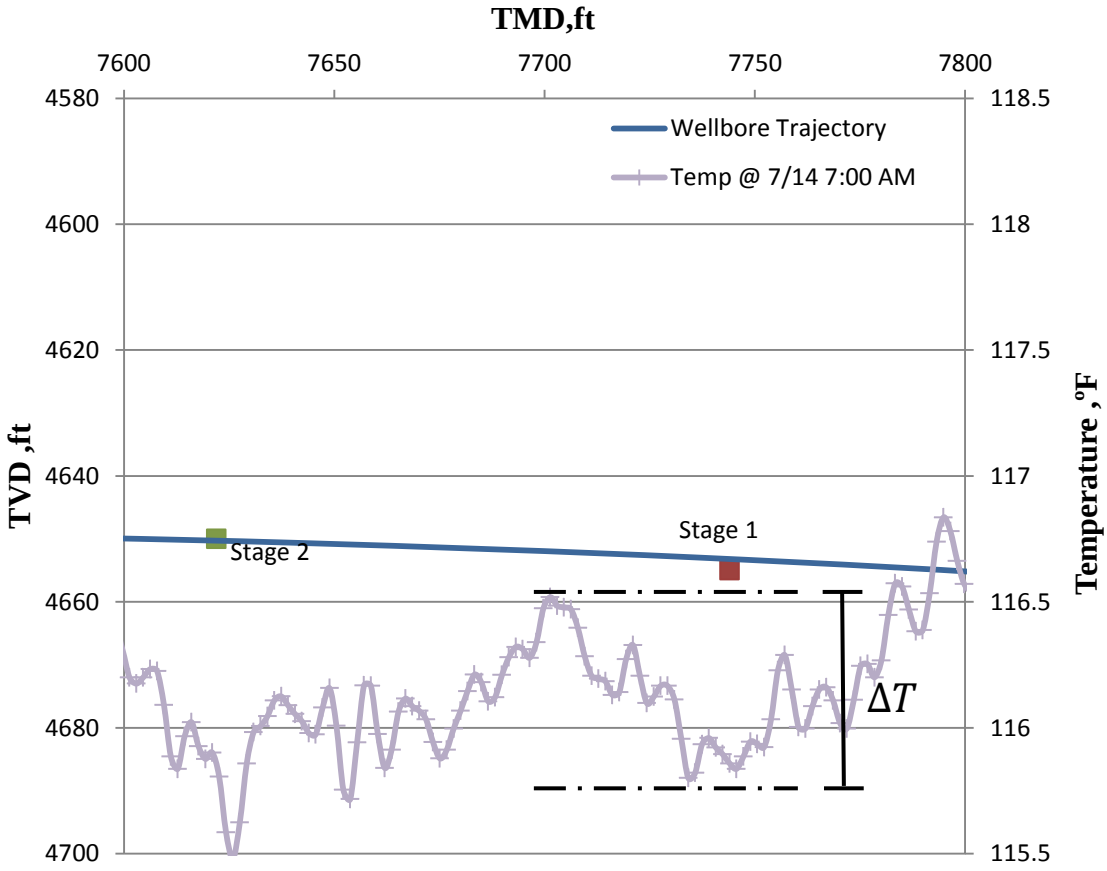

Fig. 5.12—Difference between temperature at gas inflow location and temperature at end of Stage 1. ΔTservesas observation in the execution of the EnKF.

5.4 ENKF Results

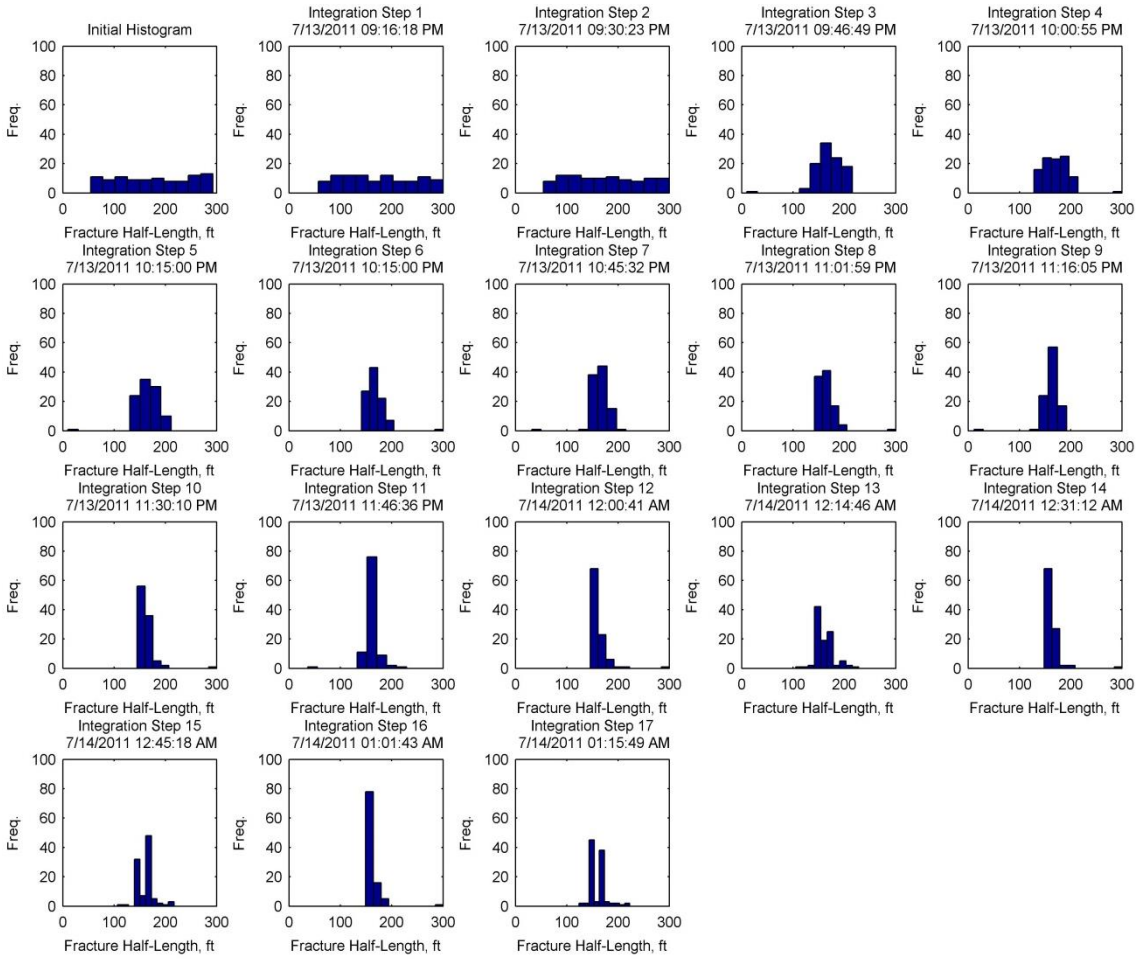

Fig. 5.13—Estimation of fracture half-length after 17 integration steps (4 hours).

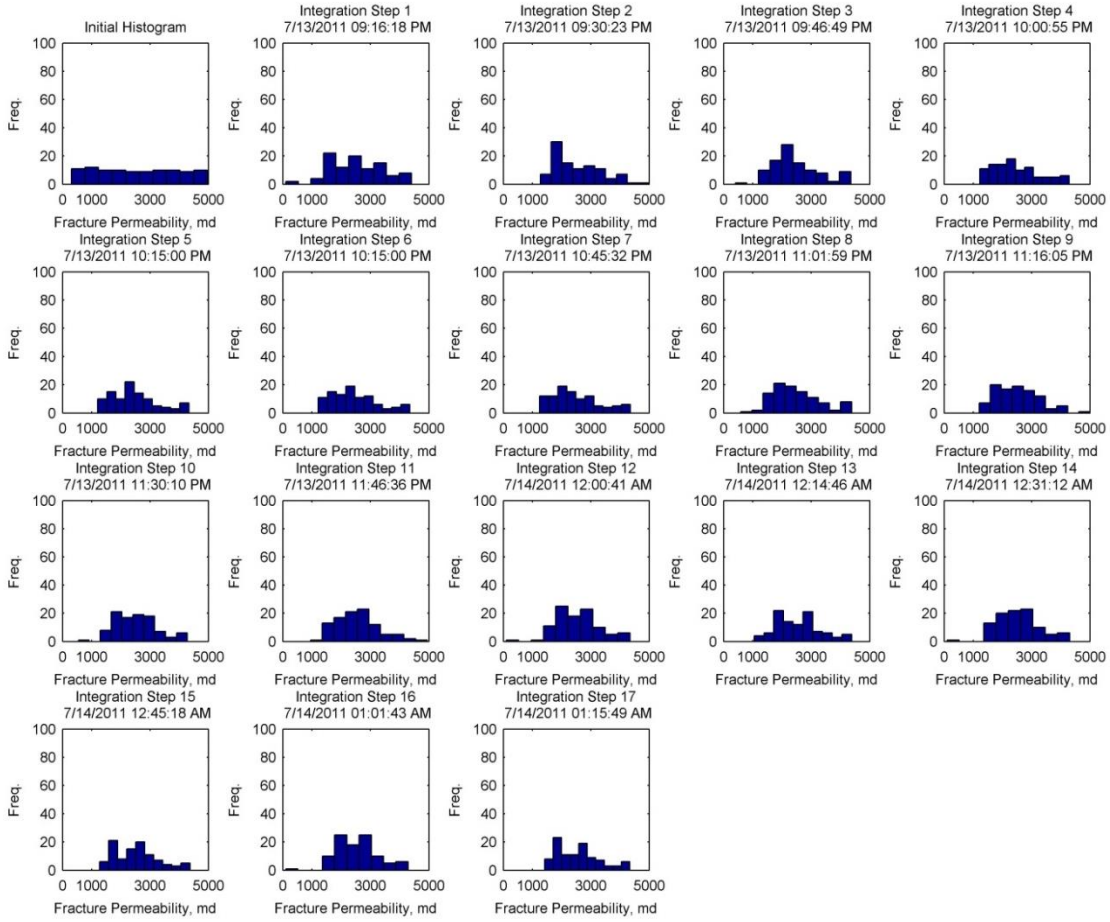

Fig. 5.14—Estimation of fracture permeability after 17 integration steps (4 hours).

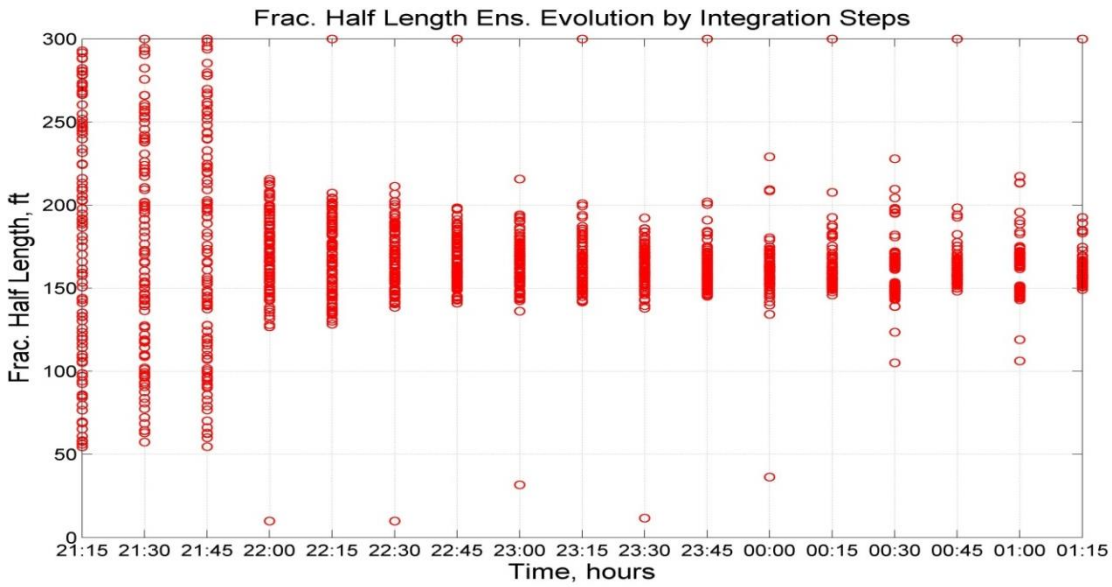

Fig. 5.15—Fracture half-length ensemble evolution by integration steps. (Field case).

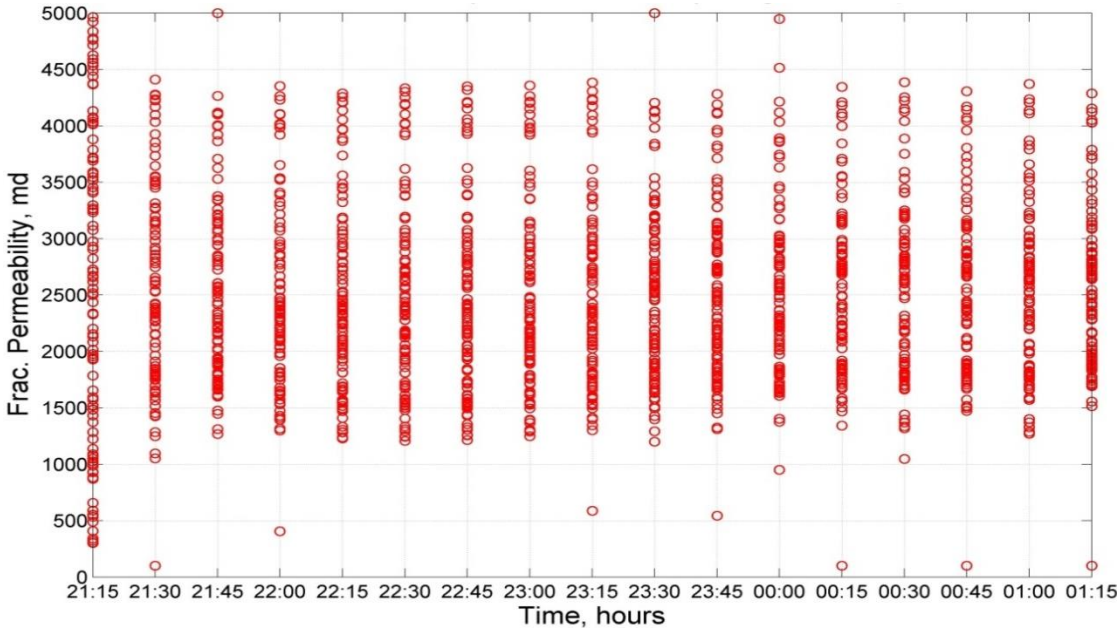

Fig. 5.16—Fracture permeability ensemble evolution by integration steps. (Field case).

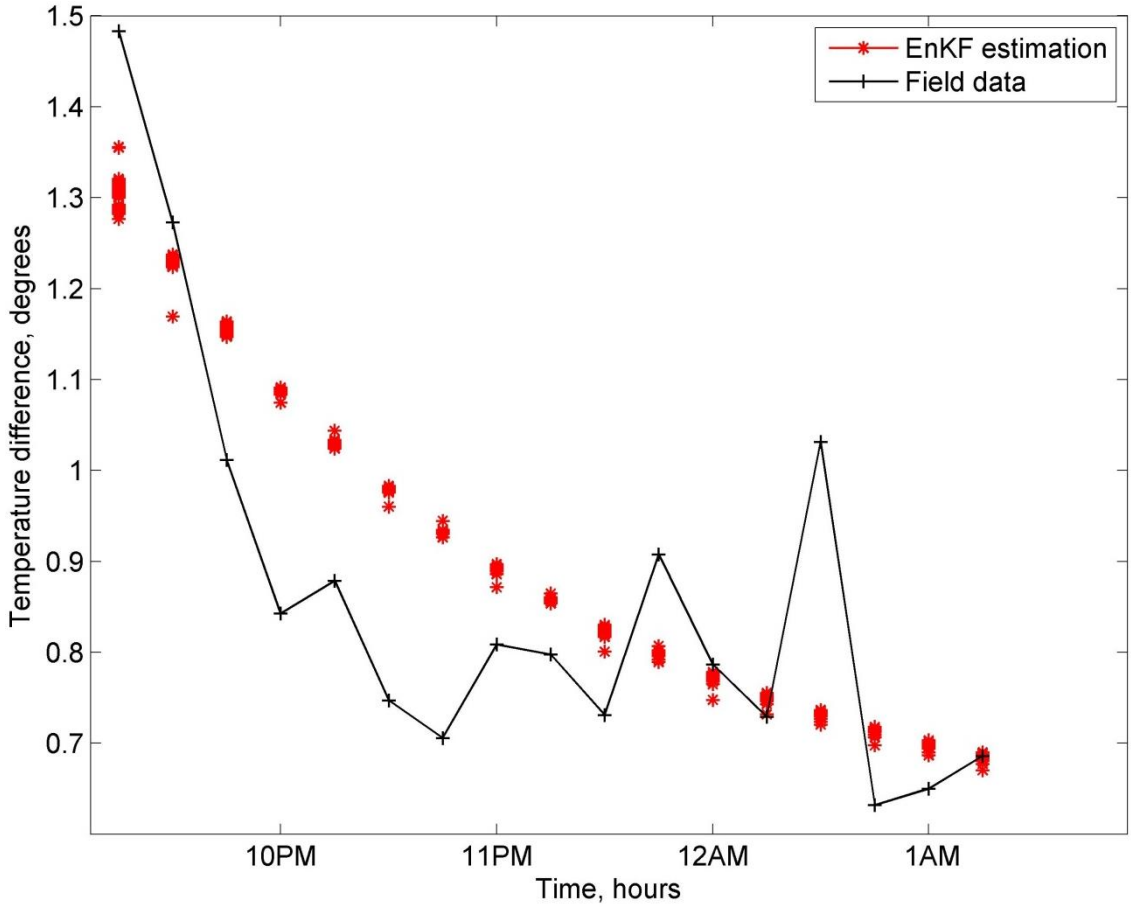

Fig. 5.17—Temperature difference of EnKF forecasts (red) and field data (black).

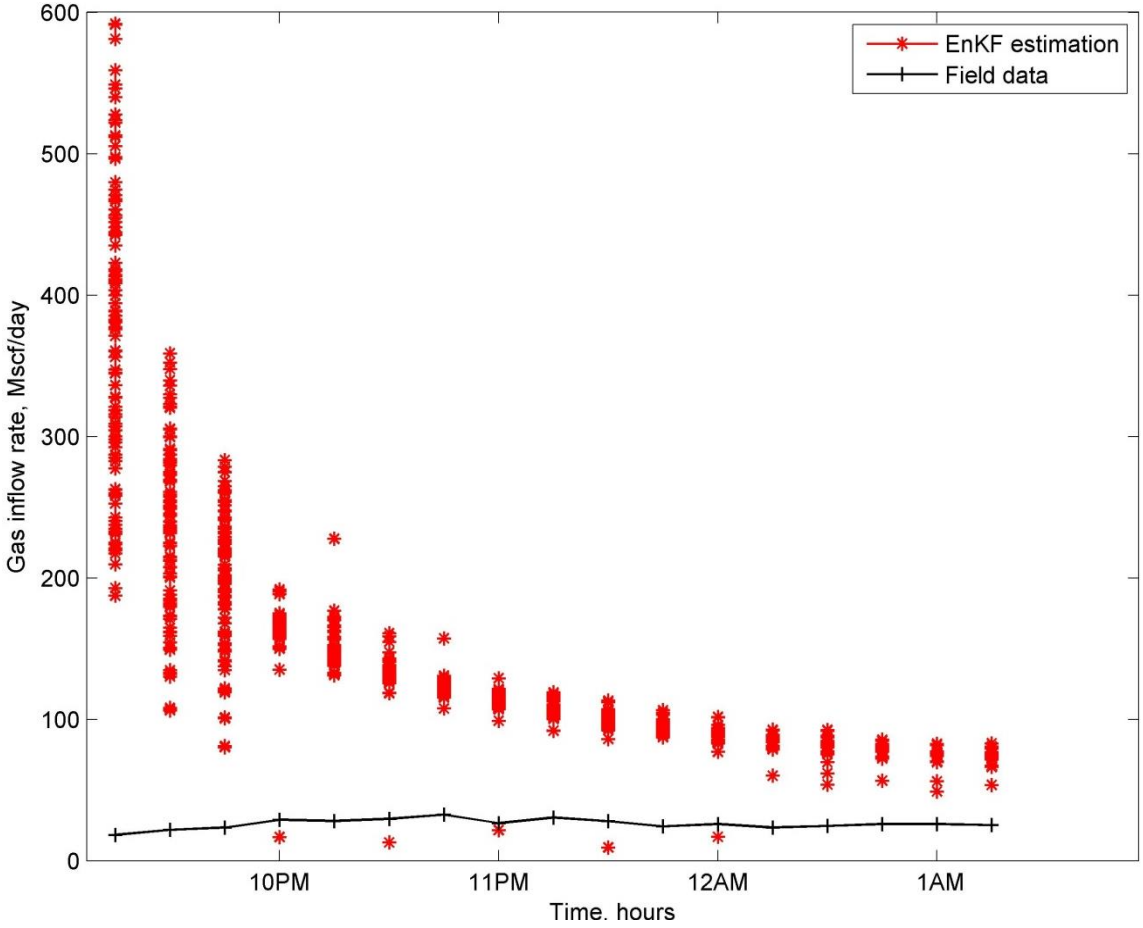

Fig. 5.18— Production performance of EnKF forecasts (red) and field data (black).

5.5 Discussion

The range of validity needs to be defined in order to test the accuracy of the estimations presented in the previous subsection. Fracture half-length values can be inferred from well spacing plans operators use in the Marcellus shale. Field studies and relevant literature specify that well spacing in the Marcellus shale is between 500 ft-1000 ft, as shown in **Fig. 5.19** (Edwards et al, 2011). This means that fracture half-length values range between **250 ft and 500 ft**.

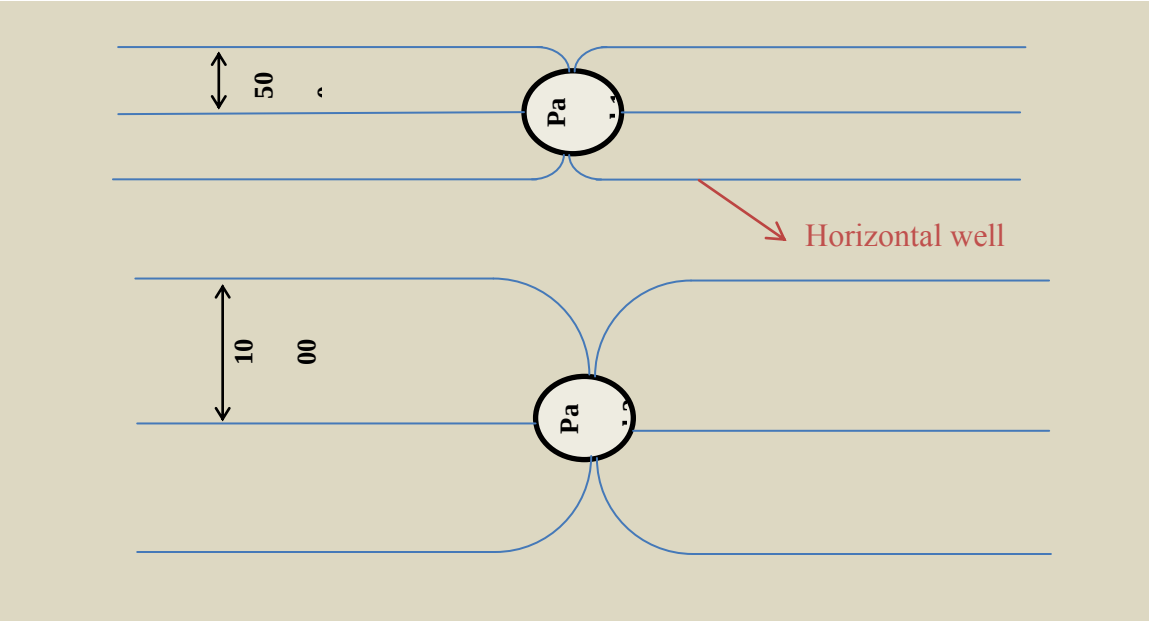

Fig. 5.19—Well spacing of horizontal wells in the Marcellus shale.

For the type of proppant mesh used in Well A (80-100, 30-50 mesh) fracture conductivity values (at closure stress levels of 3,000-3,500 psi) range between **100 md-**

ft to 1000 md-ft according to different laboratory studies (Zhang et al, 2013). When setting up the inverse problem, fracture width is assumed to be known and is defined in the construction of the LGR scheme. With a gridblock size of 10 ft in the X direction, the fracture width has a value of 0.33 ft. Fracture permeability values are calibrated in such way that fracture conductivity values are preserved. In this way, the fracture permeability range of validity is between **300** and **3000 md.**

Estimations of fracture half-length and permeability are shown in **Fig. 5.13** and **Fig. 5.14**, **Fig. 5.15** and **Fig. 5.16** show the evolution of fracture half-length and permeability ensemble evolution at each integration step. For both fracture parameters, the solution does not converge to a single value but rather to a set of values. In synthetic cases, despite converging to a single value, the final solution was in essence still a PDF where the true value had the highest frequency (e.g. 100). For the field case, given that the estimation has undergone a short period of assimilation time, a high spread of the estimations is observed. This spread is expected to decrease if more integration steps were to be executed.

History matching the forecast of the resulting estimations to the true DTS and production data is another way to test the accuracy of the EnKF results. **Fig. 5.17** and **Fig. 5.18** show the temperature and production forecast of all ensembles at each integration step. Indeed, as time progresses and data are assimilated, the forecast of the ensembles approaches the true field observation.

In the end, both parameter estimations fell within the previously established limits; however, the fracture half-length's final estimation has less spread than fracture

permeability. Additional monitoring time may change this situation and allow the permeability to reduce its spread and further approach the true value. History matching results also showed positive signs, as the simulated forecasts from the final ensembles approached the field data points. Once again, additional time may reduce the difference between the observed and the simulated forecast.

6. CONCLUSIONS

In this study, it was successfully demonstrated how to implement the EnKF in the characterization of HFT using DTS data. Different case studies along with a sensitivity analysis were set up in order to analyze the reservoir's thermal response to different fracture parameters. It was shown that the reservoir's temperature response is sensitive to fracture half-length, fracture permeability and EPA permeability.

Synthetic examples showed encouraging results in implementing the EnKF for individual and joint estimation of fracture parameters after only 30 days of production. Due to the computational expense of the EnKF forecast step (e.g. Monte Carlo simulation), higher computation capabilities are required for faster results. In addition, prolonged times are needed to allow the EnKF to evolve and converge to more accurate final estimations. This may represent an issue for real-time monitoring applications. As a result, the EnKF may not be suitable for real-time characterization of HFT.

Next, the implementation of the EnKF on field data showed accepted results as the estimations fell under a range of values that agreed with information from other field examples and relevant literature. For the field case, the conductivity induced by the network of fractures (e.g. EPA) was not estimated. Reservoir temperature is very sensitive to this parameter since it is closely linked to the pressure variations felt around the primary fractures. Because of this, a more robust model capable of accurately capturing this effect is strongly suggested.

In addition, prior knowledge of fracture parameter values is necessary for a more rigorous examination of the EnKF's performance. Integration of seismic information is suggested for fracture half-length estimations either as an observation in the EnKF or to test the accuracy of the resulting estimation. Furthermore, a thermal wellbore model is needed in order to optimally use field DTS data. In this way, the simulated parameter would be the same, thus reducing modelling errors.

In the end, the implementation of the EnKF has a myriad of applications in petroleum sciences, particularly in fracture diagnostic tools. The flexibility of the EnKF at integrating additional data sources is one of the main advantages of this technique in addition to its gradient free implementation. This study has successfully shown its flexibility at executing it and its effectiveness at accurately estimating fracture parameters using a combination of production and temperature data. The EnKF therefore represents a successful alternative to surpass DTS qualitative applications by performing a more accurate reservoir and HFT characterization, along with automatic history matching.

REFERENCES

Aanonsen, S. I., Nævdal, G., Oliver, D. S. et al. 2009. The Ensemble Kalman Filter in Reservoir Engineering--a Review. *SPE Journal* **14** (3): 393-412 http://dx.doi.org/10.2118/117274-pa

Baker, L.2007. Properties of the Ensemble Kalman Filter. http://www.reading.ac.uk/web/FILES/maths/laurabaker.pdf.(downloaded 19 June 2014)

Belvalkar, R. A., and Oyewole, S. 2010. Development of Marcellus Shale in Pennsylvania. Paper SPE 134852 presented at the SPE Annual Technical Conference and Exhibition, Florence, Italy, 19-22 September.http://dx.doi.org/10.2118/134852-MS

Cipolla, C. L., Lolon, E. P., Erdle, J. C. et al. 2010. Reservoir Modeling in Shale-Gas Reservoirs. *SPE Reservoir Evaluation & Engineering* **13** (4): 638-53 http://dx.doi.org/10.2118/125530-pa

Cipolla, C. L., and Wright, C. A. 2000. Diagnostic Techniques to Understand Hydraulic Fracturing: What? Why? And How? Paper SPE 59735 presented at the SPE/CERI Gas Technology Symposium, Calgary, Alberta, Canada, 3-5 April 2000.http://dx.doi.org/10.2118/59735-ms

Duru, O. O., and Horne, R. N. 2009. Simultaneous Interpretation of Pressure, Temperature and Flowrate Data for Improved Model Identification and Reservoir Parameter Estimation. Paper SPE 124827 presented at the SPE Annual Technical

Conference and Exhibition, New Orleans, Louisiana, 4-7 October 2009.http://dx.doi.org/10.2118/124827-ms

Edwards, K. L., Weissert, S., Jackson, J. B. et al. 2011. Marcellus Shale Hydraulic Fracturing and Optimal Well Spacing to Maximize Recovery and Control Costs. Paper SPE 140463 presented at the SPE Hydraulic Fracturing Technology Conference, The Woodlands, TX, 24-26 January.http://dx.doi.org/10.2118/140463-ms

Lake, L. W.2010.*Enhanced Oil Recovery*.Vol.Society of Petroleum Engineers

Li, Z., Yin, J., Zhu, D. et al. 2010. Using Downhole Temperature Measurement to Assist Reservoir Optimization. Paper SPE 131370 presented at the International Oil and Gas Conference and Exhibition, Beijing, China, 8-10 June.http://dx.doi.org/10.2118/131370-ms

Oliver, D. S., Reynolds, A. C., and Liu, N.2008.*Inverse Theory for Petroleum Reservoir Characterization and History Matching*.Vol.392.Cambridge, UK:Cambridge University Press

Reyes, R. P., Yeager, V. J., Glasbergen, G. et al. 2011. Dts Sensing: An Introduction to Permian Basin with a West-Texas Operator. Paper SPE 145055 presented at the SPE Annual Technical Conference and Exhibition, Denver, Colorado, 30 October -2 November.http://dx.doi.org/10.2118/145055-ms

Sierra, J. R., Kaura, J. D., Gualtieri, D. et al. 2008. Dts Monitoring Data of Hydraulic Fracturing: Experiences and Lessons Learned. Paper SPE 116182 presented at

the SPE Annual Technical Conference and Exhibition, Denver, Colorado, USA, 21-24 September 2008.http://dx.doi.org/10.2118/116182-ms

Skjervheim, J.-A., Evensen, G., Aanonsen, S. I. et al. 2005. Incorporating 4d Seismic Data in Reservoir Simulation Models Using Ensemble Kalman Filter. Paper SPE 95789 presented at the SPE Annual Technical Conference and Exhibition, Dallas, Texas, 9-12 October 2005.http://dx.doi.org/10.2118/95789-ms

Soeder, D. J. 1988. Porosity and Permeability of Eastern Devonian Gas Shale. *SPE Formation Evaluation* **3** (1): 116-24 http://dx.doi.org/10.2118/15213-pa

Yoshida, N., Zhu, D., and Hill, A. D. 2013. Temperature Prediction Model for a Horizontal Well with Multiple Fractures in a Shale Reservoir. Paper SPE 166241 presented at the SPE Annual Technical Conference and Exhibition, New Orleans, Louisiana, 30 September-2 October.http://dx.doi.org/10.2118/166241-ms

Zhang, J., Hill, D., Zhu, D. et al. 2013. Laboratory Measurement of Hydraulic Fracture Conductivities in the Barnett Shale. Paper SPE 16444 presented at the International Petroleum Technology Conference, Beijing, China, 26-28 March.http://dx.doi.org/10.2523/16444-ms